FINAL TECHNICAL REPORT

GEOLOGIC AND PALEOSEISMIC CHARACTERIZATION OF THE NEW MADRID NORTH FAULT, FARRENBURG, SOUTHEASTERN MISSOURI

Recipient:

[1]William Lettis & Associates, Inc., 1777 Botelho Drive, Suite 262, Walnut Creek, CA 94596
(925) 256-6070 phone; (925)256-6076 fax; URL: www.lettis.com

Principal Investigators:

John N. Baldwin[1], Robert Givler[1] and Robert Witter[1]
Email: baldwin@lettis.com; givler@lettis.com; witter@lettis.com

Contributors:

James D. Vaughn
KeenGeoserve; 325 East Vine Street; Dexter, MO 63841
Sue Cashman
Humboldt State University, Department of Geology, Arcata, CA 95521-4957
James Harris
Millsaps College, Geology Department; Jackson, MS 39210
Roy Van Arsdale
University of Memphis, Department of Earth Sciences, 402 Smith Chemistry, Memphis, TN 38152
Andrew Barron
University of Nevada, MS 169, Reno, NV 89957
John Sexton and Marshall Lake
Southern Illinois University, Geology Department; Carbondale, IL 62901
Steve Forman
University of Illinois, Chicago, Department of Geological Sciences; Chicago, IL 60607

Program Elements II

Keywords:

Paleoseismology; Geophysics; Recurrence interval; Slip rate; Trench Investigations; Quaternary Fault Behavior; Neotectonics

U. S. Geological Survey
National Earthquake Hazards Reduction Program
Award Number 02HQGR0024

October 2004

This research was supported by the U.S. Geological Survey (USGS), Department of the Interior, under USGS Award 02HQGR0024. The views and conclusions contained in this document are those of the Principal Investigators and should not be interpreted as necessarily representing the official policies, either expressed or implied, of the U.S. Government.

TABLE OF CONTENTS

LIST OF TABLES

LIST OF APPENDICES

LIST OF FIGURES

Award No. 02HQGR0024

GEOLOGIC AND PALEOSEISMIC CHARACTERIZATION OF THE NEW MADRID NORTH FAULT, FARRENBURG, SOUTHEAST MISSOURI

Baldwin[1], J.N, Givler[1], R., Witter[1], R.,, Vaughn[2], J.D., Cashman[3], S., Harris[4], J.B., Van Arsdale[5], R., Sexton[6], J., Lake[6] , M., Barron[7], A., and Forman[8], S.

Principal Investigators:
[1]William Lettis & Associates, Inc., 1777 Botelho Drive, Suite 262 Walnut Creek, CA 94596
balwin@lettis.com; givler@lettis.com; witter@lettis.com; phone: 925-256-6070, fax: 925-256-6076

[2]Keen GeoServe, 325 E. Vine, Dexter, MO 63841
[3]Humboldt State University, Department of Geology, Arcata, CA, 95521-4957
[4]Millsaps College, Geology Department, Jackson, MS, 39210
[5]University of Memphis, Department of Earth Sciences, 402 Smith Chemistry, Memphis, TN 38152
[6]Southern Illinois University, Geology Department, Carbondale, IL 62901
[7]University of Nevada, MS 169, Reno, NV 89957
[8]University of Illinois, Chicago, Department of Geological Sciences, Chicago, IL 60607

ABSTRACT

On the basis of the regional extent of liquefaction, contemporary northeast-trending microseismicity, and historical accounts of earthquake-related damage, the New Madrid North fault (NMNF) is inferred to have ruptured January 23, 1812, during an approximately M7 to M8 earthquake. The location of the NMNF and its role as an 1811-1812 seismic source remains enigmatic. Our recent detailed geologic characterization of the North and South Farrenburg lineaments and bedrock features beneath Sikeston Ridge provides compelling evidence that these surficial features reflect faults at depth and constrain the location of the NMNF. This study shows that the NMNF likely ruptured during the 1811-1812 earthquake sequence, as well as during earlier events in the late Holocene and late Pleistocene.

The surficial and subsurface geologic information compiled and analyzed as part of this study constrain the location and describe the style of deformation of the New Madrid North fault. The North and South Farrenburg lineaments are two northeast-trending, 3- to 4-km-long lineaments that obliquely cross Sikeston Ridge, a Pleistocene erosional remnant lying above the Mississippi River floodplain. The lineaments are defined by apparent right-laterally deflected paleodrainages, scarps, swales, linear troughs, and tonal contrasts, and align with contemporary northeast-trending microseismicity. Borehole data show a change in thickness (5 m) of post-Tertiary alluvium that reflect a buried lineament trending N35°E for 35 km across both Sikeston Ridge and a mid-Holocene fluvial surface of the Mississippi River east of the ridge. This thickness change in Quaternary alluvium coincides with microseismicity, aeromagnetic anomalies, similar northeast-trending bedrock discontinuities at the Eocene-Quaternary unconformity, and Paleozoic and Cretaceous boundaries. All of these features generally align with the North and South Farrenburg lineaments. In turn, shear wave seismic reflection profiles acquired across the Farrenburg lineaments image warped and faulted Quaternary deposits. Acquisition and interpretation of proprietary Dow Chemical Corporation vibroseis data crossing the southwest projection of the Farrenburg lineaments also show faults and folds that deform the Paleozoic and Cretaceous sediments.

Six trenches and a transect of six boreholes across the North Farrenburg lineament encountered: (1) a narrow zone of liquefaction-related dikes having a mean trend of N20°E; (2) late Holocene north- to northeast-striking near-vertical faults, (3) Pleistocene folding and possible faulting, and (4) soft sediment deformation. On the basis of soil profile development, coupled with radiometric dating of detrital charcoal in the liquefaction-related deposits, stratigraphic relations interpreted from the trenches, we interpret deformation related to: (1) the 1811-1812 sequence, (2) one and possibly several late Holocene events, and (3) one to perhaps two late Pleistocene events.

Oriented sediment samples collected from the fault zones and dikes, and analyzed with a SEM, show zones of reduced grain size and preferentially oriented sand grains along fault contacts. Similar sediment samples collected from undeformed sand and from the sand dikes show no evidence of grain fracturing or grain size reduction. Microstructural data, coupled with analyses of macro-fracture data from the trenches, indicate that the sense of slip is primarily dextral and likey of primary tectonic origin. Similar sediment samples collected from undeformed sand and from the sand dikes show no evidence of grain fracturing and reduction. Collectively, the geomorphic, geologic, seismic reflection, trench and micro-textural data support the interpretation that the Farrenburg lineaments reflect late Holocene deformation related to the NMNF.

1.0 INTRODUCTION

The New Madrid seismic zone (NMSZ) is historically the most seismically active region in the central and eastern United States, and is the source of several historical large-magnitude earthquakes (Figure 1). Contemporary seismicity and the occurrence of three M_W7 to M_W8 earthquakes (magnitude variability reflects changes in interpretation of intensity values and influence of site response) within the central Mississippi Valley during the winter of 1811-1812 (Nuttli, 1973; Johnston and Schweig, 1996; Johnston, 1996; Hough et al., 2000; Bakun and Hopper, 2004) demonstrate the seismic potential of fault sources within the NMSZ. Personal accounts and geologic studies of the 1811-1812 earthquake sequence show that the earthquakes caused widespread damage to the central and eastern United States related to strong ground shaking, landsliding, liquefaction (Tuttle et al., 2002; Tuttle and Schweig, 1995; Obermeier, 1989; Russ, 1982; and Fuller, 1912), flooding, and scarp formation (Russ, 1982; Van Arsdale, 1995; Kelson et al., 1996). However, evidence of coseismic surface rupture associated with the 1811-1812 earthquake sequence remains elusive (Schweig and Marple, 1991), with the exception of the Reelfoot fault (Kelson et al., 1992, 1996). In this study, we delineate and characterize two distinct northeast-trending lineaments traversing Sikeston Ridge directly north of New Madrid, MO, to evaluate whether the features represent the surficial expression of the poorly characterized New Madrid North fault (NMNF).

Contemporary seismic activity within the NMSZ consists of three principal trends of seismicity: two northeast-trending arms with a central connecting northwest-trending arm (Figure 1). This seismicity pattern, coupled with evaluation of focal mechanisms, and the present-day stress field of the central United States, defines a northeast-trending, dextral fault system that forms a zone of contraction within a left-stepover (Russ, 1982; Schweig and Ellis, 1994). The southern arm of seismicity coincides with the Blytheville arch, the central arm coincides with the Tiptonville Dome and Lake County uplift (LCU), and the northern arm coincides, in part, with the western margin of the Reelfoot rift and cuts northeast across the southern part of Sikeston Ridge near New Madrid (Figure 1). The northern arm of the NMSZ extends from northwest of New Madrid to the northeast across Sikeston Ridge towards Charleston, Missouri. Others have referred to the alignment of the epicenters associated with the northern arm of seismicity as the New Madrid North fault (Johnston and Schweig, 1996), which we adopt in this study. Fault plane solutions from earthquakes comprising the northern arm of microseismicity are consistent with dextral strike-slip faulting.

The January 23, 1812, large magnitude earthquake is believed to have occurred on the NMNF (Johnston and Schweig, 1996). However, no surface expression of this earthquake has been previously documented to support its occurrence on the NMNF. The existence of the fault is based on northeast-trending microseismicity (Johnston and Schweig, 1996), hypothesized rupture scenarios based on historical accounts of damage (Johnston and Schweig, 1996), and aerial distribution of earthquake-related liquefaction features (Obermeirer, 1989), and aeromagnetic anomalies (Hildenbrand et al., 1985) (Figures 1 and 2). Recently others (Mueller et al. 2004) have argued on the basis of computer modeling that the microseismicity of the northern arm is unrelated to aftershocks from the 1812 event on the NMNF. Mueller et al. (2004) argue that the January 23, 1812 earthquake occurred in the Wabash Valley hundreds of kilometers north of New Madrid. Clearly, the northern arm of northeast-trending microseismicity has been the least investigated part of the NMSZ in terms of seismic source characterization and paleoseismology.

Our previous mapping conducted in the northern part of the LCU on Sikeston Ridge identified two prominent northeast-trending lineaments (herein referred to as the North and South Farrenburg lineaments), near Farrenburg, Missouri (Figures 2 and 3) (Baldwin et al., 2002). Baldwin et al. (2002) hypothesize that the North and South Farrenburg lineaments were primary tectonic features based on northeast-trending microseismicity, geomorphology, geophysical data, trenching and microtextural analyses. Our current investigation of the Farrenburg lineaments builds upon this initial evaluation and consisted of: (1) acquisition of one shallow seismic reflection profile, (2) three ground penetrating radar surveys; (3) interpretation of a 25-km-long proprietary Dow Chemical Company vibroseis line, (4) excavation of two paleoseismic trenches, (5) drilling and documentation of six boreholes, and (6) analysis of sediment samples for microtextural analysis. This paper presents the results of these latest efforts with respect to the previous studies conducted along the Farrenburg lineaments (Baldwin et al., 2002), and draws conclusions regarding the origin of the Farrenburg lineaments, the geologic characterization of the NMNF, and preliminary event timing information for the northern NMSZ.

1.1 Tectonic and Geologic Setting

The NMSZ lies within the Mississippi embayment, a broad and gentle south-southwest-plunging syncline of Cretaceous and Tertiary age (Stearns, 1957; Stearns and Marcher, 1962; Cox and Van Arsdale, 1997). The northeast-trending Reelfoot rift (Figure 1) initially formed in Late Precambrian and Early Cambrian time during extension of the North American continent (Ervin and McGinnis, 1975; Kane et al., 1981; Hildenbrand et al., 1982; Thomas, 1989, 1991; Johnson et al., 1994; Marshak and Paulsen, 1996; Langenheim and Hildenbrand, 1997). The Reelfoot rift is approximately 300 km long, 70 km wide, and has up to 8 km of structural relief (Nelson and Zhang, 1991). Contouring of the top of the Precambrian section indicates that there may be Late Precambrian and Cambrian basins within the Reelfoot rift (Dart and Swolfs, 1998). Furthermore, these basins may be bounded by northwest-trending faults that have been mapped in the adjacent Ozark plateau (Cox, 1988; Clendenin et al., 1989).

Potentially seismogenic faults in the NMSZ are believed to have originated in Late Precambrian and Early Cambrian time during formation of the Reelfoot rift, and subsequently, have been re-activated in the present-day stress regime (Figure 1). The rift is largely defined by geophysical data (Ervin and McGinness, 1975; Hildenbrand, 1985; Langenheim and Hildenbrand, 1997). Nelson and Zhang (1991) interpreted COCORP seismic reflection lines across the rift, and suggest the presence of steeply-dipping faults and inward-dipping listric normal faults. Other seismic reflection lines (Howe, 1985; Crone et al., 1985), vibroseis lines (Zoback, 1979; Hamilton and Zoback, 1982), a Mississippi River reflection survey (Shedlock and Harding, 1982; Shedlock et al., 1997), Mini-Sosie lines (Sexton and Jones, 1986, 1988; Luzietti et al., 1992; Schweig et al., 1992; Stephenson et al., 1995; Van Arsdale et al., 1995a, 1998; Purser, 1996), and S-wave studies (Woolery et al., 1996) reveal post-Cretaceous faulting on numerous faults in the upper Mississippi embayment. In particular, Mini-Sosie lines image the uppermost crust between depths of 1,200 m and 70 m, and therefore have been obtained to locate areas of shallow deformation. Mini-Sosie surveys have revealed Tertiary and Quaternary faulting within the NMSZ and in particular beneath the Reelfoot scarp (Sexton and Jones, 1986; 1988; Purser, 1996; Van Arsdale et al., 1998), and the Blytheville arch (Stephenson et al., 1995; Van Arsdale et al., 1996).

Plio-Pleistocene Upland Gravels unconformably overlie Eocene rocks in the embayment. During the Pleistocene, the Mississippi River incised through the Upland Gravels and into the Eocene section. Coincident with Pleistocene valley incision was deposition of terrace sediments and loess blankets (Autin et al., 1991). The modern geomorphology of the Mississippi Valley began in the Holocene with the transition of the Mississippi River from a braided glacial outwash river to a meandering river (Autin et al., 1991; Saucier, 1994). The Farrenburg sites lie at the southern end of Sikeston Ridge and are composed of late Wisconsin braided stream terrace deposits of glacial outwash material (Obermeier, 1989).

2.0 FARRENBURG LINEAMENTS

The North and South Farrenburg lineaments are located on Sikeston Ridge, a 3.5- to 10-m-high, north-trending late Pleistocene erosional remnant that extends for 50 km from New Madrid to north of Sikeston, Missouri (Figures 2 and 3)(Baldwin et al., 2000). Sikeston Ridge consists of glacial outwash and braided stream channel deposits that range from 30 to 60 m in thickness (Obermeier, 1989; Baldwin et al., 2002). The lineaments trend northeast and oblique to the predominant south to southeast-flowing Pleistocene paleodrainages mapped on Sikeston Ridge, and the north-south trending ridge margins (Figures 2 and 4) (Baldwin et al., 2001). Based on interpretation of aerial photography, the 3- to 4-km-long, N30°E-trending North Farrenburg lineament is defined by several apparent right-laterally deflected paleodrainages, southeast-facing scarps, linear topographic depressions and tonal contrasts. The 3-km-long, N25°E-trending South Farrenburg lineament is defined at the surface by the presence of possible deflected paleodrainages, southeast-facing scarps, tonal variations, and linear depressions. Regionally the lineaments depict an en echelon left-stepping fracture pattern. Because the lineaments align generally with the northeast-trending band of microseismicity defining the northern arm of the NMSZ and previously inferred locations of the NMNF (Johnston and Schweig, 1996; Obermeier, 1989), we hypothesize that the lineaments represent possible surface rupture on the NMNF (Baldwin et al., 2002).

Re-interpertation of limited borehole data compiled by Obermeier (1989) across the southern part of Sikeston Ridge shows that there is a buried lineament marked by a thickness change of at least 5 m of post-Tertiary alluvial deposits beneath Sikeston Ridge (Figure 3). The thickness change is along a 35- to 40-km-long, N35°E-trending isopach lineament extending from northwest of New Madrid to the northeast across Sikeston Ridge, and onto the Holocene floodplain of the Mississippi River. Near the eastern margin of Sikeston Ridge, the isopach lineament steps left (north) about 5 km and projects to the northeast along a more northeasterly trend to the village of Bertrand (Figure 4). To the southwest, the post-Tertiary isopachs (200 ft contour) appear to merge with a similar northwest-trending isopach, which we interpret as evidence of the Reelfoot fault. We note that the topographic expression of the eastern ridge margin, where the inferred NMNF projects, shows no clear evidence of right-lateral separation (Figure 2). We hypothesize that the absence of distinct displacement at the eastern ridge margin may be because the ridge was modified by placement of levees and earlier historic incision and modification that buried or obscured the tectonic signature associated with repeated surface-fault rupture.

The northeast-trending isopach lineament is aligned, in part, with many other potentially fault-related features, including: (1) the northeast-trending band of contemporary microseismicity (Figure 1), (2) the North and South Farrenburg lineaments, (3) discontinuous northeast-trending lineaments mapped near Lilbourn (Figure 2), (4) aeromagnetic anomalies (Hildenbrand, 1985; Hildenbrand et al., 1992), and (5) Quaternary to Cretaceous deformation interpreted from recently acquired seismic reflection profiles near Farrenburg and along the central axis of Sikeston Ridge (see section 4.0 below). The post-Tertiary isopach lineament also is consistent with structural contours of an Eocene-Quaternary unconformity that upon interpretation also trends northeast near this boundary (Figure 2 of Mihills and Van Arsdale, 1999). In summary, we consider the possibility that thicker Neogene sediments on the northwest side of the isopach lineament may be related to fault displacement coincident with the NMNF, and the intersection with the Reelfoot fault.

3.0 APPROACH AND METHODLOGY

Our approach in evaluating the Farrenburg lineaments and their association with the New Madrid North fault included analysis of aerial photography, seismic reflection profiles, drilling, ground penetrating radar, and paleoseismic trenching, coupled with age dating (radiocarbon and thermoluminescence), and microtextural analysis. Geomorphic lineaments were identified through the interpretation of aerial photography of the study area. Photographs analyzed included 1:40,000-scale U.S. Geological Survey (USGS) infrared photography (1981), and black and white 1:24,000-scale photography (1966) from the U.S. Department of Agriculture. The methods of the various data acquisition techniques are described in Appendix A.

4.0 GEOPHYSICAL SURVEYS

Determining the association between seismicity and surface deformation in the Mississippi River Valley is hindered by the presence of thick, unconsolidated sediments of the Mississippi embayment. It is hypothesized that the upward continuation of basement faults into the near-surface (Tertiary and Quaternary) deposits may be masked by ductile deformation of the soft sediments, or alternatively liquefaction-related deformation that obliterates evidence of surface rupture. To evaluate the connectivity of surficial geomorphic lineaments with deeper underlying structures, such as the inferred NMNF, we evaluated: (1) a 25-km-long vibroseis profile collected in the 1960's by Dow Chemical Company (Figure 3), (2) four shear wave (S-wave) seismic reflection profiles (S-1 to S-4) totaling about 1.6 km in length (Figure 4), and (3) several ground penetrating radar surveys (GPR-1 to GPR-3) (Figure 4). These surveys intersect the lineaments or the projection of lineaments where little geomorphic evidence exists of surface-fault rupture. Collectively, the findings from the geophysical surveys indicate the presence of faults, folds and flexures offsetting the Tertiary-Quaternary boundary (S-1 to S-3), Paleozoic and Cretaceous boundary (M-8) and Pleistocene deposits (GPR-1 and GPR-2) that align, in part, with the (1) Farrenburg lineaments, (2) northern arm of NMSZ seismicity and (3) a northeast-trending post-Tertiary thickness change in alluvium. The findings of each profile are discussed below.

4.1 Vibroseis Line M-8

The 25-km-long Dow Chemical Company vibroseis line M-8 shows relatively strong reflectors that provide information on the presence of deep-seated faults and flexures disrupting the base of the Paleozoic-Cretaceous and Cretaceous-Tertiary boundaries along a north-south transect through the center of Sikeston Ridge (Figure 3). These stratigraphic reflectors in line M-8 correlate with reflectors in published lines and stratigraphic contacts from well log data in the immediate area (Hamilton and Zoback, 1982; Shedlock et al., 1997; Purser and Van Arsdale, 1998; Van Arsdale et al., 1998). Broad south-vergent flexures (A and B) and numerous high-angle faults (C to H) with apparent reverse separation are interpreted from the vibroseis data (Figure 5). From south to north the faults are interpreted from the vibroseis data and project updip near stations VP 420 (C), VP 380 (D), VP 355 (E), VP 340 (F and G), and VP 315 (H) (Figure 5).

The largest reverse displacement is across fault D, which is interpreted as near-vertical and having a down-to-the-north displacement of 0.05 seconds (approximately 50 m). Because fault D is vertical and is the dominant structure in this line, we speculate that fault D may be a transpressive strike-slip fault in the present tectonic regime. The down-to-the-north vertical displacement across the fault agrees well with the Quaternary isopach map that delineates thicker deposits north of fault D. Along an up dip and northeast projection of fault D, parallel to the Farrenburg lineaments, fault D lies less than 2 km north-northwest of the North Farrenburg lineament (Figure 3).

Fault D also closely coincides with the northern margin of the LCU suggesting it may represent a structural boundary between uplift associated with the LCU and oblique strike-slip displacement on the NMNF. As interpreted by Russ (1982), the northern LCU lies close to the hinge of distinct south dipping bedding beginning near fault D (Figure 5). South of fault D to at least flexure A the strata dip southerly as part of a broad antiform, whereas north of fault D, the strata exhibit extensive faulting, short amplitude folds, and only a gentle southerly dip. Interpreted faults A through C that fall within the northern limits of the LCU are interpreted as having south-side down apparent vertical displacement combined with south-dipping strata. A simple southwest projection of the Farrenburg lineaments indicates that faults C and B most closely coincide with the Farrenburg lineaments, respectively; however, fault D lies closely north of the Farrenburg lineaments.

We note that fault A falls within our linear northwest-trending post-Tertiary isopach that is interpreted as the subsurface expression of the Reelfoot fault (Figure 3). Interestingly, directly northwest of fault A, where data is missing along line M-8, it is permissible to interpret southwest-side up vertical displacement across the Cretaceous-Tertiary boundary (Figure 5). This sense of displacement is consistent with the overall sense of displacement on the Reelfoot fault, and that interpreted by Harris and Street (1998) directly southwest of New Madrid along the east-facing banks of Des Cyprie Slough (Figure 2). We believe that the coincidence of these subsurface features is strongly suggestive of the northernmost expression of the Reelfoot fault. This interpretation is further supported by the subtle tectonic-related geomorphology on this part of Sikeston Ridge: (1) topography is higher directly to the southwest of Des Cyprie Slough consistent with hanging wall deformation above a southwest-dipping Reelfoot reverse fault, and (2) Des Cyprie Slough flows anomously northwest presumably up against the scarp of the Reelfoot fault and opposite of the regional southerly gradient. Review of circa 1870's topographic maps show the Des Cyprie Slough as a topographic low, partially submerged, and occupied by bald cypress trees, all of which are consistent with other geomorphic features noted along the Reelfoot scarp (e.g., Reelfoot Lake). Regionally, the northwest projection of the Reelfoot fault between the Kentucky Bend and southwestern Sikeston Ridge also is consistent with our re-interpretation of reconstructed bedrock structure contours of the Paleozoic (Crone and Brockman, 1982; Purser and Van Arsdale, 1998), Cretaceous (Purser and Van Arsdale, 1998), and an Eocene-Quaternary unconformity (Mihills and Van Arsdale, 1999). These studies, delineate a broad, poorly defined linear structure extending northwest across the Mississippi River to New Madrid and the southwestern Sikeston Ridge.

Identifying unequivocal geomorphic evidence indicative of dextral surface-fault of the NMNF rupture directly overlying vibroseis line M-8 is difficult. There are subtle geomorphic expressions on Sikeston Ridge suggestive of regional deformation. Our surficial geologic mapping of Sikeston Ridge (Baldwin et al., 2000), however, identified several Pleistocene paleochannels that exhibit geomorphology suggestive of deflection and changes in gradient as they intersect the northern limits of the LCU and inferred location of the NMNF (Figure 2). This observation agrees well with Russ (1982), who found a shallowing of gradients of paleodrainages on Sikeston Ridge where the paleodrainages encountered the northern limit of the LCU.

Finding distinct geomorphic features right-laterally displaced where faults B-D intersect the ground surface is problematic given the absence of post Cretaceous-Tertiary boundary stratigraphic data from vibroseis line M-8. Thus, we examined stereo-paired aerial photography and existing USGS 7.5-minute topographic maps in an initial attempt to document the surface expression of faults B thru D directly above vibroseis line M-8. For example, we evaluated a broad 1-to 2.5-km-wide southeast-flowing Pleistocene paleochannel that intersects faults B through D (Figure 2). The margin of the paleochannel is defined by an approximately 1.5-to 3-m-high, 60-to 150-m-wide southwest facing topographic escarpment that can be traced from the western margin of Sikeston Ridge to southwest of Farrenburg (Figure 2). Typically, such erosional features provide excellent piercing points from which to assess surface-fault rupture. Yet from the available photography, we only recognize an extensive field of liquefaction-related sand blow deposits and several short discontinuous northeast-trending tonal lineaments northeast and southwest of the paleochannel margin in the area of the up dip intersection of faults B through D. We do not observe distinct geomorphic evidence suggestive of a displaced paleochannel margin. The absence of such evidence may be because: (1) surface-fault rupture occurred northeast of the channel margin in the vicinity of the Farrenburg lineaments, (2) cultural modifications (grading and plowing) across the channel margin(s) have obliterated any geomorphic evidence of displacement, (3) existing USGS 7.5-minute topographic maps lack the elevation control to accurately delineate subtle elevation changes and deflected patterns in the topographic contours across several of the paleochannel margin(s), or (4) the cumulative surface displacement at the southern end of the rupture is so minor that it is unresolvable at the scales of existing USGS maps and photography reviewed during this study. Regardless, the presence of faulting in vibroseis line M-8 that locally aligns with the

Farrenburg lineaments coupled with the suggestion of regional tectonic influence on the Pleistocene geomorphology of Sikeston Ridge, and other interpreted northeast-trending bedrock structures supports our interpretation that the NMNF can be defined in the subsurface both by geophysical and borehole data.

4.2 Seismic Reflection Survey and Ground Penetrating Radar

Vibroseis line M-8 only images bedrock up to the Cretaceous-Tertiary boundary, therefore we collected three high-resolution seismic reflection profiles (S-1 to S-4) to assess the presence or absence of disrupted Tertiary-Quaternary reflectors beneath the North and South Farrenburg lineaments. Profiles S-1 to S-3 intersect the North Farrenburg lineament and S-4 intersects the South Farrenburg lineament (Figure 4). These profiles are located east of vibroseis line M-8.

4.2.1 North Farrenburg Lineament

Seismic reflection lines S-1 to S-3 image disrupted Quaternary reflectors that are faulted, folded and warped across the mapped location of the North Farrenburg lineament (Figure 6). Profile S-1 shows that the basal Quaternary deposit (0.35s) is warped into an antiform between CMP 300 and 400, and possibly faulted between CMP 300 and 350 (Figure 6). The location of the warped reflectors is coincident, in part, with the mapped surface expression of the North Farrenburg lineament. In profile S-2, the upper reflection in the basal Quaternary gravel section between 0.30s and 0.35s shows a pronounced change in dip at CMP 290 that may be from apparent drag folding along the interpreted near-vertical fault (Figure 6). In profile S-3, we interpret disruption at the base of the Quaternary gravels between CMP 310 and 350, slightly east of the mapped photo-lineament (Figure 6). The S-wave reflection data across the North Farrenburg lineament typically image two closely spaced, near-vertical faults similar to our interpretation of aerial photography that identified two closely-spaced northeast-trending photolineaments (Figure 4).

Three ground penetrating radar surveys also were collected at the North Farrenburg site. Two of the GPR surveys (GPR-1 and GPR-2) shadow seismic reflection lines S-1 and S-2, whereas GPR-3 intersects the North Farrenburg lineament 0.6 km northeast of seismic line S-3 (Figure 4). A 290-m-long, east-west oriented transect (GPR-1) located along an unmarked farm road intersects County Road 707 on the east and the North Farrenburg lineament to the west near the central part of the profile. GPR-1 images one primary reflector at a depth of about 3 m from the east near CR707 to station 160 that is relatively horizontal and shows no clear evidence of warping or faulting. West of station 160, the same reflector appears to rise in elevation and merge with a gentle east-facing reflector that is suggestive of a channel margin or an east-facing monocline. Underlying this east-dipping reflector are two moderately distinct reflectors that also dip east, but appear to be faulted and folded along their length (Figure 7). The overall apparent separation across the zone of faulting is down to the east. Minor faults, folds, and a southwest-trending paleochannel exposed in trenches T-1 and T-4 (see section 5.3) align with this interpreted zone of deformation in GPR-1 (Figure 7).

A second GPR survey (GPR-2) was acquired along County Road 707 to reoccupy seismic reflection line S-2 and the inferred zone of faulting interpreted from this profile (Figure 4). The 400-m-long, north-south transect images several distinct reflectors to a depth of about 5 meters. Similar to GPR-1, a broad "u-shaped" feature is imaged between stations 0 and 150, that is strongly suggestive of channel morphology or a broad monocline. Along the southern margin of the inferred paleochannel or monocline are several anomalous, incoherent reflectors that are interpreted as faults (Figure 7). South of station 150 m, the stratigraphy is relatively horizontal. The zone of interpreted faulting in GPR-2 coincides with the mapped location of the North Farrenburg lineament, and poorly constrained faulting interpreted from seismic reflection line S-2.

Additional ground penetrating radar data (GPR-3) were collected about 0.6 km northeast of seismic line S-3 along an unmarked farm road trending east-west across the ridge. GPR-3 line is approximately 800 m long and intersects the northeast projection of the North Farrenburg lineament, a broad zone of liquefaction-related deformation, and extends just beyond the eastern margin of Sikeston Ridge (Figure 4). At least three, and possibly up to four, "u-shaped" features suggestive of channel morphology are imaged between stations 0 and 220. The channels appear to be less than 3 m deep and about 20 to 30 m wide (Figure 8). Near station 225 there is a strong disturbance from an irrigation well. This is the approximate location of the mapped trace of the North Farrenburg lineament. East of the irrigation well to about station 680, there are few shallow (<3 m) reflectors to assess faulting or folding. East of station 680, we interpret another buried paleochannel near the eastern margin of the ridge. Across the ridge margin there are no distinct faults or folds, however the reflectors at the eastern end of the profile become incoherent because of the moderately dense vegetation present at the ridge margin. Where the profile intersects the North Farrenburg lineament, the reflectors are of poor quality and not useful for the assessment of faulting. The most interesting aspect of the profile is the position of paleochannels west of the mapped location of the lineament.

4.2.2 South Farrenburg Lineament

S-wave profile S-4 provides information on the presence or absence of faulting along the northeast-trending South Farrenburg lineament. The seismic reflection line is located about 1.2 km southwest of Farrenburg, MO, and 2.5 km south of profiles S-1 to S-3 (Figure 4). The seismic line begins near an abandoned St. Louis-Southwestern railroad line and extends north along County Road 719 for about 0.56 km. Seismic line S-4 intersects the South Farrenburg lineament at an oblique angle near the central part of the profile.

The processed seismic section (un-interpreted and interpreted) is shown in Figure 9. Coherent reflection energy, primarily in the 0.3 s (Quaternary) to 0.5 s range (Tertiary-Quaternary reflector), is visible along the entire length of the line. Between distance positions 140 and 290 m, a broad 150-m-wide u-shaped reflector is imaged near the base of the Quaternary section. On the basis of channel morphology and apparent truncation of horizontal reflectors, we interpret this feature as a buried Quaternary paleochannel present near the south-central part of the line at a depth between 30 and 50 m. The northern margin of the paleochannel appears to be, in part, controlled by steeply dipping faults. Directly north of the paleochannel, offset reflections between 0.5 and 0.3s, changes in reflection amplitude and coherency, and diffraction patterns suggest the presence of high-angle faults in the subsurface (Figure 9). Fault displacements on the reflection at 0.5 s are interpreted as normal, although shallower displacements near 0.3 s (30 to 40 m below the ground surface) appear to be reverse, suggesting reactivation of older extensional faults in the late Quaternary compressional stress field. We would interpret this as evidence of transpressive deformation responding to the present-day stress field. The position of the paleochannel is conspicuously aligned with the fault, and may have been controlled by fault movement along this interpreted shear zone. In addition, the location of the South Farrenburg lineament appears to coincide with the up dip surface projection of the southernmost interpreted fault. Therefore, the South Farrenburg lineament coincides with interpreted faulting at depth, as well as a buried Quaternary paleochannel. The orientation of the paleochannel is unknown based on the single S-wave profile.

5.0 PALEOSEISMIC INVESTIGATION

We excavated six (T-1 to T-6) paleoseismic trenches totaling 132 lineal meters, and drilled six (B-1 to B-6) cores oblique to the North Farrenburg lineament to determine the origin and age of the lineament, and to collect event timing information (Figure 4). Trenches T-1 to T-4 were excavated west, and trenches T-5 and T-6 were excavated east, respectively, of County Road 707 (Figure 4). All of the trenches, including the borehole transect, obliquely intersect northeast-trending photolineaments associated with the North Farrenburg lineaments. Trenches T-1, T-2 and T-4 are located in a precision-graded field void of the geomorphology previously interpreted from aerial photography, whereas the remainder of the trenches (T-3, T-5 and T-6) occupy land that according to the owners has not been graded, but has been heavily plowed. Despite the cultural disturbance of the pre-existing surficial geomorphology along the North Farrenburg lineament, our aerial reconnaissance (Baldwin et al., 2002) shows that some of the northeast-trending geomorphic features previously interpreted from 1966 and 1981 aerial photography correlate with distinct tonal lineaments traversing northeast across the site and intersect our trenches.

5.1 Near-Surface Stratigraphy

Trenches T-1 to T-6 encountered surficial deposits consisting primarily of late Pleistocene glacial outwash and boverbank and floodplain deposits overlain by discontinuous Holocene alluvial deposits and pedogenic soil horizons. The late Pleistocene deposits consist of well-stratified unconsolidated silt and sand and discontinuous clay lenses. These strata provide superb stratigraphic markers for documenting the presence or absence of surface fault rupture and/or tectonic warping inferred from geophysical and GPR transects crossing the North Farrenburg lineament. For the ease of discussion and correlation purposes, descriptions on the near-surface-stratigraphy of the North Farrenburg site are divided between subsurface explorations conducted east (trenches T-1 to T-4) and west (trenches T-5 to T-6) of New Madrid County Road 707 (CR707) respectively. These trenches evaluate about an 1-km-long section of the North Farrenburg lineament. The logs for trenches T-1 to T-6 are presented in Figures 10 through 15. Detailed descriptions of dike deposits and stratigraphic units encountered in trenches T-5 and T-6 are presented in Appendix B. Soil descriptions for the three soil profiles SP-1 to SP-3 are presented in Appendix C.

5.1.1 Trenches T-1 to T-4 West of County Road 707

Trenches T-1 to T-4 excavated west of CR707 exposed laterally continuous well-bedded fluvial clay, silt and sand (Figure 10 to 13). In addition, two well to moderately developed pedogenic B horizons that formed in the glacial outwash deposits provide key marker units for correlating stratigraphy between trenches T-1 to T-4. The deposits are subdivided into alluvial, liquefaction-related deposits, and soils.

1. Alluvial Deposits

The oldest alluvial deposits encountered west of CR707 include unit A, which consists of well laminated, fine-to coarse-grained sand with lenses of silty clay. These alluvial deposits are unconformably overlain by an interbedded sand (unit B), silty sand and silt (units C and D) that partly comprise a distinct south-flowing paleochannel in trenches T-1 and T-4 that may correlate with a similar “channel-like” feature imaged in GPR-1. Outside of the paleochannel margins, these deposits are relatively flat-lying with the exception of where the deposits encounter zones of faulting, folding and venting. The estimated age of the alluvial deposits in trenches T-1 to T-4 is based on two peat and two charcoal samples that yield C^{14} age ranges from about 34,300 to 38,700 yr B.P (Table 1). The C^{14} age range is slightly greater than the infrared stimulated luminescence (IRSL) age of 28.1 ± 2.5 ka for similar sediment analyzed from trench T-6 (Table 1). The age of these deposits are similar to Saucier’s (1974) age of Sikeston Ridge.

Interestingly, these C^{14} and IRSL ages are older than the late Wisconsin age (isotope stage 2, ca 20 ka) inferred for these deposits from regional geologic and geomorphic relations by Blum et al. (2000). We believe that the relatively close correlation between IRSL and C^{14} ages of sediments exposed at the North Farrenburg site indicate that parts of Sikeston Ridge may be older than currently modeled by Blum et al., (2000). Our age data support Saucier's (1974) model, where the ridge is comprised of late Pleistocene braided stream deposits that likely formed more than 30,000 years ago. The reason for the absence of loess on the ridge is unclear, but the well-preserved (e.g., not buried by loess) fluvial geomorphology of paleodrainages traversing across Sikeston Ridge appears to support the inference that Pleistocene loess is not present in the southern part of Sikeston Ridge.

2. Pedogenic Soil Horizons

A moderately developed Bt horizon, unit Bs, overprints unit B in trenches T-1, T-3 and T-4 (Figures 10 to 13). Unit Bs consists of massive silty fine-grained sand with well-developed pedogenic structure. Unit Bs is unconformably overlain by a laterally discontinuous, massive fine-to medium-grained Pleistocene sand designated unit C that has eroded sections of unit B and unit Bs. Developed within this massive sand is a second pedogenic Bt-horizon, designated unit Cs, that is best expressed in trenches T-1, T-3 and T-4. Unit Cs represents a pedogenic Bt-horizon merging to the west with unit Bs. Overlying unit Cs is a massive grayish-brown to light yellowish-brown Pleistocene silty sand to sandy silt (unit D; Figures 10 to 13). Based on stratigraphic relations (overlying sand blow deposits), soil pedologic features, and age constraints, we interpret the top of unit D as the pre-1811 ground surface or former historical buried soil (unit Ds; present only in trench T-3). A single radiocarbon sample collected from this unit yielded a C^{14} age of 34,660 ± 340 yr BP (Table 1). This age is stratigraphically consistent with sample FBT3-RC-20 collected about 2.5 m below unit D that yielded a C^{14} age of 38,180 ± 250 yr BP. Pedogenic unit Ds, however, is considered to be much younger because it would have been at the ground surface during the 1811-1812 sequence.

3. Liquefaction-Related Deposits

Cross-cutting units A through D are clastic dikes containing grayish-white to white, fine to medium-grained sand (unit E; Figures 10, 12 and 13). At least one sand blow deposit overlies unit Ds and connects downsection with dikes exposed in trench T-3. The dikes range from 0.05 to < 0.5 m wide and contain lignite clasts and rip-up clasts acquired from the "wall-rock" material. Four detrital charcoal samples from the sand blow and dike deposits (unit E) were analyzed. These lab dates display a wide scatter of ages that probably reflect the mixing of charcoal from the underlying Pleistocene source material and younger deposits near the ground surface at the time of venting (Table 1). The radiocarbon results for the liquefaction deposits range from Pleistocene to modern. The two late Pleistocene ages yielded by samples FBT3-RC3 and FBT4-RC1 are interpreted to reflect the age of the liquefied parent material consistent with the late Pleistocene age of the deposits as shown by peat and charcoal samples collected in unit B in trenches T-1, T-3 and T-4 (Table 1) and nearby IRSL analyses of similar alluvial material exposed in trench T-6 (see section 5.1.2). Because of the proximity of unit E sand blow deposits relative to the ground surface, an absence of substantial soil development in units E and F, and the presence of historical debris in unit F, we interpret that the unit E liquefaction deposits formed during the 1811-1812 earthquakes (Table 1).

5.1.2 Trenches T-5 and T-6 East of County Road 707

Trenches T-5 and T-6, located about 0.75 km northeast of trenches T-1 to T-4, exposed a 2-to 3-m-thick section of well-bedded Pleistocene fluvial stratigraphy that is overprinted by a well developed pedogenic (soil) horizon (Figures 14 and 15). The Pleistocene material is cross-cut by clastic dikes, faults and occasionally is unconformably overlain by discontinuous Holocene fluvial material deposited within a narrow 1-to 2-m-wide liquefaction-related swale. The trenches exposed interbedded clay, silt, and fine-grained sand of which we subdivide into at least 15 stratigraphic and pedologic units (see detailed descriptions in Appendix B). The exposed stratigraphic relations and textural characteristics are consistent with a braided glacial outwash origin for the deposits.

Correlation of stratigraphy between trenches T-5 and T-6 is based on the presence of a distinct olive-gray to pinkish clay (unit 3), an iron-oxide-stained silty sand (unit 9), as well as several well-developed pedogenic soil horizons (units 10 to 12). For the purpose and ease of discussion, the stratigraphic and pedologic units exposed in trenches T-5 and T-6 are subdivided into lower and upper alluvium, pedogenic soil horizons, liquefaction-related deposits, and historic plow-zone. Because of the significant separation between trenches T-1 to T-4, and trenches T-5 and T-6, respectively, correlation of stratigraphy is unreliable, and therefore no attempt at stratigraphic correlation is made. However, because of similar stratigraphic positions and pedogenic development between the trenches, pedologic correlations are inferred between all the trenches under the assumption that the landscape of Sikeston Ridge has been relatively stable throughout much of the Holocene epoch.

1. Lower Alluvium

The lower alluvium (unit 1) is exposed near the base of the southeastern end of trenches T-5 and T-6, and is encountered in borings B-1 to B-6 (Figures 14 to 16). The lower alluvium consists of a friable, light brown to reddish brown fine-grained sand with planar laminae and cross-bedded sedimentary structures. On the basis of the boreholes drilled directly to the northeast of trench T-6, the lower alluvium is discontinuous and appears to be interbedded with a massive finer-grained clay and silt deposit, or alternatively is located entirely east of the zone of faulting and liquefaction deformation (Figure 16). Stratigraphic unconformities exposed in trenches T-5 and T-6 show that the lower alluvium is incised into by the upper alluvium (units 2 to 9). We interpret the age of the lower alluvium as Pleistocene based on radiocarbon analyses of charcoal collected from similar glacial outwash deposits in trenches T-1 to T-4, and ISRL dating of unit 9 from the upper alluvium (Table 1).

2. Upper Alluvium

The upper alluvium (units 2 to 9) is exposed nearly continuously throughout trenches T-5 and T-6, except where bedding (units 2 to 6) projects beneath the base of the trenches. The upper alluvium consists of well-bedded material ranging from clay, silt to silty sand and fine-grained sand. The coarse-grained deposits, such as silty sand and fine-grained sand are up to as much as 2 m thick. The fine-grained deposits, such as, clayey silt and clay, often are thin (< 0.6 to 0.2 m) and become laterally diffuse as they grade into slightly coarser clayey silt to the northeast. Typically, the deposits exhibit normal grading with basal contacts noted by fine-grained sand or silty sand that is coarser than overlying material. Rare planar laminations of medium- to fine-grained sand occur randomly throughout the deposits. Cutting vertically across these deposits are thin (<0.5 cm) fractures, many of which are filled with dark brown to gray clay (shown by the abbreviation “vc” on logs of Figures 14 and 15), with a lesser number filled with fine-grained sand (shown by the abbreviation “sd” on Figures 14 and 15). Most of these fractures are interpreted as pedogenic in origin, with a few representing root filled casts and tectonic fractures.

Bedding attitudes from the lower and upper alluvial packages in trenches T-5 and T-6 indicate that the deposits locally strike northeast, and generally dip southeast. The units strike subparallel to the North Farrenburg lineament, and have a shallow to moderate southeast dip in the northwest end of the trenches, and typically flatten or dip gently to the northwest in the southeast end of the trenches. The deposits thin at the northwest end of the trench and thicken to the southeast across the zone of deformation. The age of these deposits are estimated as late Pleistocene on the basis of radiocarbon analyses of charcoal collected from similar glacial outwash deposits observed in trenches T-1 to T-4, and an IRSL date from Unit 9 in trench T-6 (Table 1).

3. Pedogenic Soil Horizons

Several pedogenic soil horizons (units 10 to 12) are recognized in the trench exposures (see Appendices B and C. These pedogenic units (A, A/E, and Bt-soil horizons) overprint and obscure pre-existing bedding of the upper alluvium (Figures 14 and 15). We use: (1) the accumulation of massive dark brown to grayish brown organic material accompanied by granular and platy soil structure to define the former A-horizon; (2) the presence of prominent pedogenic fractures and a grayish white silt with light-colored blotches (skeltans) to define the A/E horizon; and (3) the presence of clay films bridging sand-sized grains and a distinct yellowish-red brown hue and closely spaced fractures to define the Bt-soil horizon. The Bt-soil horizon correlates with unit 10 in trenches T-5 and T-6, and likely parts of both units Bs and Cs in trenches T-1 to T-4 west of CR707. The E-soil horizon (unit 11) consists of a silt that has been leached of iron compounds and thus has a light grayish color. Silty soil tongues of the E horizon penetrate the pedogenic fractures of the Bt-soil horizon giving the clay-rich unit a mottled grayish white to brown appearance. Directly overlying the E-soil horizon is a thin remnant of the A-soil horizon (unit 12) that is characterized by a massive dark brown to grayish brown silty fine-grained sand with granular and platy soil structure. Unit 12 represents the surficial A-soil horizon present during the 1811-1812 earthquake sequence. It is unclear how much of the unit has been removed by grading.

In comparison to the bedding of the upper alluvium, the pedogenic soil horizons are relatively flat, and exhibit minor undulations along the length of the trench exposures. The most prominent undulations of the pedogenic horizons occur in zones of faulting and liquefaction-related deformation. Based on pedogenic characteristics (e.g., hue, texture, clay film development) and depth, we speculate that the soil horizon is at least middle Holocene to possibly as old as early Holocene to late Pleistocene.

4. Liquefaction-Related Units

Cutting vertically across the lower and upper Pleistocene alluvial packages, as well as pedogenic soil horizons, are numerous clastic dikes and sills, some which come close to the present-day ground surface (Figures 14 and 15). The clastic sand dikes are preferentially constrained to a 5-to 7-m-wide zone of near-vertical dikes in trenches T-5 and T-6. At least six distinct dikes are recognized in these trenches. Descriptions of the individual sand dikes are provided in Appendix B, shown graphically on the trench logs, and are described briefly in Table 2. Associated with the sand dikes are liquefaction-related deposits (units 13, 14, 14a, and 14b) that usually overlie and merge downward with the sand dikes. These surficial deposits typically have a bowl-shaped or crater morphology, and are coarser-grained than the surrounding bedded upper alluvium and pedogenic soil horizons. Radiocarbon samples analyzed from the liquefaction deposits yield ages ranging from $\geq$ 45 ka to modern. Unlike the clastic dikes exposed in trenches T-1 to T-4, trenches T-5 and T-6 encounter sand dikes with various stages of soil development that provide stratigraphic evidence for several poorly constrained events: 1811-1812 and possibly several late Holocene events.

5. Historic Plow Zone Deposits

Across the upper part of trenches T-5 and T-6 exists a thin veneer of light-brown silt with very fine-grained sand. The deposit is noted by granular to platy soil structure, rootlets, and a sharp basal contact. The deposit is considered to be a mix of aeolian and plowed Pleistocene glacial outwash deposits.

5.2 Near-Surface Structural Relations

Exploratory trenches (T-1 to T-6) across the North Farrenburg lineament provide direct evidence of tectonic-related surface deformation including: (1) liquefaction-related structures (e.g., clastic dikes and craters), (2) faulting, and (3) folding of Pleistocene-Holocene material. The zone of deformation defined by these features overlies regions suspected of faulting and folding based on interpretation of aerial photography, GPR and seismic reflection profiles acquired across the site. The stratigraphic and structural relations exposed in the trenches provide evidence of tectonic deformation related to the 1811-1812 earthquake sequence, and events from the late Holocene and late Pleistocene. See Appendix D for descriptions of sand dikes and faults.

5.2.1 Liquefaction-Related Structures

Each of the trenches (T-1 to T-6) encountered either a main single clastic dike or a complex zone of clastic dikes that align with the mapped location and trend of the North Farrenburg lineament (table 2; Figure 4). The dikes are vertical to subvertical and cross-cut Pleistocene glacial outwash deposits. In places the dikes reach the ground surface as sand blow dikes with crater-like deposits. The sand dikes are typically about 5 to 15 cm wide, with the largest dike approaching 50 cm in width. Orientations of the liquefaction dikes range from due north to N55°E with a mean dike orientation of approximately N20°E subparallel to parallel to the North Farrenburg lineament (Figure 17a and 17b). The liquefaction-related deposits are overprinted by various stages of soil development which we use to differentiate the relative age of the dikes at the North Farrenburg site. Also, soft sediment deformation of numerous clay and granular deposits is spatially associated with dikes in trenches T-1, T-3, T-4, and T-5 as a result of sand/fluid injection during strong-ground shaking.

5.2.2 Faulting

Faulting was observed in nearly all of the trenches excavated across the North Farrenburg lineament (Table 2). The faulting typically consisted of near-vertical, southwest-dipping faults within a 1- to 2-m-wide zone that exhibited both northwest- and southeast-side-down vertical separation (≤ 0.20 m), and often coincided with the margin of a clastic dike. Faults measured in T-1, T-4, and T-6 strike northeast subparallel to the North Farrenburg lineament, with subvertical dips (>80°) (Figures 17c and 17d), and can be traced to within 1.5 to 0.2 m of the ground surface. Between trenches T-1 to T-4, and T-5 and T-6, the faults exhibit a northward rotation in strike. There also is an upsection variation in fault strike (T-1 [042-061°] that may reflect clockwise rotation of shearing as the rupture encounters the ground surface. We infer that the sense of shearing is consistent with right-lateral displacement. Faulting in trench T-1 consists of a 1-m-wide zone of numerous small steeply east-dipping to near-vertical faults, with the main near-vertical fault characterized by several anastomosing shear planes and possible drag folding of the upper alluvium (Figure 11). In the southwall of trench T-6, faulting can be traced to within 0.2 m of the ground surface, where it appears to offset the base of an A/E-soil horizon (unit 12). The fault zones typically are associated with a complex set of fracture patterns defined by two sets of greyish clay-filled, near-vertical fractures trending northeast and northwest, respectively, that show no offset (Figure 17d). Some of these fractures may be tectonic-related, however, most are probably related to soil forming processes. See Appendix D for detailed descriptions of the fault zones exposed in each trench.

Analysis of fracture and fault orientation data collected from trench T-6 was performed to more precisely define the orientation and structural style of the exposed fault zone. We loosely interpret the sense of shear of faults in trench T-6 as right-lateral based on the measured angles between faults and the two distinctly different sets of fractures. For instance, faults exposed in trench T-6 strike between N7E° and N26E°, and have a mean strike of ~N17E°. In contrast, the north-east trending set of fractures in trench T-6 vary in orientation between N24E° to N58E° with a mean of ~N37E°. We note that the angle between the mean fault orientation (N17°E) and the mean northeast-trending fracture orientation (N37°E) is ~20° (clockwise orientation), consistent with Reidel (R1) shears within a dextral strike-slip fault regime. This is consistent with the anomalous drag folding of the upper alluvium, occasional abrupt changes in stratigraphic thickness across faults and a decrease in vertical displacement down-section (e.g., similar to a flower structure formed along a strike-slip fault) in trench T-1. The absence of apparent displacement across the inferred Reidel shears is unclear, however, because there only is minor displacement across the main fault zone of trench T-6, perhaps the Reidel shears reflect primarily fracturing. We acknowledge that these fractures also may have been formed by pedogenic process, but our preferred interpretation is of tectonic origin based on their proximity to the zone of faulting and folding, and their orientation being consistent with dextral strike-slip deformation. The northwest-striking set of fractures strike between N57°W to N70°W and have a mean strike of N56°W. The angle between the mean fault orientation (N17°E) and the mean northwest-striking fracture orientation (N56W) is ~126°, and is more difficult to interpret under strike-slip conditions. It is likely that the northwest-striking fractures reflect pedogenic development, and are of non-tectonic origin.

5.2.3 Folding

At least two distinct varieties of folding are expressed in the Pleistocene deposits along the trace of the North Farrenburg lineament. One variety of folding includes minor secondary folding of deposits at discrete fault traces (e.g., drag folding in trench T-1). The second type of folding includes relatively broad tilting or warping of deposits into northeast-trending asymmetrical synclines at or near the zone of faulting and/or venting (i.e., trenches T-5 and T-6).

5.2.3.1 Drag Folding

Possible drag folding in trench T-1 occurs along several anastomozing shear planes that extend upward to within 1.5 m of the ground surface. The drag folding appears to be constrained to deposits as much as 2 to 2.5 m below the ground surface (Figure 11). The overlying prominent soil horizon (unit Cs) shows only minor warping across the zone of faulting but is not distinctly faulted. The sense of displacement reflected by the drag folding of the Pleistocene deposits is inconsistent with the observed vertical separation of the same faulted fluvial units across the main shear. We infer from the pattern of folded bedding in trench T-1 that a component of lateral displacement may be accommodated by the fault zone.

5.2.3.2 Broad Folding

Broad synformal folding across the zone of faulting and venting in some of the trenches coincides with the complex pattern and style of deformation inferred from seismic reflection lines S-1 to S-3. On the basis of bedding attitudes across the length of trenches T-5 and T-6, we speculate eastward directed tilting of the Pleistocene glacial outwash deposits. Generally, strike and dip data between these trenches is very similar and characterizes a broad, asymetrical syncline with limb dips as high as 17-24°. Based on the borehole profile northeast of trench T-6, the folding appears to extend along trend to the northeast (Figures 15 and 16). The fold axes of the syncline(s) are approximately symmetrical and trend parallel to the North Farrenburg lineaments (N30°E) and plunge ≤5° to the northeast. Notably the upper part of the upper alluvium, unit 9, appears to thin to the west where the deposits are moderately dipping, and thicken to the east where the deposits flatten. The total vertical separation of the base of the upper alluvium, unit 9, across the zone of deformation unrelated to faulting is ~ 0.7 m (minimum) in trench T-5 and 0.8 m (minimum) in trench T-6. Conversely, the total vertical separation of the base of the pedogenic horizon (unit 10) is 0.05 (or zero since it falls within the limit of resolution) for trench T-5 and 0.4 m (minimum) for trench T-6. The sense of vertical separation across the folds and style of folding is consistent with the interpreted zones of anomalous disruption, warping and faulting interpreted from seismic reflection lines S-1 to S-3, and in particular line S-3 closest to trenches T-5 and T-6 (see Figure 6).

Lastly, a transect of six sediment cores (B-1 to B-6) collected 8 m northeast of trench T-6 and along the projection of the zone of deformation exposed in trenches T-5 and T-6 provide additional subsurface information on the lateral continuity of the northeast-trending zone of warping and broad folding exposed elsewhere at the site (Figure 4). A simplified cross-section developed from interpretation of the six cores demonstrates the existence of inferred faulting, folding, and graben formation along a northeast projection from trench T-6 (Figure 16). The units encountered in the cores are correlated to deposits exposed in trench T-6, with the exception of parts of units B and A that extend beyond the base of the trench T-6. The deposits and pedogenic units encountered in boreholes B-1 to B-6 reflect a component of southeast-down vertical separation (minimum of ≤ 0.7 m using the base of unit 4) across a graben as much as 2 m wide (Figure 16). The sense of displacement and zone of deformation is consistent with the faulting and folding observed in trenches T-5 and T-6. Upsection the graben morphology becomes less distinct across pedogenic units 10 and 11, suggesting that these soil units have undergone less deformation than the underlying Pleistocene glacial outwash deposits, which also is consistent with the trench exposures. We noted the presence of a liquefaction-related sand intrusion in borehole B-1 between 1.3 to 1.45 m in depth within the region of the graben. The pattern, style and location of the inferred zone of deformation from interpretation of the boreholes is correlative with the findings in trench T-6, thus providing additional evidence on the lateral extent of northeast-trending tectonic-related deformation along the North Farrenburg lineament.

6.0 EVENT TIMING INFORMATION

Recognition of several surface deforming events at the North Farrenburg site are based on absolute and relative age dates of vented sand as well as warped stratigraphy, and paleosols. On the basis of stratigraphic and structural relations interpreted from the trenches, we interpret deformation related to: (1) the 1811-1812 sequence, (2) one and possibly several late Holocene events, and (3) one to perhaps two late Pleistocene events.

6.1 Evidence for 1811-1812 Surface Deformation

Trenches T-1 to T-3, and T-5 contain earthquake-induced liquefaction deposits that are likely correlative with the 1811-1812 earthquake sequence (Table 2). Primary depositional and textural characteristics indicative of the 1811-1812 earthquakes include: (1) loose and unconsolidated well sorted sand at or near the present-day ground surface, (2) clean sand burying a pre-existing organic-rich, pedogenic A-horizon (unit Ds of trench T-3) within which cultural items are entrained, and (3) the absence of distinct pedogenic development of near-surface clastic dikes and vented sand. The most compelling evidence for historical (1811-1812) liquefaction-related deformation is present in trenches T-1 to T-3. Please refer to Appendix B for more detailed descriptions of the liquefaction deposits encountered in the trenches. These trenches exposed either sand dikes or sand blow deposits consisting of unconsolidated clean sand at or near the present-day ground surface, with little to no soil development (Figures 10 to 12). The absence of pedogenic features in the liquefaction deposits of trenches T-1 to T-3 indicate that the clastic dikes and sand blow deposits are very young. Trench T-3 also exposed a sand blow deposit (unit E) containing historic cultural debris that buries an organic-rich surficial deposit (unit Ds) interpreted as the former 1811-1812 ground surface. In trench T-2, relatively clean, loose sand deposited within a crater-like feature interpreted as liquefaction-related yielded C^{14} ages consistent with the 1811-1812 earthquake sequence (Table 1). Sand dikes interpreted as 1811-1812 events listed in Table 2, and described in more detail in Appendix B.

Less well constrained evidence suggestive of 1811-1812-related clastic dikes also exists in trench T-5. Dike 2 in trench T-5 consists of two separate deposits near the ground surface: (1) a relatively clean brownish fine-grained sand, and (2) a mixed slightly coarser-grained brown sand with soil development and mixed organics from the A/E-soil horizon. The relatively clean brown sand has a slightly more silt- and clay-rich texture than similar liquefaction-related deposits encountered in trenches T-1 to T-3 that are interpreted as 1811-1812 events. However, because the soil development of this relatively clean fine-grained sand of dike 2 is so weak compared to other liquefaction-related deposits interpreted as pre-1811-1812 events in trenches T-5 and T-6, it is permissible to interpret this particular liquefaction deposit as an 1811-1812 event.

6.2 Evidence for Late Holocene Surface Deformation

Stratigraphic and limited age control from deposits exposed in trenches T-2, T-5 and T-6 provide evidence for one and possible several late Holocene events (Table 2). We differentiate between late Holocene and 1811-1812 events using diagnostic pedogenic criteria that are suggestive of greater age: (1) chemical weathering along dike margins, (2) presence of relatively mature pedogenic textures in the upper part of the sand dikes, and (3) liquefaction-related sand craters or grabens overprinted by soil development processes (e.g., contain a pedogenic organic horizon, accumulation of clay, as well as iron and mangenese oxide staining).

Trenches T-5 and T-6 expose numerous clastic dikes that lack clean, friable sand typical of the 1811-1812 liquefaction deposits observed in trenches T-1 to T-3. The clastic dikes exposed in these trenches are overprinted by weak to moderate pedogenic structure that includes leaching of minerals, iron-oxide staining, weak cementation, and a higher clay content. In particular, dike 2 in trench T-5 contains two different liquefaction deposits: one inferred as an 1811-1812 sand deposit (as discussed above) and a second coarse-grained sand that was injected and mixed with an overlying A/E pedogenic horizon (unit 12a). A charcoal sample (FN-T5S-RC-1) from the liquefaction deposit (unit 14), where it intersects the A/E-soil horizon, yielded a calibrated age of AD 130 to AD 340 (Table 1). On the basis of stratigraphic position, the charcoal likely was derived from the adjacent A/E-soil horizon during injection of the liquefied material. Assuming this age reflects the approximate timing of the event, it overlaps with the estimated age of a prehistoric event occurring in the northern NMSZ at about AD 300 (Tuttle et al., 2002). Clastic dikes 4 and 5 in trench T-5 contain similar stratigraphic and lithologic relations to that of clastic dike 2 and may also be related to this event. Detrital charcoal samples collected from these other dikes and adjacent pedologic units were submitted for analyses, but were too small for AMS analysis. The age of this event remains poorly constrained.

Based on the cross-cutting relationship between sand dikes and overlying crater-like structures that truncate the buried A/E-pedogenic horizon in trenches T-5 and T-6, we interpret a second poorly constrained late Holocene event at the site. Limited radiocarbon age data from the buried liquefaction-related crater-like features (units 14 and 14a) range from about 45,000 yr B.P. to modern (Table 1). The anomalously old ages are considered erroneous based on: (1) IRSL and radiocarbon age data that indicate a Pleistocene age for the underlying glacial outwash deposits, and (2) the presence of weak to moderate pedogenic textures developed in the crater-like deposits suggesting an age likely less than middle Holocene but older than the 1811-1812 events. We believe the approximately 45,000 yr B.P. age yielded by one charcoal sample (FN-T6N-RC-2) reflects reworking of older charcoal into the crater either through entrainment within rapidly ejected sand originating below the base of the trench, or reworking of near-surface Pleistocene material by creeks re-occupying the graben structure. In turn, the modern age yielded by samples from the graben probably reflects younger charcoal being mixed into the subsurface, deposition within the swale by late Holocene intermittent water occupying the northeast-trending swale, and plowing of the ground surface.

Because the anomalous older and younger ages can be dismissed based on stratigraphic relations and pedogenic textures, we consider the ages on the remaining radiocarbon samples to be more representative of the crater's age. A single C^{14} age of cal AD 1210 to AD 1300 (95% probability of calibrated age interval) yielded by a sample (FN-T6S-RC-1) from the crater deposit (unit 14) in trench T-6 suggests that the crater formed prior to AD 1210 to AD 1300, or possibly as early as BC 1220 to BC 970 (FN-T5N-RC-4) from radiocarbon data for a similar crater deposit (unit 14a) encountered in trench T-5 (Table 1). Detailed characterization of liquefaction features in the Upper Mississippi embayment by Tuttle et al. (2002) show that the NMSZ has produced earthquakes sequences similar to the 1811-1812 event on average every 500 years for the past 1,200 years, with hypothetical events occurring around AD 1450, AD 900, and AD 300, and pre BC 400. Based on the radiocarbon samples from the swales, and assuming the swales are correlative, the swale likely formed sometime between BC 1220 and AD 1300, thus overlapping with the three older known northern NMSZ events. These older ages for the crater-like deposits are consistent with the presence of weak-to moderately-developed soil and chemical staining expressed in the crater deposit, as well as occasional clay seams lining the upper margins of the sand dikes, suggesting that the crater-like deposit formed prior to 1811-1812, and likely even before the NMSZ's penultimate event of AD 1450 (Tuttle et al., 2002). We acknowledge these events are poorly constrained. Additional radiocarbon analyses and better stratigraphic relations may help refine these age estimates.

Using the trench T-2 exposure, we also infer a late Holocene event based on the presence of a grayish-brown, slightly organic-rich, silty sand that has been deposited within a graben-like feature. This sand has been buried, and is bounded partly by clean white sand likely derived from the 1811-1812 earthquake sequence. We interpret the organic silty sand as an older liquefaction deposit having undergone minor soil development, and subsequent collapse into a reactivated graben. The age of the organic silty sand is unknown, however the presence of a weak soil horizon with small (1-3 mm in diameter) concretions and 1811-1812 liquefaction related deposits that bury the unit, it is permissible to interpret this deposit as a pre-1811-1812 event. The exact age of the event is unknown, but it is believed to predate the 1811-1812 sequence based on age, pedogenic and stratigraphic relationships. Alternatively, the deposit reflects the base of the former A-horizon and subsequently collapsed into the 1811-1812 graben.

6.3 Evidence for Late Pleistocene Surface Deformation

The trenches also exposed faulted and tilted late Pleistocene stratigraphy that provide evidence for one and possibly two surface-deforming events in the late Pleistocene. In trenches T-5 and T-6, Pleistocene deposits are warped into a southeast-facing monocline (Figures 14 and 15). The late Pleistocene deposits are overprinted by a well-developed soil (units 10 to 12). Pedogenic units 10 and 11 do not exhibit the same amount of warping as the underlying late Pleistocene material. For instance, the total vertical separation of the base of the upper alluvium (unit 9 located below the pedogenic soil horizon), across the zone of deformation, and unrelated to faulting is ~ 0.7 m (minimum) in trench T-5, and 0.8 m in trench T-6. Comparatively, the well developed pedogenic horizon of unit 10 is generally flat-lying along the length of the trench, except where it encounters the zone of younger liquefaction-related deformation and faulting. The total vertical separation of Unit 10 (unrelated to faulting) ranges to as much as 0.4 m (minimum). The decrease in vertical separation upsection between units 9 and 10 indicates that much of the warping preceded pedogenic development of units 10 to 12, which based on pedogenic textures and stratigraphic relations are possibly late Pleistocene to early Holocene in age. The IRSL age date of unit 9 indicates that the folding post dates 28.1 ± 2.5 ka and predates the development of unit 10. The subsequent minor folding of unit 10 likely reflects deformation related to the 1811-1812 and/or other possible Holocene event(s) discussed above. The apparent absence of numerous Holocene liquefaction-related deposits is supported by the minor amount of folding and warping observed in unit 10.

Lastly, the presence of upward fault terminations within unit B in trench T-1 (between stations 7 and 8.5 m; Figure 11) and possibly trench T-3 (between stations 1.5 and 4 m; Figure 12) also provides circumstantial evidence in support of an earlier event. Radiocarbon ages from the Pleistocene deposits faulted in trench T-1 at the depth of fault termination range from about 34,000 to 37,000 yrs B.P. (Figure 11). Alternatively, these ruptures may have formed during the late Holocene and were modified or truncated by liquefaction-related deformation of the glacial outwash material. This may be the case with trench T-3, but it is more difficult to explain with trench T-1.

6.4 Summary

Assuming that the deformation interpreted from the trenches is directly related to the New Madrid North fault, the event timing information, although extremely limited, appears to indicate temporal behavior of the fault. We believe that this is a reasonable assumption given the apparent spatial occurrence of the faulting, folding and venting along the North Farrenburg lineament, and their relationship with underlying deep-seated deformation interpreted from seismic reflection lines S-1 to S-3. From the trench data, we interpret between 3 and 6 earthquakes in the last approximately 30 ka. In summary, late Pleistocene deformation is dominated by broad folding, and generally an absence of faulting and venting. The minor exception of possible late Pleistocene faulting includes shears exposed in trenches T-1 and T-3 that exhibit upward fault terminations. The late Holocene and 1811-1812 events are clearly characterized by faulting and venting, and a minor amount of folding and warping. The minor warping recorded by the pedogenic units overlying zones of faulting and venting also supports the likelihood that only a few surface deforming events occurred in the Holocene at the North Farrenburg site.

7.0 TEXTURAL CHARACTERISTICS

We collected oriented sediment samples from the fault zone, dikes and undeformed sand layers of the trenches at the North Farrenburg site for computer-based image analysis of grain size and orientation with the purpose of assessing microtextural characteristics indicative of coseismic surface-fault rupture (e.g., grain size reduction, preferred grain orientation, and development of shear zones) (Cashman and Cashman, 2000). Sediment samples collected from fault zones exposed in trenches T-1 and T-6 identified distinctive microstructures and grain size distributions suggestive of primary faulting.

7.1 Fault Microtextures

At the microscale, a N42°E-striking, steeply southeast dipping fault exposed in trench T-1 with 5 cm of down to the northwest vertical separation (sample 12, horizontal; Figure 11), shows primary fault-related features. SEM images from a horizontal thin-section of the sediment sample delineate the fault zone as a 1 cm wide band of fine-grained material with low porosity and strong preferred orientation (oblique to the fault zone) of elongate grains (Figure 18). Maximum grain size in the fault zone is 125µm (very fine sand) while most grains of the same faulted unit directly outside of the fault zone are 125 to 250µm in size (fine sand). Within the fault zone is a 1.5 mm wide very fine-grained fault core that is characterized by an anastomosing pattern in which extremely fine-grained zones with very low porosity surround lenses of higher porosity, and more coarse-grained sediment (Figure 18). SEM images from a vertical thin section of an adjacent sample (sample 11) also show a fine-grained fault zone, approximately 1 cm in width, containing grains that are generally smaller than and more closely-packed than those in adjacent sediments. Preferred orientation (steeply dipping, parallel to the fault) of elongate grains also is locally developed in the vertical fault zone sample.

A near-vertical, N03°E-striking fault with < 0.5 cm of vertical offset located at the primary fault zone exposed in trench T-6 also shows fault-related features when viewed at microscale (sample 4-6, horizontal; Figures 15 and 19). Photomicrographs and SEM images from a horizontal thin-section show a well-defined 0.5 mm wide fault zone characterized by significantly lower porosity, smaller grain size than the adjacent country rock, and a preferred grain orientation roughly parallel to the fault zone boundaries (Figure 20). Mean grain size in the fault zone is < 50µm (silt and clay), while most grains in the unit offset by the fault are in the 62-125µm range (very fine sand). Unlike the sample from trench T-1, neither strong preferential grain alignment nor anastomosing shear zone texture is observed on this fault. We hypothesize that the absence of these features may be because this fault records less offset than the fault sampled in trench T-1.

7.2 Sand Dike Microtextures

Microscale texture (e.g. size, shape, orientation, and spatial distribution of grains) in the faults exposed in trenches T-1 and T-6 is distinctly different from that at the margins of sand dikes exposed in the same trenches. Both a 0.15 m wide, vertical sand dike in trench T-1 and the silty sand it intrudes have relatively loosely-packed sand grains (high porosity), larger grain sizes (most grains 125-500µm, fine to medium sand), and no preferred grain orientation, except in locally-developed bands of closely packed grains near the dike margin (sample 17, vertical; Figure 21). A 0.2 m wide sand dike in trench T-6 displays similar high porosity, 125-500µm grain size, and lack of preferred grain orientation to that of the sand dike in T-1 (Figures 22 and 23). These observations of texture in New Madrid sand dikes are consistent with those of similar sediment samples collected along sand dikes and secondary non-seismogenic faults formed during the 1906 San Francisco earthquake (Thompson and Witter, 2004).

Although some sand dikes appear to intrude faults at the North Farrenburg site, microscale texture of the fault sediments is distinctly different from that of sand dikes.

7.3 Style of Deformation

Intergranular textures observed in SEM images of oriented samples from the faults described above provide insight into the processes that operated during faulting at the North Farrenburg site. Larger sand grains in proximity to the fault zone, and many of those preserved within the fine-grained material of the fault zone, display pervasive grain cracking. The abrupt grain size reduction that characterizes the fault zones of trenches T-1 and T-6 therefore appears to be the result of grain breakage (Figure 24). In addition, sand and silt grains in the fault zone of trench T-1 show stronger preferred orientation than do those outside of the fault zone. The dominant orientation of grain long axes from a vertical thin-section (sample 11) across the fault in trench T-1 is vertical, while in a horizontal thin-section (sample 12) the strongest concentration of grain long axes extends from fault-parallel to 50° counterclockwise from the fault (Figure 25). This pattern suggests that grain rotation played a role in development of the fault. In addition, preferred grain orientations in the horizontal sample from trench T-1 suggest that rotation in the horizontal plane accompanied right-lateral shear. The primary process in formation of the fault zone appears to have been cataclasis (i.e., the fracturing and rotation of grains) within the unconsolidated fluvial sediments. Similar cataclastic textures have been observed by faulting in unconsolidated sediment offset by the active McKinleyville fault in northern California (Cashman and Cashman, 2000). Both the microstructural similarities between samples from the North Farrenburg lineament and those of the McKinleyville fault, and the contrast between microscale characteristics of fault zones and those of sand dike contacts provide petrographic evidence for primary faulting on the North Farrenburg lineament. Although the analysis of textures of sediment at the North Farrenburg site is preliminary and additional evaluation of thin-sections is forthcoming, this technique appears to be a powerful tool for differentiating primary faulting from secondary (non-seismogenic) faulting.

8.0 DISCUSSION

In this comprehensive geologic characterization of potentially active seismogenic structures underlying southern Sikeston Ridge, we assessed two northeast-trending photo-lineaments (North and South Farrenburg lineaments) preserved in Pleistocene braided stream deposits with respect to their origin and relation to the dextral strike-slip New Madrid North fault. It is difficult to differentiate the origin of the northeast-trending Farrenburg lineaments as secondary (e.g., liquefaction-related) or primary (co-seismic surface fault rupture) tectonic deformation based entirely on trench exposures. However our compilation of geologic, geophysical, paleoseismic and microtextural data indicate that the Farrenburg lineaments, in particular the North Farrenburg lineament, most likely represent northeast-trending clastic dikes, faults and folds that formed during strong ground shaking from New Madrid-like events, and primary (coseismic) surface fault rupture on a northeast-striking, dextral strike-slip fault. We believe that the causative fault is the New Madrid North fault. Below, we present two alternative models to explain the origin of the Farrenburg lineaments: (1) settlement related to liquefaction, or (2) primary surface-fault rupture.

8.1 Model 1: Liquefaction-Related Deformation

As is well documented in published literature and review of aerial photography, fissuring produced by the 1811-1812 earthquakes was a common and widespread phenomena in the New Madrid region (Lyell, 1849; Fuller, 1912; Obermeier, 1989). For instance, Fuller (1912) describes fissures forming in regions of extensive sand-blow development as having an average trend of about N30°E, similar to the Farrenburg lineaments. However, fissures with these northeast-trending orientations appear to be observations made along low-lying stream courses and not from the surrounding elevated ridges. Fuller (1912) further describes the distribution of fissures in the upland as *"limited to the vicinity of the edges of steep bluffs and are not seen where the surface is flat* (e.g., Sikeston Ridge) *or the slopes gentle."* Obermeier et al. (1992) also demonstrate that fissure patterns in the NMSZ, as well as the Wabash fault zone, tend to be strongly controlled by the local geologic setting. For example, earthquake-related fissures have a tendency to form along the tops and be parallel to the scrolls of point-par deposits, and tend to parallel stream channels (Obermeier et al., 1992). Based on our geomorphic mapping, the majority of paleodrainages flow south to southeast on Sikeston Ridge, or oblique to the northeast trend of the Farrenburg lineaments. In addition, most of the liquefaction phenomena mapped in the southern part of Sikeston Ridge (Baldwin et al, 2001) consist of sand blows of considerable size and variable dimensions, and usually do not form lineaments similar to the Farrenburg lineaments, or along a northeast orientation. Except for the Farrenburg lineaments few, if any, of the N30°E-trending lineaments described by Fuller (1912) are visible from the interpretation of aerial photography suggesting that the northeast-trending fissures observed by Fuller (1912) must have been localized features not associated with Sikeston Ridge.

We acknowledge that much of the faulting and folding exposed in the trenches also can be explained by secondary deformation related to liquefaction (e.g., settlement). Similar secondary faulting and folding has been documented in trenches related to the great 1906 San Francisco earthquake (Thompson and Witter, 2004) and the 1994 Northridge earthquake (Hecker et al., 1995). Microtextural data of the fault zone and clastic dikes at the Farrenburg lineament indicate two distinct styles of deformation. The fault zone samples indicate that the faulted sediments exhibit grain size reduction through grain breakage, a decrease in porosity, alignment of sand grains parallel to the orientation of the faulting, and a pattern of grain alignment suggestive of dextral displacement. Conversely, sediments associated with sand dikes show no grain size reduction or loss of porosity and no evidence of aligned sand grains parallel to the clastic dike wall. Furthermore, evaluation of faulted Holocene fluvial sediments displaced by liquefaction-related lateral spread during the 1906 earthquake exhibit microtextural characteristics similar to the microtextures observed along the Farrenburg clastic dikes. Collectively, these data suggest deformation of sand grains along faults and dikes forms distinct patterns and textures.

We believe that the microtextural characteristics of the faulted sediments at the North Farrenburg site are best explained by coseismic surface-fault rupture. Therefore, it is not unreasonable to interpret the faults and folds exposed in the trenches as related to primary tectonic surface deformation related to faulting. We acknowledge that some of the deformation documented along the Farrenburg lineaments is related to strong-ground shaking, however, because of the apparent connection between underlying deeper faults imaged in geophysical profiles, geomorphic mapping and the microtextural data that the Farrenburg lineaments most likely represent the surface expression of a northeast-trending tectonic structure rather than a 3 to 4 km long settlement fracture (see below).

8.2 Model 2: Coseismic Surface-Fault Rupture Deformation

One of the most obvious observations to be made regarding the connectivity of the Farrenburg lineaments to an underlying seismic source is their alignment with contemporary microseismicity interpreted as the NMNF, or the northern arm of the NMSZ. Similarly, previous geomorphic and paleoseismic studies performed within the NMSZ, such as within the Tiptonville Dome of the Lake County uplift (Russ, 1982; Kelson et al., 1992, 1996; Van Arsdale et al., 1995a), Manila high and Big Lake "sunklands" (Guccione et al., 2000), indicate that contemporary NMSZ microseismicity coincides with geomorphic landforms (e.g., Tiptonville Dome, Ridgely Ridge, Blytheville arch; and, in part, the Bootheel lineament) and seismogenic structures at depth such as the active Reelfoot fault (Chiu et al., 1992; Schweig et al., 1992a and 1992b; Van Arsdale et al., 1995b; Odum et al., 1998; Mueller et al., 2001). Our geophysical surveys identified several deep to shallow complex structures associated with faulting, folding and warping coincident, in part, with the northern arm of NMSZ seismicity and the Farrenburg lineaments. We interpret this as subsurface evidence of potential seismogenic sources directly beneath the lineaments. We identified at least three faults (faults B thru D) in vibroseis line M-8 that may represent the subsurface expression of the New Madrid North fault, and one fault (fault A) representing the possible northwestern extension of the Reelfoot fault. By default, fault D with the greatest amount of apparent vertical displacement (about 50 m of down-to-the-north separation) of Paleozoic-Cretaceous and Cretaceous-Tertiary reflectors is the strongest candidate for the New Madrid North fault. In addition, a simple projection of fault D about 0.5 km to the southwest shows that fault D aligns with a zone of complex Quaternary faulting and folding (displaying west-side down separation consistent with line M-8) previously interpreted by Sexton (1992) in seismic reflection line K-2 (Figure 2). If these features are correlative, then seismic line K-2 indicates that the zone of deformation associated with the New Madrid North fault is complex and possibly up to 500-m-wide. We also note that fault D partly aligns with the distinct linear change in thickness of the Quaternary deposits underlying Sikeston Ridge, and poorly defined northeast-trending bedrock structural contours (Crone and Brockman, 1982; Purser and Van Arsdale, 1998; Milleps and Van Arsdale, 1999) all of which collectively suggest a strong spatial association. Furthermore, high-resolution seismic-reflection profiles (S-1 to S-4) image disrupted Quaternary reflectors beneath the Farrenburg lineaments. Although the orientation of the faults interpreted from line M-8 are unknown, we believe that based on deformation imaged in seismic line K-2 (Sexton, 1992) and the presence of northeast-trending bedrock structural lineaments, that it is reasonable to assume that faults B thru D strike northeast across Sikeston Ridge, and roughly align with the faulting interpreted from seismic reflection lines S-1 to S-4.

Our geomorphic mapping and shallow subsurface exploration of northeast-trending photolineaments using ground penetrating radar, trenching and drilling techniques define the North Farrenburg lineament as a 3-to 4-km-long zone of northeast-oriented clastic dikes, faults and folds that deform late Pleistocene glacial outwash material. The zone of deformation is oriented subparallel to parallel to the overall trend of contemporary microseismicity, and northeast-trending structures inferred from bedrock contouring.

The presence of porosity loss, grain-size reduction, grain rotation and anastomosing shear bands developed in the poorly consolidated glacial outwash sediment exposed in trenches at the North Farrenburg site is consistent with similar fault-developed textures observed in unconsolidated late Pleistocene marine sand deformed by the McKinleyville fault (Cashman and Cashman, 2000). Crude kinematic indicators interpreted from trenches T-1 and T-6, and the alignment of sand grains in trench T-1 suggest that the faults exposed at the North Farrenburg site have accommodated right-lateral co-seismic displacement. We strongly believe that when all of the subsurface and surficial evidence of deformation is evaluated, that for at least the well-studied North Farrenburg lineaments, these geomorphic features represent the surficial expression of coseismic rupture on the New Madrid North fault.

9.0 SUMMARY

This paper presents the findings of a geologic characterization of the inferred New Madrid North fault, and its possible tectonic correlation to the North and South Farrenburg lineaments. We believe that the combined geophysical and bedrock structural data support our interpretation of a northeast-trending bedrock structure beneath Sikeston Ridge that is coincident with contemporary northeast-trending microseismicty. We infer that this bedrock structure, which also is expressed as a linear, northeast-trending thickness (5 m) change in post-Tertiary deposits, delineates the location of the New Madrid North fault. In turn, these features generally coincide with the northeast-trending Farrenburg lineaments preserved in late Pleistocene braided stream deposits comprising the southern part of Sikeston Ridge. High-resolution seismic reflection surveys indicate that the North and South Farrenburg lineaments are associated with faulting, folding and warping of Quaternary reflectors. Our surficial geologic mapping and trenching of the lineaments also show that they are associated with tectonic geomorphology, near-surface faults, folds and liquefaction sand dikes. Interestingly, textural analysis of sediment samples from the fault zones exposed in trenches T-1 and T-6 exhibit microtextural characteristics (cataclasis, anastomosing shear bands, porosity loss and preferred orientation of grains) typical of textures associated with fault zones. Preferred grain orientations from samples collected from the fault zone of trench T-1 are consistent with a component of dextral shear on the fault. Similarly, analyses of fracture and fault information collected from trench T-6 supports our conclusion that the deformation observed in the trenches is compatible with dextral shear. We conclude from the preponderance of geomorphic, geophysical, structural and stratigraphic evidence that the Farrenburg lineaments, especially the North Farrenburg lineaments, are of primary tectonic origin, and reflect late Holocene and historic deformation on the NMNF.

Previous paleoseismic searches for evidence of neotectonic deformation related to the New Madrid seismic zone have focused primarily on anomalous elevated topography within the Mississippi embayment, such as the Tiptonville Dome, Blytheville arch, Lake County uplift, Manila high and Big Lake "sunklands". These studies have been relatively successful in providing information on the timing and rate of activity and regional deformation. With the exception of detailed paleoseismic studies of the Reelfoot fault, however, many of these studies provide little evidence on the surface trace of the fault(s) believed to be responsible for the 1811-1812 earthquakes. The absence of surface expression of coseismic surface-fault rupture is probably the result of one or more processes: (1) obliteration of the surface rupture by extensive liquefaction, (2) inability of the rupture to propagate through poorly consolidated saturated sediments (Woolery et al., 1997), (3) burial of the rupture by thick quantities of late Holocene flood plain material, or (4) removal of the surficial evidence by fluvial erosion. The North Farrenburg lineament and its alignment with 1811-1812 venting, closely associated near-surface faulting and folding, and linkage with deeper bedrock faults, appears to be the rare case in which evidence of the 1811-1812 surface rupture is preserved in an older elevated topographic surface.

If, as we believe, the Farrenburg lineaments represent the surface expression of coseismic rupture, then these features may provide direct stratigraphic information on the timing of previous events on the NMNF. The event timing information, although extremely limited and poorly constrained, appears to indicate temporal behavior of the New Madrid North fault. For instance, late Pleistocene deformation is dominated by broad folding, and generally an absence of faulting and venting, with perhaps the minor exception of faulting in trenches T-1 and T-3 that exhibit upward fault terminations. Pedologic horizons (units Bs and Cs, and units 10 to 12) estimated to be possibly late Pleistocene to early Holocene in age, but at least middle Holocene in age, show minor deformation across the primary zone of faulting and folding. Based on the apparent minor deformation of the pedogenic horizons and the comparatively smaller degree of pedogenic development of the dikes and faults cross-cutting pedogenic units Bs, Cs, 10 and 12, we interpret that the deformation occurred relatively recently (i.e., late Holocene), and may be from a few surface-deforming events on the NMNF. These late Holocene and 1811-1812 events are clearly characterized by faulting and venting, and a lesser amount of folding and warping. Little is known about the timing of events on the South Farrenburg lineament, therefore the South Farrenburg lineament, if fault related, could be accommodating some of the strain associated with the NMNF.

In summary, this investigation provides an initial geologic characterization of the poorly understood New Madrid North fault. On the basis of the findings of this study, the New Madrid North fault exhibits the following characteristics:

- Based on post-Tertiary isopachs, an Eocene/Quaternary unconformity, and the linear nature of the deeper bedrock structures, the New Madrid North fault merges with the Reelfoot fault about 5 to 8 km northwest of New Madrid, Missouri. This is supported, in part, by the geophysical data of vibroseis line M-8 and Harris and Street (1998), as well as possible subtle tectonic-related geomorphology along Des Cyprie Slough.

- Aligns with a northeast-trending subsurface escarpment defined as an Eocene/Quaternary unconformity, and linear Paleozoic and Cretaceous bedrock structures underlying Sikeston Ridge. The Eocene/Quaternary unconformity can be traced laterally about 12 km from northwest of New Madrid to the eastern margin of Sikeston Ridge, where it steps left and aligns with another weak northeast-trending bedrock structure (Figure 2 of Mihills and Van Arsdale, 1999). The left-stepping nature of the subsurface expression of the fault, also may be expressed geomorphically by the left-stepping pattern of fracturing between the North and South Farrenburg lineaments.

- Re-interpretation of post-Tertiary isopachs (Obermeier, 1989) across southern Sikeston Ridge indicate that there is a linear change in thickness (about 5 m) defined by a northeast-trending lineament that coincides with the Eocene/Quaternary unconformity and fault(s) imaged in vibroseis data (M-8). The Quaternary deposits are thicker on the northwest side of the lineament than on the southeast side suggesting a vertical component across the fault zone.

- Based on the trench exposures, surface-fault rupture is discontinuous, but the geomorphic surficial expression of the fault is delineated by the alignment of one or all of the following: laterally continuous sand dikes, folding and warping, and near-surface faulting.

- Assuming that the deformation observed along various trenches excavated at the North Farrenburg site is directly related to faulting at depth, and is unrelated to another unidentified nearby seismogenic source, the deformational history of the New Madrid North fault appears to be episodic: pedogenic units and liquefaction-related deposits suggest relatively recent late Holocene activity and little deformation during the early and middle Holocene, preceded by Pleistocene deformation in the form of folding and possible faulting.

10.0 ACKNOWLEDGEMENTS

This research was supported by the U.S. Geological Survey's National Earthquake Hazard Reduction Program, under Award #99-HQGR-0096 and #02-HQGR-0024. The views and conclusions contained in this document are those of the authors and should not be interpreted as necessarily representing the official policies, either expressed or implied, of the U.S. Government. Additional support for this study was provided by the Professional Development Program of William Lettis & Associates, Inc. We are thankful to those people who made this project possible, including K. Cashman who provided SEM images and helpful discussion of sample textures. Dan Childress and members of the Dexter U.S. Department of Agriculture provided use of the Giddings rig and helped describe the soils encountered in the trenches and cores at the site. We are indebted to the Ling and Wescoat families who kindly allowed us the opportunity to conduct this investigation on their properties. Larry Hamilton excavated and backfilled the trenches with expertise. Jim Farrenburg and Tom Bradley also provided much needed local landowner information and helped with access. The Brotherton's of New Madrid put up with our gear, late nights of work, as well as providing a fine room and board.

Table 1. Results of Radiocarbon Analyses, North Farrenburg Site, Farrenburg, Missouri

Unit	Trench	Sample	Lab Number (Beta)	Sample Material	Conventional Radiocarbon age ± 1σ (yr BP)[a]	$13_c/12_c$ (%)[b]	Calibrated Age[c] (calibrated 2σ) (yrBP)	Probability Distriuction (95%) Probability of Calibrated Age Interval	IRSL Age of Unit (Ka)[d]	Interpreted Age of Unit
West of County Road 707										
Unit E	T-2	FB-T2-RC1	151038	Charred material	200±40	26.4	AD1640-AD1700	0.27		
							AD1720-AD1810	0.54		
							AD1830-AD1880	0.05		
							AD1920-AD1950	0.15		
	T-2	FB-T2-RC7	151039	Charred material	160±40	25.4	AD1660-AD1710	0.18		
							AD1720-AD1890	0.65		
							AD1910-AD-1950	0.18		
	T-3	FB-T3-RC3	151030	Charred material	(41,570±320)	25.1				
	T-4	FB-T4-RC1	151043	Charred material	(31,190±230)	22.7				1811-1812 deposit
Unit Ds	T-3	FB-T3-RC14	151041	Charred material	(34,660±340)	22.3				Pleistocene-Holocene soil
Unit B	T-1	FB-T1-RC4	151035	Charred material	(510±40)	25	AD1330-AD1450			
	T-1	FB-T1-RC6N	151036	peat	34,730±240	26.2	-	-		
	T-1	FB-T1-RC8N	151037	peat	36,710±270	25.1	-	-		
	T-3	FB-T3-RC20	151042	Charred material	38,180±520	26.3	-	-		
	T-4	FB-T4-RC8	151044	Charred material	(320±40)	29.5	AD1460-AD1660			Pleistocene
East of County Road 707										
Unit 14-Dike 2	T-5	FN-T5S-RC1	192072	Charred material	1780±40	23.7	AD130-AD340	0.98		
							AD350-AD360	0.004		
							AD370-AD380	0.017		AD130-AD340
Unit 14-Crater	T-6	FN-T6S-RC1	192075	Charred material	760±40	25.2	AD1190-AD1200	0.005		
							AD1210-AD1300	0.995		AD1210-AD1300
Unit 14-Crater	T-6	FN-T6N-RC2	192074	Charred material	(>45,320)	24.8				
Unit 14a-Crater	T-5	FN-T5N-RC1	192070	Charred material	110±40	25.0	AD1680-AD1760	0.34		
							AD1770-AD1780	0.01		
							AD1800-AD1940	0.63		
							AD1950-AD1955	0.03		
Unit 14a-Crater	T-5	FN-T5N-RC4	192963	Charred material	2900±50	27.2	BC1260-BC1230	0.04		
							BC1220-BC970	0.91		
							BC960-BC930	0.05		late Holocene
Unit 10-Soil	T-6	FN-T6S-RC6	192077	Charred material	(1870±40)	29.1	AD30-AD40	0.003		
							AD60-AD240	0.997		Pleistocene
Unit 9-Sediment	T-6	FN-T6S-TL2	UIC1433	Sediment					28.1±2.5	Pleistocene

a) Reported ages are corrected for \d13C and include a laboratory error multiplier of 1.0 in reported laboratory uncertainty; samples analyzed by Beta Analytic, Inc.
(radiocarbon years before present; "present"=1950AD)
b) Read -25 as value of 25% measured for 13C/12C ratio.
c) Calibrated using Stuiver and Reimer (2000)
d) Sample analyzed by Steve Forman of University of Chicago. IRSL = infrared stimulated luminescence.
( ) parenthesis refer to incositent ages relative to C^{14} data and stratigraphy.

Table 2. Liquefaction-related dikes associated with the North Farrenburg lineament, Farrenburg, Missouri

Trench Designation	Dike Designation	Orientation	Width (cm)	Associated with Surficial Deposit	Associated with Faulting (>0.05m)	Pedogenic Indicators	1811-1812 Event	Pre 1811-1812 Event
T-1	Dike 1	N19°E	5-10	Y-c, t	Y	N	Y	N
	Dike 2	N55°E	10-15	N-c, t	Y	N	Y	N
T-2	Dike 1	NE (approximate)	5-15	Y-f; c	Y	W	Y	Y
T-3	Dike 1	N37°E	5-50	Y-b	N	N	Y	N
	Dike 2	N23°E	5-10	P-b	N	N	P	N
T-4	Dike 1	N30°-33°E	5-15	N	Y	N	P	N
T-5	Dike 1	N10° to 45°W	5-15	N-t	N	W	N	P
	Dike 2	N16°E	5	Y-s; c	N	W	P	Y
	Dike 3	N	5	P-b	N	W	N	Y
	Dike 4	N25°E	5-15	Y-b; c	N	M	N	Y
	Dike 5	N	5-10	Y-f	N	W	N	Unknown
	Dike 6	NE (approximate)	5-10	Y-f	N	W	N	Y
T-6	Dike 1	N25°-30°E	5	Y-s; c	N	M	P	P
	Dike 2	N25°-30°E	1-12	N	N	-	N	P
	Dike 3	N7° to 20°E	30	Y-c; s	Y	M	N	Y
	Dike 4	N16°E	5-10	N	Y	W-M	N	Y

Y - yes
N - no
P - possible

b - blow
c - crater
s - swale
t - truncated (Ap – horizon)
f - fissure

W - weak
M - moderate

11.0 REFERENCES

Autin, W.J., Burns, S.F., Miller, B.J., Saucier, R.T., and Snead, J.I., 1991, Quaternary geology of the Lower Mississippi Valley, *in* Morrison, R.B., ed., Vol. K-2, Quaternary nonglacial geology: Conterminous U.S., Geological Society of America, Boulder, CO, p. 547-582.

Bakun, W.H. and Hopper, M.G., 2004, Historical seismic activity in the central United States: Seismological Research Letters, v. 75, n. 5, p. 564-574.

Baldwin, J.N., Barron, A.D., and Kelson, K.I., 2000, The origin and paleoseismic history of Sikeston Ridge, New Madrid seismic zone, Missouri: U.S. Geological Survey National Earthquake Hazard Reduction Program Final Technical Report, dated May 30, 2000, 36 p.

Baldwin, J.N., Barron, A.D., and Kelson, K.I., 2001, Sikeston Ridge: Pleistocene erosional remnant or Quaternary fault-bounded block within the New Madrid seismic Zone?[abs]: North-Central Geological Society of America Abstract and Programs, North-Central Section (35th) Annual Meeting (April 23 to 25, 2001).

Baldwin, J.N., Barron, A.D., and Kelson, K.I., Harris, J.B., and Cashman, S.M., 2002, Preliminary paleoseismic and geophysical investigation of the North Farrenburg lineament, Farrenburg, Missouri: Deformation associated with the New Madrid North fault?: Seismological Research Letters-Eastern Section, v. 73, n. 3, p-393-413.

Berman, S.A., 2000, An integrated high-resolution P- and SH-wave seismic reflection investigation of neotectonic deformation of Sikeston Ridge in the New Madrid seismic zone: Lexington, University of Kentucky, M.S. thesis dated August 7, 2000, 77 p.

Berman, S., Street, R., McDowell, S., and Harris, J., 2000, Results of a seismic and GPR investigation over Sikeston Ridge near New Madrid, Missouri [abs]: Seismological Research Letters, v. 71, n. 1, p. 115.

Blum, M.D., Guccione, M.J., Wysocki, D.A., Robnett, P.C., and Rutledge, E.M., 2000, Late Pleistocene evolution of the lower Mississippi River valley, southern Missouri to Arkansas: Geological Society of America Bulletin, v. 112, n. 2, p. 221-235.

Cashman, S. and Cashman, K., 2000, Cataclasis and deformation-band formation in unconsolidated marine terrace sand, Humboldt County, California: Geology, v. 28, n. 2, p. 111-114.

Chiu, J.M., Johnston, A.C., and Yang, Y.T., 1992, Imaging the active faults of the central New Madrid seismic zone using PANDA array data: Seismological Research Letters, v. 63, p. 375-393.

Clendenin, C.W., Niewendorp, C.A., and Lowell, G.R., 1989, Reinterpretation of faulting in southeast Missouri: Geology, v. 17, n. 3. p. 217-220.

Cox, R.T., 1988, Evidence of late Cenozoic activity along the Bolivar-Mansfield tectonic zone, midcontinent, USA: The Compass, v. 65, p. 207-213.

Cox, R.T., and Van Arsdale, R.B., 1997, Hotspot origin of the Mississippi embayment and its possible impact on contemporary seismicity: Engineering Geology, v. 46 (3/4), p. 5-12.

Crone, A.J., and Brockman, 1982, Configuration and deformation of the Paleozoic bedrock surface in the New Madrid seismic zone, *in* A. McKeown and L.C. Pakiser, eds., Investigations of the New Madrid, Missouri, Earthquake Region, F: U.S. Geological Survey Professional Paper 1236, p. 113-135.

Crone, A.J., McKeown, F.A., Harding, S.T., Hamilton, R.M., Russ, D.P., and Zoback, M.D., 1985, Structure of the New Madrid seismic zone in southeastern Missouri and northeastern Arkansas: Geology, v. 13, p. 547-550.

Dart, R.L., and Swolfs, H.S., 1998, Contour mapping of relic structures in the Precambrian basement of the Reelfoot rift, North American mid-continent: Tectonics, v. 17, n. 2, p. 235-249.

Ervin, C.P., and McGinnis, L.D., 1975, Reelfoot rift-reactivated precursor to the Mississippi Embayment: Bulletin of Geological Society of America, v. 86, p. 1287-1295.

Fuller, M.L., 1912, The New Madrid earthquake: U.S. Geological Survey Bulletin 494, 119 p.

Guccione, M.J., Van Arsdale, R.B., and Hehr, L.H., 2000, Origin and age of the Manila high and associated Big Lake "sunklands" in the New Madrid seismic zone, northeastern Arkansas: Geological Society of America Bulletin, 112, p. 579-590.

Hamilton, R.M., and Zoback, M.D., 1982, Tectonic features of the New Madrid seismic zone from seismic-reflection profiles, *in* F.A. McKeown and L.C. Pakiser, eds., Investigations of the New Madrid, Missouri, Earthquake Region: U.S. Geological Survey Professional Paper 1236-F, p. 55-82.

Harris J.B., 1996, Shear-wave splitting in Quaternary sediments: Neotectonic implications in the central New Madrid seismic zone: Geophysics, v. 61, p. 1871-1882.

Harris, J.B., and Street, R.L., 1998, Shallow seismic reflection investigations of neotectonic activity of the Lower Mississippi Valley: Annual meeting of the 1998 Society of Exploration Geophysicists, New Orleans meeting, September 13-18, 1998.

Hecker, S., Ponti, D.J., Garvin, C.D., and Hamilton, J.C., 1995, Characteristics and Origin of Ground Deformation Produced in Granada Hills and Mission Hills During the January 17, 1994 Northridge, California, Earthquake in Woods, Mary C. and Seiple, W. Ray, eds., The Northridge, California, Earthquake of 17 January 1994: California Department of Conservation, Division of Mines and Geology Special Publication 116, p. 111-131.

Hildenbrand, T.G., 1985, Rift structure of the northern Mississippi Embayment from the analysis of gravity and magnetic data: Journal Geophysical Research, v. 90, p. 12,607-12,622.

Hildenbrand, T.G., Kane, M.F., and Hendricks, J.D., 1982, Magnetic basement in the upper Mississippi embayment region - A preliminary report, *in* F.A. McKeown and L.C. Pakiser, eds., Investigations of the New Madrid, Missouri, earthquake region: U.S. Geological Survey Professional Paper 1236, p. 39-53.

Hildenbrand, T.G., Rosenbaum, J.G., and Reynolds, R.L., 1992, High resolution aeromagnetic study of the New Madrid seismic zone: A preliminary report: Seismological Research Letters v. 63, n. 3, p. 209-221.

Hough, S.E., Armbruster, J.G., Seeber, L., and Hough, J.F., 2000, On the modified mercalli intensities and magnitudes of the 1811-1812 New Madrid earthquakes: Journal of Geophysical Research, v. 105, n. B10, p. 23,839-23,864.

Howe, J.R., 1995, Tectonics, sedimentation, and hydrocarbon potential of the Reelfoot aulogcogen: Norman, University of Oklahoma, unpublished M.S. Thesis, 109 pp.

Johnson, P.R., Zietz, I., and Thomas, W.A., 1994, Possible Neoproterozoic-early Paleozoic grabens in Mississippi, Alabama and Tennessee: Geology, v. 22, n. 1, p. 11-14.

Johnston, A.C., 1996, Seismic moment assessment of earthquakes in stable continental regions III, New Madrid 1811-1812, Charleston 1886, and Lisbon, 1755: Geophysical Journal Int., 126, p. 314-344.

Johnston, A.C., and Schweig, E.S., 1996, The enigma of the New Madrid Earthquakes of 1811-1812: Annual Reviews of Earth and Planetary Science, v. 24, p. 339-384.

Kane, M.F., Hildenbrand, T.G., and Hendricks, J.D., 1981, Model for the tectonic evolution of the Mississippi embayment and its contemporary seismicity: Geology, v. 9, p. 563-568.

Kelson, K.I., Van Arsdale, R.B., Simpson, G.D., and Lettis, W.R., 1992, Assessment of the style and timing of surficial deformation along the central Reelfoot scarp, Lake County, Tennessee: Seismological Research Letters, v. 63, p. 349-356.

Kelson, K.I., Simpson, G.D., Van Arsdale, R.B., Haraden, C.C., and Lettis, W.R., 1996, Multiple late Holocene earthquakes along the Reelfoot fault, central New Madrid seismic zone: Journal Geophysical Research, v. 101, n. B3, p. 6151-6170.

Langenheim, V.E., and Hildenbrand, T.G., 1997, Commerce geophysical lineament-Its source, geometry, and relation to the Reelfoot rift and New Madrid seismic zone: Bulletin of Geological Society of America, v. 109, n. 5, p. 580-595.

Luzietti, E.A., Kanter, L.R., Schweig, E.S., Shedlock, K.M., and Van Arsdale, R.B., 1992, Shallow deformation along the Crittenden County fault zone near the southeastern boundary of the Reelfoot rift, northeast Arkansas: Seismological Research Letters, v. 63, n. 3, p. 263-275.

Marshak, S., and Paulsen, T., 1996, Midcontinent U.S. fault and fold zones: a legacy of Proterozoic intracratonic extensional tectonism?: Geology, v. 24, n. 2, p. 151-154.

Mihills, R. K. and Van Arsdale, R.B., 1999, Late Wisconsin to Holocene deformation in the New Madrid seismic zone: Seismological Society of America Bulletin, v. 89, no. 4, p. 1019-1024.

Mueller, K and Pujol, J., 2001, Three-dimensional geometry of the Reelfoot blind thrust: Implications for moment release and earthquake magnitude in the New Madrid seismic zone: Seismological Society of America Bulletin, v. 91, p. 1563-1573.

Mueller, K., Hough, S.E., and Bilham, R., 2004, Analysing the 1811-1812 New Madrid earthquakes with recent instrumentally recorded aftershocks: Nature, v. 429, p. 284-288.

Nelson, K.D., and Zhang, J., 1991, A COCORP deep reflection profile across the buried Reelfoot rift, south-central United States: Tectonophysics, v. 197, p. 271-293.

Nuttli, O.W., 1973, The Mississippi Valley earthquakes of 1811-1812: Intensities, ground motion and magnitudes: Seismological Society of America Bulletin, v. 63, p. 227-248.

Obermeier, S.F., 1989, The New Madrid earthquakes: an engineering-geologic interpretation of relict liquefaction features: U.S. Geological Survey Professional Paper 1336-B, 21 pp.

Odum, J.K., Stephenson, W.J., Shedlock, K.M., and Pratt, T.L., 1998, Near-surface structural model for deformation associated with the February 7, 1812, New Madrid, Missouri, earthquake: Bulletin of Geological Society of America, v. 110, n. 2, p. 149-162.

Purser, J.L., 1996, Shallow seismic reflection survey along the southern margin of Reelfoot Lake, Tennessee, and regional implications: Memphis, University of Memphis, unpublished M.S. thesis, 76 pp.

Purser, J.L. and Van Arsdale, R.B., 1998, Structure of the Lake County Uplift: New Madrid Seismic Zone: Seismological Society of America Bulletin, v. 88, n. 5, p. 1204-1211.

Rhea, S., Wheeler, R.L., and Tarr, A.C., 1995, Map showing seismicity and sandblows in the vicinity of New Madrid, Missouri: U.S. Geological Survey Miscellaneous Field Studies Map-2264-A, 1:250,000.

Russ, D.P., 1982, Style and significance of surface deformation in the vicinity of New Madrid, Missouri, *in* F.A. McKeown and L.C. Pakiser, eds., Investigations of the New Madrid Missouri, Earthquake Region: U.S. Geological Survey Professional Paper 1236, p. 95-114.

Saucier, R.T., 1974, Quaternary geology of the lower Mississippi Valley: Arkansas Archaeological Survey Research Series 6, 25 p.

Saucier, R.T., 1994, Geomorphology and Quaternary geologic history of the lower Mississippi Valley: U.S. Army Corps of Engineers, Waterways Experiment Station, 364 pp.

Schweig, E.S., III, and Marple, R.T., 1991, The Bootheel lineament: A possible coseismic fault of the great New Madrid earthquakes: Geology, v. 19, p. 1025-1028.

Schweig, E.S., Fan, Shen, Kanter, L.R., Luzietti, E.A., Van Arsdale, R.B., Shedlock, K.M., and King, K.W., 1992a, Shallow seismic reflection survey of the Bootheel lineament area, southeastern Missouri: Seismological Research Letters, v. 63, n. 3, p. 285-295.

Schweig, E.S., Marple, R.T., and Li, Y., 1992b, An update of studies of the Bootheel lineament in the New Madrid seismic zone, southeastern Missouri and northeastern Arkansas: Seismological Research Letters, v. 63, n. 3, p. 277-284.

Schweig, E.S., and Ellis, M.A., 1994, Reconciling short recurrence intervals with minor deformation in the New Madrid seismic zone: Science, v. 264, p. 1308-1311.

Sexton, J.L., 1992, Collaborative research SIUC-USGS high resolution seismic reflection surveying of the Bootheel lineament in the New Madrid seismic zone: U.S. Geological Survey NEHRP Final Report, 35 pp.

Sexton, J.L., and Jones, P.B., 1986, Evidence for recurrent faulting in the New Madrid seismic zone from Mini-Sosie high-resolution reflection data: Geophysics, 51, n. 9, p. 1760-1788.

Sexton, J.L., and Jones, P.B., 1988, Mini-Sosie high-resolution reflection survey of the Cottonwood Grove fault in northwestern Tennessee: Bulletin of Seismological Society of America, v. 78, n. 2, p. 838-854.

Shedlock, K.M., and Harding, S.T., 1982, Mississippi River seismic survey: Geophysical Research Letters, v. 9, p. 1275-1278.

Shedlock, K.M., Harding, S.T., and Luzietti, E.A., 1998, Near-surface faulting under the Mississippi River near New Madrid, Missouri (abs.): Eos (Transactions, American Geophysical Union), v. 69, p.14.

Shedlock, K.M., Stephenson, W.J., Luzietti, E.A., Zihlman, F.N., Oliver, H.L., Rhea, S.B., and Collins, D.R., 1997, Mississippi River shallow seismic survey: U.S. Geological Survey CD-ROM, 3-discs.

Stearns, R.G., 1957, Cretaceous, Paleocene, and Lower Eocene geologic history of the northern Mississippi embayment: Bulletin of Geological Society of America, v. 68, p. 1077-1100.

Stearns, R.G., and Marcher, M.V, 1962, Late Cretaceous and subsequent structural development of the northern Mississippi embayment area: Bulletin of Geological Society of America, v. 73, p. 1387-1394.

Stephenson, W.J., Shedlock, K.M., and Odum, J.K., 1995, Characterization of the Cottonwood Grove and Ridgely faults near Reelfoot Lake, Tennessee, from high-resolution seismic reflection data: U.S. Geological Survey Professional Paper 1538-I, p. 1-10.

Stuiver, M., and Reimer, D.J., 2000, Radiocarbon calibration program, CALIB rev. 4.3: Radiocarbon, v. 35, p. 215-230 (from website).

Thomas, W.A., 1989, The Appalachian-Ouachita orogen beneath the Gulf Coastal Plain between the outcrops in the Appalachian and Ouachita Mountains, *in* Hatcher, R. D., Thomas, W. A., and Viele, G. W., eds, The Appalachian-Ouachita Orogen in the United States: Geological Society of America, The Geology of North America, v. F-2, p. 537-553.

Thomas, W.A., 1991, The Appalachian-Ouachita rifted margin of southeastern North America: Bulletin of Geological Society of America, v. 103, p. 415-431.

Thompson, S.C., and Witter, R.C., Evaluating the repeatability of lateral spreading, U.S. Geological Survey National Earthquake Hazard Reduction Program Final Technical Report for award no. 03-HQGR-0075, dated July 2004, p. 22.

Tuttle, M.P., Schweig, E.S., Sims, J.D., Lafferty, R.H., Wolf, L.W., Haynes, M.L., 2002, The earthquake potential of the New Madrid seismic zone: Seismological Society of American Bulletin, v. 92, n. 6, p. 2080-2089.

Van Arsdale, R.B., 1998, Seismic hazards of the upper Mississippi embayment: U.S. Army Corps of Engineers Waterways Experiment Station Contract Report GL-98-1, 100 pp.

Van Arsdale, R.B., Williams, R.A., Schweig, E.S., Shedlock, E.S., Odum, J.K., and King, K.W., 1995a, The origin of Crowley's Ridge, northeastern Arkansas: erosional remnant or tectonic uplift?: Bulletin of Seismological Society of America, v. 85, n. 4, p. 963-985.

Van Arsdale, R.B., Kelson, K.I., and Lumsden, C.H., 1995b, Northern extension of the Tennessee Reelfoot scarp into Kentucky and Missouri: Seismological Research Letters, v. 66, n. 5, p. 57-62.

Van Arsdale, R.B., Guccione, M., Stephenson, W., and Odum, J., 1996, Collaborative research - University of Memphis and University of Arkansas: Mini-Sosie seismic reflection surveys at Reelfoot Lake, Tennessee, and Big Lake, Arkansas: U.S. Geological Survey NEHRP Final Report, 25 pp.

Van Arsdale, R.B., Purser, J. Stephenson, W., and Odum, J., 1998, Faulting along the southern margin of Reelfoot Lake, Tennessee: Bulletin of Seismological Society of America, v. 88, n. 1, p. 131-139.

Woolery, E.W., Wang, Z., Street, R.L., and Harris, J.B., 1996, AP-and SH-wave seismic reflection investigation of the Kentucky bend scarp in the New Madrid seismic zone: Seismological Research Letters, v. 67, n. 2, p. 67-74.

Zoback, M.D., 1979, Recurrent faulting in the vicinity of Reelfoot Lake, northwestern Tennessee: Bulletin of Geological Society of America, Part 1, v. 90, p. 1019-1024.

Zoback, M.D., Hamilton, R.M., Crone, A.J., Russ, D.P., McKeown, F.A., Brockman, S.R., 1980, Recurrent intraplate tectonism in the New Madrid Seismic Zone: Science, 209, p. 971-976.

APPENDIX A

DATA ACQUISITION AND METHODOLOGIES

Seismic Reflection and Vibroseis Data Acquisition

Numerous shear wave (S-wave) profiles were acquired across the North Farrenburg lineament (S-1 to S-3) and South Farrenburg lineament (S-4). S-wave profiles S-1 (360 m long) and S-3 (290 m long) were oriented east-west, and S-2 (290 m long) was oriented north-south along New Madrid County Road 707 (Figure 4). The reflection data for these three profiles were collected in SH-mode (sensitive to horizontally polarized shear waves) on a 12-channel engineering seismograph. The active spread consisted of 12 receivers (30 Hz horizontal geophones oriented perpendicular to the seismic line) spaced at 3-m intervals. The seismic profiles were shot off-end with 3-m-shotpoint spacings and 3-m source offsets. Seismic energy was generated by five horizontal impacts of a 4.5-kg sledgehammer on a 10-kg steel I-beam oriented perpendicular to the spread. Acquisition parameters on the seismograph included filter settings of 30 Hz (lowcut) and 250 Hz (highcut), a 1.0 s record length, and 0.5 ms sampling interval. Processing followed a standard sequence for shallow common midpoint (CMP) reflection data and included trace editing, bandpass filtering, and velocity analysis. The seismic data were stacked as 6-fold sections and enhanced with post-stack F-K (frequency wave number) filtering and automatic gain control. The processed seismic sections are discussed in Section 4.0 and have a resolution of about 5 m.

The seismic data for profile S-4, which crosses the South Farrenburg lineament, were collected in SH mode (sensitive to horizontally polarized shear waves) on a Seistronix RAS-24, 24-channel engineering seismograph. The 0.56 km long profile S-4 was collected on New Madrid County Road 719, southwest of Farrenburg (Figure 4). The active spread consisted of 24 receivers (14 Hz horizontal geophones oriented perpendicular to the seismic line) spaced at 3-m intervals. The reflection profiles were shot in a split spread configuration with 3-m shotpoint spacings and 1.5-m source offsets. Seismic energy was generated by five horizontal impacts of a 1.8-kg sledgehammer on a 5-kg steel I-beam oriented perpendicular to the spread (Figure 2). Profile S-4 has a resolution of about 5 m.

The portion of vibroseis line M-8 collected by Dow Chemical Company and re-interpreted for this study includes a 25 km long section that runs along Highway 61/62 between Matthews and New Madrid, MO. The north-south trending profile obliquely crosses the southwest projections of both the North and South Farrenburg lineaments. Line M-8 was collected by vibroseis technique, using four vibrating sources and sixteen sweeps. The geophones included models GS20D- 10HZ phones along a grid of 36 phones. The VP interval and group interval were at each at 220 feet, respectively. The field sample rate was at 2 msec and the record length 16 sec. The data were processed using coherency stack and bandpass filters.

Paleoseismic Trenching and Drilling

Paleoseismic trenches (T-1 to T-6) were excavated at the North Farrenburg site to document near-surface stratigraphy and structure across previously interpreted zones of disturbance imaged in the seismic reflection and GPR profiles (Figure 4). General stratigraphic and structural relations exposed in the trenches were cleaned, flagged, surveyed, and logged at a scale of either 1 in. = 0.5 m or 1 in. = 1m. Zones of faulting were logged at a scale of 1 in. = 0.5 m. Pedogenic descriptions also were made of trenches T-5 and T-6 for the purpose of correlating site-specific pedogenic development with respect to age. The soil profile descriptions are presented in Appendix C. All the trench locations and dimensions, including boreholes (see below), were surveyed using a Topcon GRS-303 total station relative to nearby cultural features, such as roads, drainage ditches, telephone poles, and structures.

Six sediment cores were collected 8 m northeast of trench T-6 and along the projection of the zone of deformation exposed in trenches T-5 and T-6 to provide additional subsurface information on the lateral continuity of deformation. The 5-cm-diameter push cores were collected in 1.2 m lengths using a Giddings drill operated by the United States Department of Agriculture. The cores were extruded into split plastic pipe, lithologically described, and correlated with trench stratigraphy. The maximum depth explored was 4.7 m. The core locations were surveyed along with the trenches. The profile location is shown on Figure 4.

Age Dating

The ages of the sedimentary deposits at the site were estimated from radiocarbon and thermoluminescence analyses and pedologic development of the sediments. Sixteen samples of detrital charcoal and peat collected from the trenches were submitted for radiocarbon analysis by accelerator mass spectrometry at Beta Analytic Inc., in Miami, Florida. The radiocarbon dates were dendrochronologically corrected to calibrated years according to the procedure of Stuiver and Reimer (2000). The results of the radiometric analysis are presented in Table 1. In addition a sediment sample collected from trench T-6 was analyzed by thermaluminescence techniques at the University of Illinois at Chicago (Table 1). Pedologic descriptions also were made of trench T-5 and T-6 for the purpose of correlating site-specific pedologic development with respect to age. The soil profile descriptions are presented in Appendix C.

Microtextural Analyses

We collected oriented sediment samples from the fault zone, dikes and undeformed sections of the trenches of the North Farrenburg site for computer-based image analysis of grain size and texture with the purpose of identifying microtextural characteristics indicative of coseismic surface-fault rupture (e.g., grain size reduction, preferred grain orientation, and development of shear zones) (Cashman and Cashman, 2000). Samples were collected in clear 1x10x10 cm plastic boxes, and were later cemented using a low viscosity, slow curing, clear epoxy. Thin sections and polished sections were prepared and analyzed using a petrographic microscope and SEM. Grain dimensions and orientations were measured from thin sections and polished sections using the computer program NIH Image. Individual measurements included lengths of long and short axes of grains, aspect ratio, and long axis orientation. Cashman and Cashman (2000) found that grain size counts using this method correlated fairly closely (within 10%) with those from sieve and pipette analyses.

APPENDIX B

LITHOLOGIC DESCRIPTIONS FOR TRENCHES T-5 AND T-6
NORTH FARRENBURG LINEAMENT, FARRENBURG, MISSOURI

Trench T-5

Bedding attitudes (see log of trench T-5 for locations)

A: N35°E, 11°E
B: N30°E, 12°E
C: N30°E, 24°E
D: N14°E, 14°E
E: S31°W, 17°W
F: S2°W, 5-10°W

Unit 1: Light brown to reddish brown fine-grained SAND; planar to cross-bedded, moist, friable, mottled orange brown and contains prominent manganese and iron oxide staining (Pleistocene fluvial deposit)

Unit 2: Olive gray silty SAND that becomes finer-grained with depth (increase in silt); massive, firm, moist, basal contact not observed (Pleistocene fluvial deposit)

Unit 3: Reduced olive gray CLAY with occasional pinkish tint, massive, stiff, contains common orange root concretions of iron oxide staining up to 3 cm diameter, damp; plastic, lower contact is gradational (Pleistocene fluvial deposit).

Unit 4/5: Interbedded oxidized orange fine-grained SAND, dark brown SILT and light brown silty CLAY; sand is bedded with fine laminations; friable; iron oxide nodules; silt is massive but with normal grading, well sorted; stiff and damp; silt-filled veins common; few to rare manganese oxide nodules; very little secondary clay accumulation (Pleistocene fluvial deposit).

Unit 6: Oxidized orange brown clay to silty CLAY (20 to 30% clay); massive, stiff, damp, plastic, mottled; vertical clay seams cutting across unit merges with lower clay unit to the east (Pleistocene fluvial deposit).

Unit 7: Light brown to dark brown fine-to medium-grained SAND, massive with some planar laminations, stiff, damp, oxidation produces dark staining, fines upward, base of unit sometimes marked by silt content; lower contact is gradational to smooth (Pleistocene fluvial deposit).

Unit 7A: Light brown to dark brown fine-grained SAND with trace of sandy lenses; few to common manganese oxide nodules; strong oxidization throughout unit; deposit cut by clastic dikes; lower contact gradational to smooth and often marked by manganese and iron oxide staining (Pleistocene fluvial deposit).

Unit 8: Light orange brown mottled SILT with very fine-grained sand, massive, gradational basal contact.

Unit 9: Orange brown silty very fine-grained SAND with clay and silt; massive, stiff and damp; weak prismatic structure, common filaments of manganese oxide along root pores as well as nodules; grades to a clayey silt, clay- and silt-filled fractures (vertical) cut deposit; clay likely pedogenic and mobilized from overlying units; few horizontal silt and clay-filled fractures occur in some areas; lower contact gradual and smooth (Pleistocene fluvial deposit).

Unit 10: Oxidized orange brown to yellowish dark brown clayey SILT to silty CLAY; massive dry to damp and hard; highly fractured with well developed prismatic to blocky structure. Upon exposure to air this unit develops cracks along pedogenic surfaces that are filled with grayish white silty skeltans. Peds coated with thin dark clay films; few manganese oxide nodules; no relict bedding preserved; occasional soil tongues penetrate unit; prominent gray skeltans (silt stringers) characterize the unit lower boundary very diffuse (5-10 cm) to gradational (Bt2/E pedogenic soil horizon).

Unit 11: Mottled light gray, light brown and orange brown silty SAND to sandy SILT with trace of clay; massive; sand is very fine-grained; damp and soft; strongly mottled grayish white skeltans common as vertical seams and roundish pods; weak fine granular soil structure with occasional vertical pedogenic fracture; rare to few manganese oxide nodules (1-2 mm diameter); common root pores; lower boundary is diffuse and wavy (Bt1/E pedogenic soil horizon).

Unit 12b: Dark grayish brown very fine-grained SAND with silt and trace of clay; damp, soft, light gray mottles are silt pods (skeltans); weak angular blocky structure; few very fine roots and root pores; moderate accumulation of organics noted by dark brown color; lower contact is gradual (over 2 cm) and wavy (unit contains soil properties of A and E-soil horizons).

Unit 12a: Light grayish brown silty fine-grained SAND, massive, granular texture, compared to Unit 12b it contains more properties similar to an E-horizon, gradational basal contact (soil properties of E-horizon).

Unit 14a: Dark gray to brown very fine-grained SAND and SILT; contains fine root pores and manganese oxide nodules; deposit is defined as a bowl-shaped feature with gradual margins that are defined, in part, by light gray irregular mottles; continued excavation of deposit identified no connecting dike, but deposit is interpreted as a swale within the zone of deformation that may, in part, be liquefaction-related; unit contains charcoal and maintains a grayish tint suggesting high organic debris mixed within unit (Holocene swale with liquefaction-related deposits).

Unit 14b: Dark gray to brownish gray mottled poorly sorted fine-grained sand with silt; generally massive but contains fine laminae; friable and dry; orange oxidization mottles more pronounced at the east end of this feature; contains 4 to 10 mm diameter silt clasts (rip-up?) and silt laminae; deposit is overprinted by soil pedogenic processes as evident by the presence of skeltans (leaching); root pores replaced by manganese oxide staining and nodules; basal contact is gradational and wavy (cross-cutting relations with Unit 11 indicate unit is likely an injected sand dike that has undergone moderate soil development processes).

Unit 15: Light brown to light gray SILT with very fine-grained sand; fine moderately to well-developed granular to platy soil structure; common very fine roots; lower contact very sharp, horizontal and smooth (Plow zone material).

TrenchT-6

Bedding attitudes (see log of trench T-6 for locations)

A: N43°E, 14°E
B: N47°E, 10°E
C: N53°E, 5°E
D: S5°E/S5°W, 10°W
E: S12°W, 10°W

Unit 1: Light brown to reddish brown fine-grained SAND; planar to cross-bedded, moist, friable, mottled orange brown and contains prominent manganese and iron oxide staining (Pleistocene fluvial deposit)

Unit 3: Reduced olive gray CLAY with occasional pinkish tint, massive, stiff, contains common orange root concretions of iron oxide staining up to 3 cm diameter, damp; plastic, lower contact not observed, but gradational in trench T-5; similar clay unit observed in cores to the northeast show offset (Pleistocene fluvial deposit).

Unit 4: Oxidized orange fine-grained SAND with trace of silt; sand is bedded with fine laminations; friable; iron oxide nodules; unconformably rests on Unit 3 and thins to the east on the north wall; moist; lower contact is sharp and smooth (Pleistocene fluvial deposit).

Unit 5: Orange brown (iron oxide stained) very fine-grained SAND with silt to SILT, massive but with normal grading, well sorted; stiff and damp; silt-filled veins common; few to rare manganese oxide nodules; very little secondary clay accumulation, lower contact is not observed (Pleistocene fluvial deposit).

Unit 6: Oxidized orange brown clay to silty CLAY (20 to 30% clay); massive, stiff, damp, plastic, mottled; vertical clay seams cutting across unit; unit offset 12 cm across N16°E-striking shear; unit increases in clay content to east; lower contact gradational to smooth (Pleistocene fluvial deposit).

Unit 7: Orange brown silty very fine-grained SAND with trace of clay; few to common manganese oxide nodules; strong oxidization throughout unit; abundant vertical clay seams and silt-rich skeltans cutting across unit; lower contact gradational to smooth (Pleistocene fluvial deposit).

Unit 8: Oxidized gray to orange brown clayey silt with very fine-grained SAND to silty CLAY to east, massive, stiff, damp; clay content increases to the east; becomes diffuse to east and grades into a unit with textures similar to Units 5 and 7; unit also characterized by iron oxide banding and staining; lower contact is gradational to smooth (Pleistocene fluvial deposit).

Unit 9: Orange brown silty very fine-grained SAND with clay and silt; massive, stiff and damp; weak prismatic structure, common filaments of manganese oxide along root pores as well as nodules; grades to a clayey silt, clay- and silt-filled fractures (vertical) cut deposit; clay likely pedogenic and mobilized from overlying units; few horizontal silt and clay-filled fractures occur in some areas; lower contact gradual and smooth (Pleistocene fluvial deposit).

Unit 10: Oxidized orange brown to yellowish dark brown clayey SILT to silty CLAY; massive dry to damp and hard; highly fractured with well developed prismatic to blocky structure. Upon exposure to air this unit develops cracks along pedogenic surfaces. Peds coated with thin dark clay films; few manganese oxide nodules; no relict bedding preserved; occasional soil tongues penetrate unit; prominent gray skeltans (silt stringers) characterize the unit lower boundary very diffuse (5-10 cm) to gradational (Bt2/E pedogenic soil horizon).

Unit 11: Brownish gray sandy SILT to silty very fine-grained SAND with trace of clay; massive; sand is very fine-grained; damp and soft; strongly mottled grayish white skeltans common as vertical seams and roundish pods; weak fine granular soil structure with occasional vertical pedogenic fracture; rare to few manganese oxide nodules (1-2 mm diameter); common root pores; lower boundary is diffuse and wavy (Bt1/E pedogenic soil horizon).

Unit 12: Dark grayish brown very fine-grained SAND with silt and trace of clay; damp, soft, light gray mottles are silt pods (skeltans); weak angular blocky structure; few very fine roots and root pores; moderate accumulation of organics noted by dark brown color; lower contact is gradual (over 2 cm) and wavy (unit contains soil properties of A and E-soil horizons).

Unit 13: Grayish brown very fine-grained sandy SILT; massive, damp, stiff; grayish brown mottles of silt (skeltans) common; trace of clay; weak angular blocky structure; few very fine roots and pores; manganese oxide nodules approximately 2 mm in diameter; prominent light gray skeltans make up 15% of unit; eastern boundary with Bt1/E soil horizon is diffuse across 5 cm (unit is interpreted as an A/E pedogenic horizon that has collapsed into liquefaction-related crater; alternatively, preferential percolation of water into the sand crater overlying unit 12 may have stripped iron and clay from the Bt1/E soil horizon (Complex Bt/E soil horizon developed in liquefaction deposits).

Unit 14: Dark grayish brown poorly sorted silty medium- to very fine-grained SAND; massive, damp, stiff, no clay present; irregular shaped crater-like sandy body; contains rare dark reddish brown fine-grained sand as pockets in deposit; no soil structure within unit; possible faint horizontal laminae on north wall of trench T-6 suggesting fluvial deposition post event; few very fine rootlets and pores; few skeltans present in the unit; margins of feature are sharp to gradational. East margin is more gradual than the west; crater shape tapers downward to sand-filled dike (dike number 3); however, the texture of the deposit is notably poorly sorted compared to well sorted sand within dike (sand blow mixed with A/E horizon and modified by pedogenesis; or sand blow modified by low surface water flow within a swale).

Unit 15: Light brown to light gray SILT with very fine-grained sand; fine moderately to well-developed granular to platy soil structure; common very fine roots; lower contact very sharp, horizontal and smooth (Plow zone material).

APPENDIX C

PEDOLOGIC DESCRIPTIONS
NORTH FARRENBURG LINEAMENT

APPENDIX D

STRUCTURAL RELATED OBSERVATIONS
LIQUEFACTION AND FAULTING

Liquefaction-related Features

Trench T-1

Trench T-1 encountered two clastic sand dikes that approach the present-day ground surface with crater-like morphology; however they both are truncated by historic tilling of the field and do not develop as laterally continuous sand blow deposits. Based on the absence of little to no soil development within the upper portion of the dike, or along the margins of the sand dikes, we interpret these clastic sand dikes formed during the 1811-1812 earthquake sequence.

Trench T-2

Trench T-2 encountered a narrow northeast-trending sand dike that includes two relatively prominent sand bodies, one of which is bounded by graben faults that connect with the walls of the dike down section. Two distinct sands are present in the upper part of the dike: one dark grayish brown silty sand with iron oxide concretions, and a second grayish white, clean friable sand that fills most of the graben or swale-like structure. The darker silty sand also lines one wall of the graben that is filled with clean friable sand. We interpret the two sand bodies and the presence of more advanced pedogeic soil processes within the dark grayish brown sand as evidence of two separate liquefaction events. The clean sand with little soil development is interpreted as a liquefaction deposit associated with the 1811-1812 earthquake sequence.

Trench T-3

A 5-m-wide zone of near-vertical sand filled dikes were exposed in trench T-3. The dikes trend approximately N23E to N38E across the base of the trench, and are up to 0.5 m wide. The sand filling the dikes is characterized as white, medium- to fine-grained and loose to friable. Many of the dikes come within <0.1 m of intersecting the former interpreted 1811-1812 ground surface and connect with a sand blow deposit that buries the former surface. Where the vented sand deposits are close to the ground surface, they appear to form about 14 m wide and 0.5 m thick liquefaction-related sand blow deposit. The sand blow exhibits horizontal bedding of lignite grains and charcoal. The sand blow deposit is overlain by historic fluvial deposits and debris that contain metal and tile fragments and form a horizontally bedded liquefaction-related sand blow deposit.

Trench T-4

A 0.2 m wide sand-filled dike occupies the southwall of trench T-4. The dike trends N30°E to N33°E across the trench and connects with a similar fracture on the northwall of the trench that shows primarily faulting (east-side down) and lesser amounts of sand-filled fractures. The sand is vertically mixed containing clean light-brown fine- to medium-grained sand to dark brown medium- to coarse-grained sand. Upsection the sand dike narrows and branches out laterally to thin discontinuous sand stringers in the overlying soil profile, but does not intersect the ground surface as exposed in the trench. It is unclear if the venting is associated with the 1811-1812 earthquake sequence or an earlier event.

Trench T-5

Up to as many as six liquefaction-related sand dikes were exposed in trench T-5 across a 7 to 8 m wide zone of deformation. The dikes are designated from east to west as dike 1 to dike 6. Each of the dikes are described in detail below.

Dike Trend Data (see log of trench T-5 for location)

D1: N10°W to N30°W, 90°
D2: N16°E, 90°

D3: N
D4: N25°E, 90
D5: N
D6: NA (approx. N-NE)

Dike 1

Sand dike 1 contains light gray fine- to medium-grained sand and rare silt rip-ups. Sand occurs in subvertical 5 to 15 cm thick sand dike. Dike trends N10°W to N30°W. On the north wall and upsection the dike connects with several thin, wavy near-vertical sand stringers that project up to the base of the A/E-soil horizon. On the southwall, the dike connects with a narrow crater-like feature that is filled with grayish brown silty very fine-grained sand to fine-grained sandy silt (soil development within deposit); penetrates the A/E-horizon of unit 12a.

Dike 2

Dike 2 is a prominent 4-5 cm thick vertical clastic dike. Sand is fine- to medium-grained well sorted, light gray, contains multiple silt-rich, 5-to 25-cm-long rip-up clasts. Flow bands are composed of silty sand and are approximately 2 mm thick and sub-parallel to dike margins. Dike appears to correlate with prominent sand dike in south wall and strikes N16°E across trench. Dike continues upsection on southwall and connects with crater-like feature composed of two separate sand bodies possibly of different events; on north wall dike 2 is located below a sand-filled crater or swale. Doesn't penetrate swale in wall; may do so three-dimensionally elsewhere in wall. In south wall, crater-like feature contains a light-brown (cleanish-1811-1812?) very fine-grained sand on the east, and a medium-grained sand with mixed E-horizon material on the west (older event?). We interpret these separate sand bodies as evidence of two separate liquefaction-related events.

Dike 3

Dike 3 consists of a discontinuous sand dike that anastomoses in and out of the plane of exposure and may bifurcate upward into dikes (Dikes-3a and Dike-3b of the north wall). Dike 3 is well expressed in the north wall, but not as well as expressed in south wall. Connects with thin sand dike having angular silt clasts of 5 to 25 cm long. Dike trends approximately due North across trench. Doesn't connect with an overlying deposit, but is stratigraphically below the crater-like deposit of the north wall.

Dike 4

Prominent sand dike appears to correlate with large sand dike in south wall and trends N25°E across trench. Contains well sorted fine- to medium-grained sand with common silt rip-up clasts. The central part of the dike is mixed with sand and irregular chunks of surrounding material. The sand dike is best defined in the silt rich deposits. Sand dike 4 connects upsection with a possible fissure-like feature that appears to stop near the base of the E-horizon (Unit 12a); however, E-horizon contains blebs of sand that are similar to vented material suggesting it continued upward. No clay along dike margins. Upper part of sand is partially modified by pedogenic processes (pre-1811-1812). E-soil horizon doesn't penetrate dike similar to all other dikes.

Dike 5

Characterized by an anastomosing 5-to 10-mm thick clean sand intrusion that goes in and out of the plane of the exposure. It's unclear whether this dike has a correlative match in the south wall. Possible that the sand dike splits from prominent dike in south wall that appears to correlate with sand dike 4. Trend across the trench is about due north. It is possible that dike 5 connects with an overlying crater- to fissure-like feature. The possible fissure is between 4 and 14 cm wide, and contains dark brown sandy silt (pedogenic development) with silty rip-up clasts, and pieces of former organic A-horizon. Cross-cuts unit 12a.

Dike 6

Dike 6 consists of a 1-3 cm wide clastic intrusion. The basal portion of the dike is characterized by white-gray silty sand. The margins of the dike are often lined with silty clay seams. Upper part of the dike consists of fine- to medium-grained sand. Dike continues upsection and connects with crater-like feature. Crater-like fissure contains dark brown fine-grained sand with some sub-horizontal laminations. Light-gray clay lines margins of crater. Dike is not correlative with any dikes on the north wall of trench T-5, but occurs directly opposite convolute bedding in north wall that is interpreted as soft-sediment deformation from strong-ground shaking.

<u>Trench T-6</u>

Dike Trend Data (see log of trench T-6 for location)

D1: N25-30°E
D2: N20-30°E or N26°E, 81°SE
D3: N7°E to N20°E, 90°
D4: N16°E, 90°

Trench T-6 encountered a 5-m-wide zone of clastic dikes cutting across bedded braided stream deposits and approaching the ground surface. In trench T-6, we recognize at least four distinct sand dikes designated from east to west as dike 1 to dike 4. Two of the dikes, dikes 3 and 4, are associated with apparent vertical separation of braided stream channel deposits.

Dike 1

Sand dike 1 is 2-to-5 cm-wide and filled with clean loose, medium-to fine-grained sand near the base of trench. In the floor of the trench, the dike is interconnected with multiple sand dikes, and silty clay seams in the southwall suggesting antiquity to the deposit. The dikes connect through an anastomosing network of sand-filled fractures ranging from 2 mm to 30 mm wide. Orientations of the dikes in the floor of the trench range from N25°E to N30°E. Upsection the dike forms bowl-shaped depression that cuts across the A-E-soil horizon; however the sand from the dike cannot be directly traced into the crater-like feature. In addition, the walls of the dike become clay-lined with 2-5 mm thick clay seams. Possibly correlative with dike 1 (easternmost) of trench T-5.

Dike 2

The dike trends N20°E to N30°E across the trench and is best expressed on the north wall of the trench. The dike consists of sandy silt and fining upwards to clayey silt; no clean sand is present on either trench wall suggesting antiquity to the deposit. The dike ranges between 1 and 12 cm wide and tapers downward and is vertical. At the base of the southwall deformation associated with the dike is best expressed as convoluted bedding and clay-rich seams, and upsection as a 0.5 to 2 cm wide dike. Soil formation has obscured and modified the upper part of the dike near units 9 and 10. Prominent dessication cracks suggest that secondary clay was preferentially translocated downward into the fissure from units overlying it. Toward its base the dike tapers substantially and becomes discontinuous. It does not reach the floor of the trench. Based on the soil development of the fissure fill material, we interpret this sand dike as an older event.

Dike 3

Clastic dike 3 trends N7°E to N20°E across the trench, and consists of well sorted fine- to medium-grained clean sand (near base) with subhorizontal bedding; chaotic mixed zones of material composed of poorly sorted silty sand and clay. The dike consists of a single clastic dike on the north wall and two clastic dikes on the south wall. The sand filled dikes contain subhorizontal lower and upper contacts, and material from overlying units that have become mixed in the clastic dike. Lower stratigraphic contacts show evidence of 4 to 6 cm of east-side down vertical displacement. Upper soil horizon also appears to be deflected or offset about 5 cm down to the east. Overlying dike 3 are crater-like features filled with dark grayish brown silty sand with occasional cleaner zones of reddish brown fine-grained sand. Based on the shape of the feature and its association with sand dike 3, we interpret the feature as liquefaction-related structure (combination of a fissure and topographic low filled with sand blow material). Faint horizontal laminae that are subparallel to the present-day topography suggest possible fluvial deposition within the swale, or represent laminations from sand blow deposit. Soil development processes (e.g., stripping of clay), organic accumulation indicate that the sand blow deposit may have been subjected to soil forming processes over several hundred to thousands of years. We interpret the liquefaction-related deposits as old and sourced from sand dike 3.

Dike 4

Sand dike 4 contains well sorted fine to medium-grained sand with rip-ups. Sand content diminishes upsection but relict sand dike is perhaps modified by soil development that occurs in the overlying near-surface soils of Units 10 and 12. The dike trends N16°E across the trench. The lower portion of the dike is lined by 1 to 2 cm thick vertical zone of fine to medium-grained sand with abundant clayey rip up clasts. The presence of manganese-stained and dark-colored sandy material lining the dike that is distinctly different than the grayish white clean sand that fills the remainder of the dike suggests two episodes of venting within this dike. Up to 12 to 15 cm of east side down vertical separation of stratigraphy is associated with this dike. In the southwall of trench, it appears that faulting offsets the A-horizon (unit 12)

Faulting

<u>Trench T-1</u>

In trench T-1, the fault zone is defined by a 1-m-wide fault zone striking N42°E that consists of numerous small steeply east-dipping to near vertical faults. Most of these faults can be traced up to the base of the well-developed pedogenic Bt soil horizon (Units Bs and Cs) or within 1.5 m of the ground surface. The main near-vertical fault of trench T-1 is characterized by several anastomozing shear planes and drag folding of bedding in Unit B. The sense of displacement reflected by the drag folding is not consistent with the observed vertical displacement of Unit B across the main shear, suggesting a component of lateral displacement. Lateral displacement along the faults also is suggested by the abrupt changes in stratigraphic thickness across faults and by a decrease in vertical displacement down-section (e.g., similar to a “flower structure” formed along a strike-slip fault).

Within the fault zone, at least two of the faults appear to be truncated by an overlying clay deposit, or become diffuse and obliterated by liquefaction-related deformation upsection. Stratigraphic units are displaced as much as 15 cm across individual faults, with predominantly northwest-side down vertical displacement. The smaller faults in trench T-1 appear to terminate at the base of silty sand units or are imperceptible where they enter areas of soft-sediment deformation. Along several faults, where brittle deformation is not continuous upsection, folding and tilting of the deposits occurs.

The two sand dikes present in trench T-1 show evidence of displacement across the dike boundaries. The two sand dikes border a central block that has undergone less than 15 cm of uplift relative to the adjacent sediments. Because the amount of apparent vertical separation of stratigraphic markers is not the same across the dike margins (at about stations 19 and 25.5 m), the block may have undergone lateral translation.

Trench T-4

Trench T-4 exposed a steep N30°E-striking, west-dipping fault that is associated with a clastic dike on the south wall of the trench. The fault zone is relatively narrow at depth and broadens upsection (~1 m wide). The fault zone projects toward the faulting exposed in the eastern end of trench T-1. The dike is absent when projected across the trench to the northeastern wall, and instead, is expressed as a N30°E-striking near-vertical, 1-m-wide fault zone. The maximum apparent vertical displacement across the dike in the southeastern wall is about 5 cm; whereas across the trench on the northeastern wall the displacement is about 15 cm. Laminated and bedded sand near the base of the trench and on the west side of the fault zone exhibits extensive folding and tilting that is not expressed upsection.

Trench T-6

An approximately 2-m-wide zone of faulting also was encountered in the northwest part of trench T-6. The fault zone is characterized by several near-vertical N20°E to N30°E striking faults that commonly are associated with clastic sand dikes (dikes 3 and 4). Vertical displacements across individual faults range from 5 to 15 cm and all faults exhibit southeast side down apparent vertical separation. Total separation across the fault zone exposed in trench T-6 is 17 to 28 cm. Faulting encountered along dike 4 can be traced confidently across the basal contact of Unit 10, and less confidently across the base of the former ground surface, or base of the buried A/E soil horizon (Unit 12). The fault associated with dike 4 appears to displace the base of the buried A/E soil horizon 5-10 cm. On the basis of deflected basal stratigraphic and pedogenic boundaries, faulting can be traced upward across Units 8, 9 and 10 along dike 3. The westernmost fault exposed in trench T-6, located directly west of vent 4 is characterized by minor vertical separations of ≤ 5 cm, discontinuous, thin liquefaction-related intrusions, and clay seams along the shear. The overall down to the southeast vertical separation across the 2-m-wide zone of faulting is consistent with the borehole profile that indicates deformation extending down depth to at least four meters below the ground surface (maximum depth explored).

FIGURES

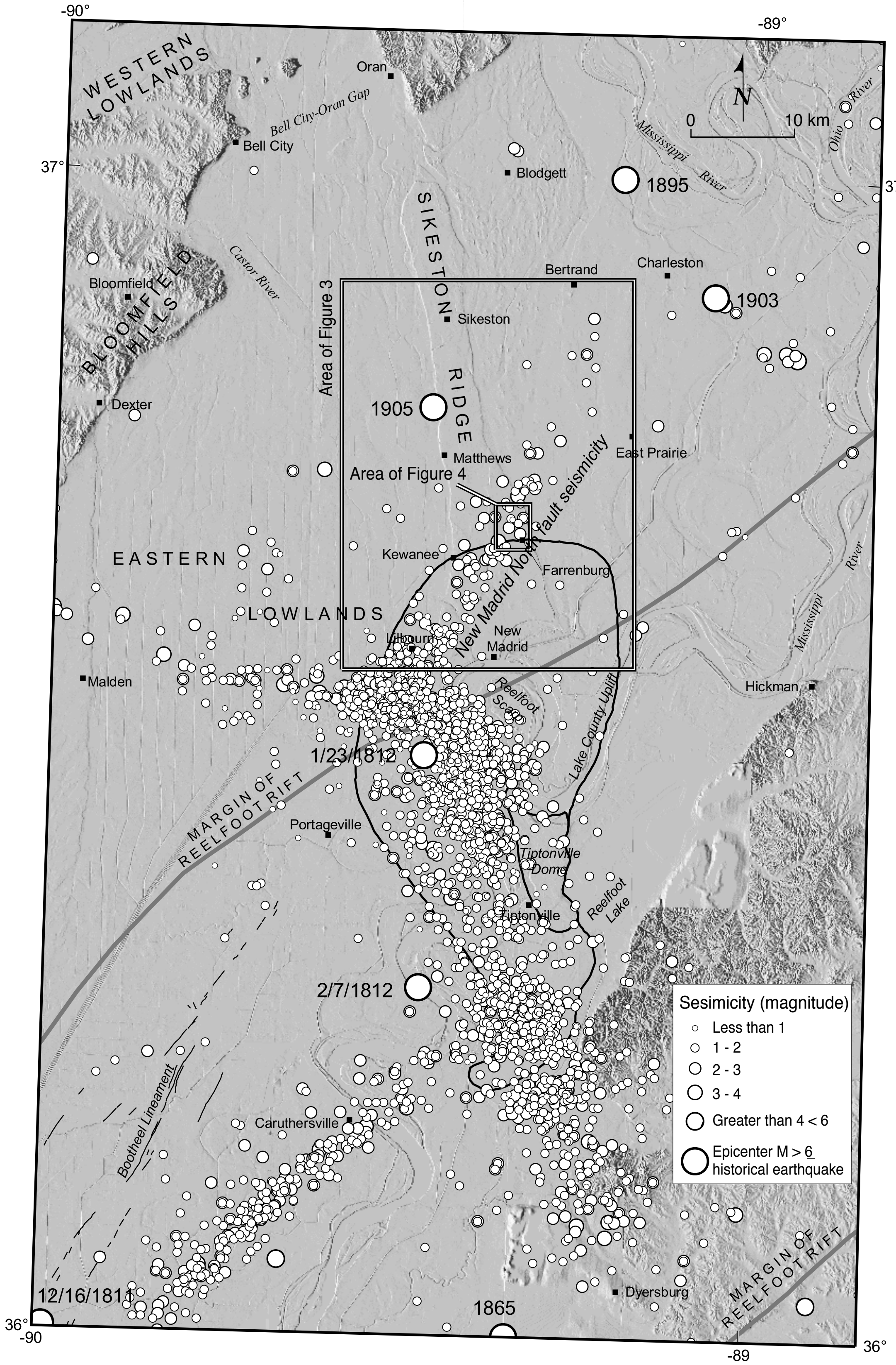

Figure 1. Map showing tectonic setting and historical seismicity (1974 - 1991) of the New Madrid seismic zone (after Rhea and Wheeler, 1995; Johnston and Schweig, 1996). Vertical exaggeration of shaded-relief base map is 7.5 times.

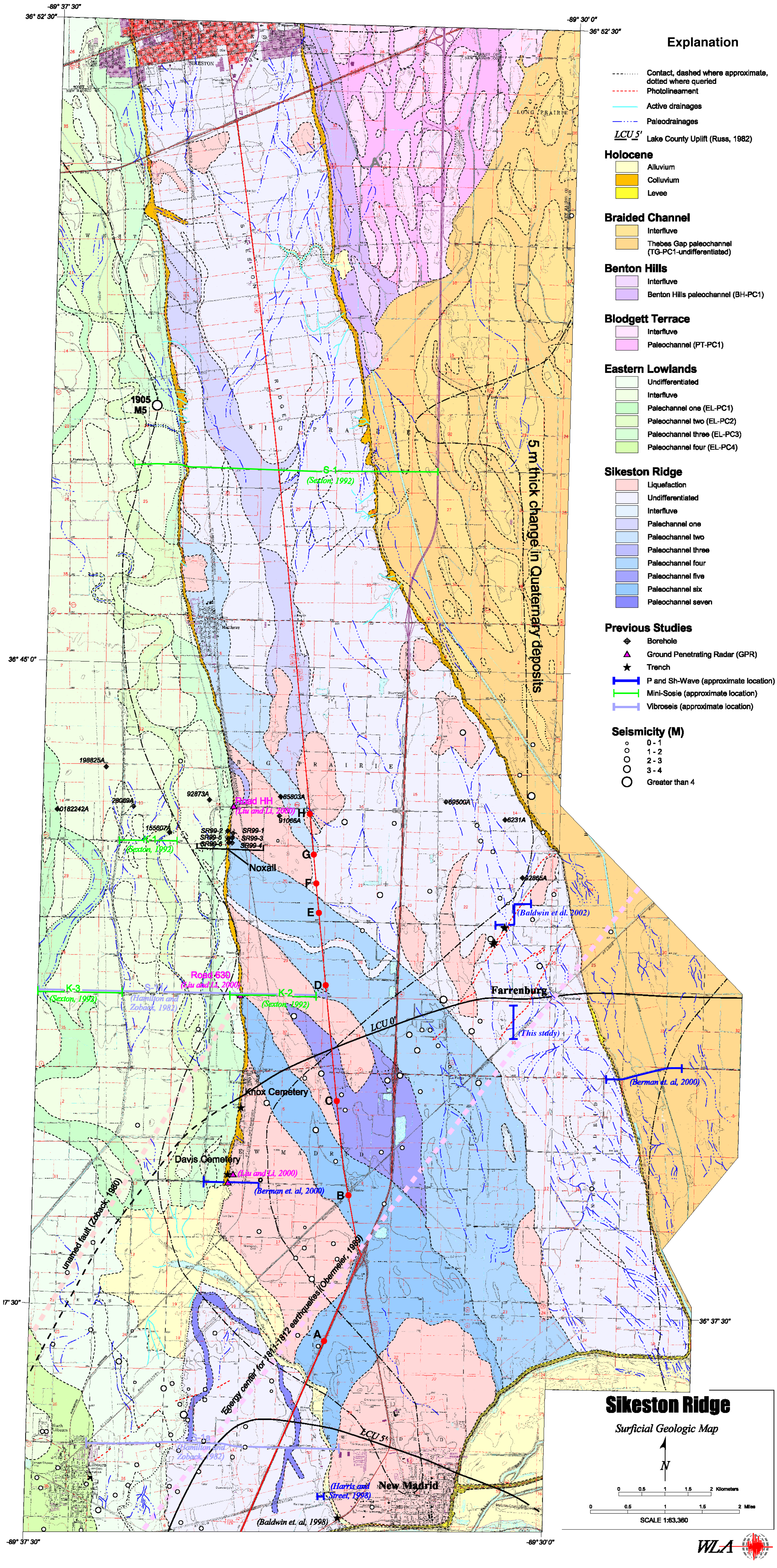

Figure 2. Preliminary surficial geologic map of southern Sikeston Ridge, New Madrid and Scott Counties, Missouri.

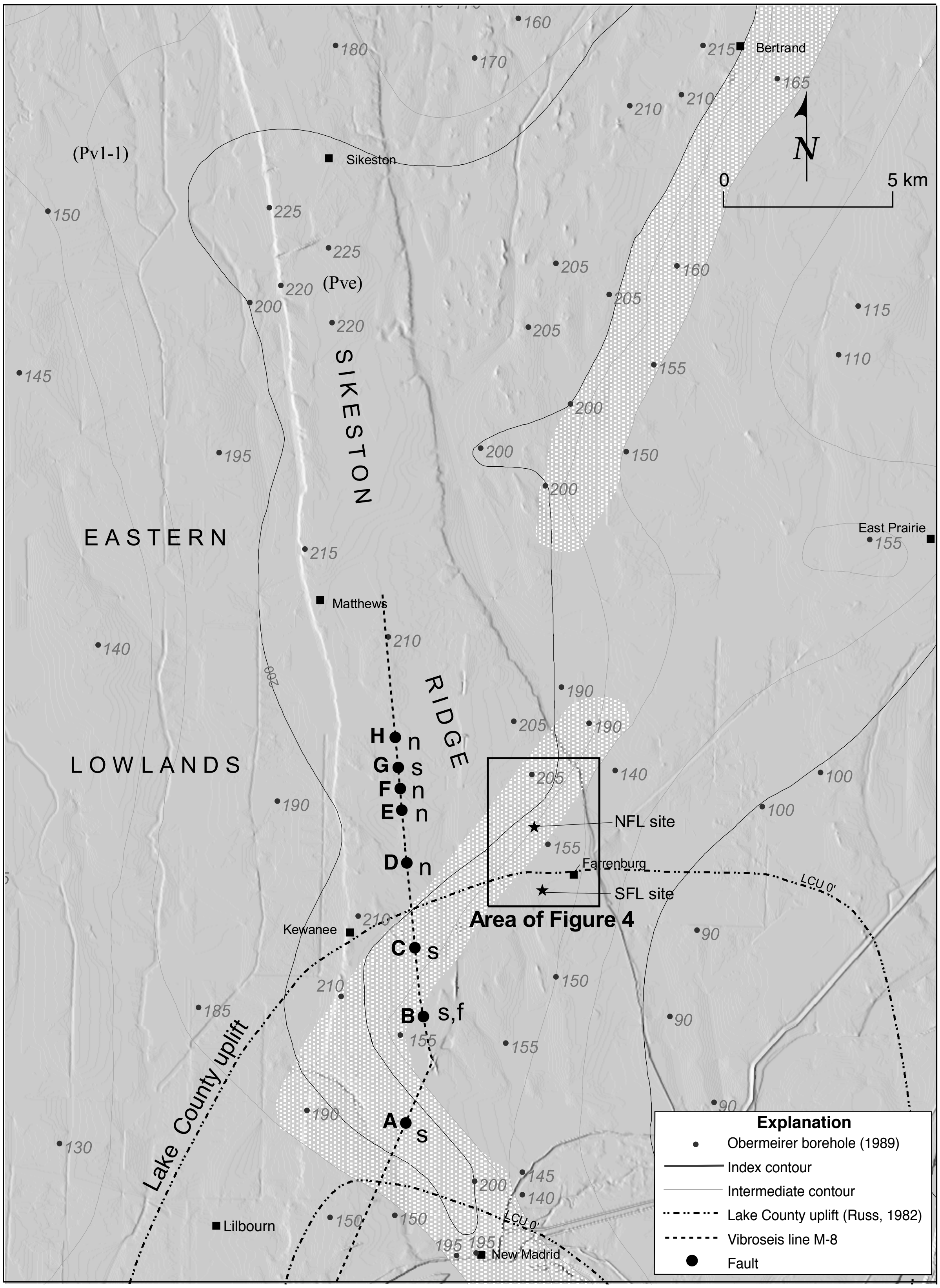

Figure 3. Shaded-relief map showing isopach contours (in feet) of post-Tertiary alluvial deposits (modified from Obermeier, 1989). Note the prominent NE-trending isopach lineaments (stippled pattern) extending from near Kewanee to at least Bertrand, Missouri. Isopach lineament possibly associated with the NMNF and Reelfoot fault. Faults (A - H) identified in vibroseis line M-8 marked by dot. N = north side up, S = south side up, F = flexure, NFL = North Farrenburg lineament site, SFL = South Farrenburg lineament site. Vertical exaggeration of shaded-relief map is 7.5 times.

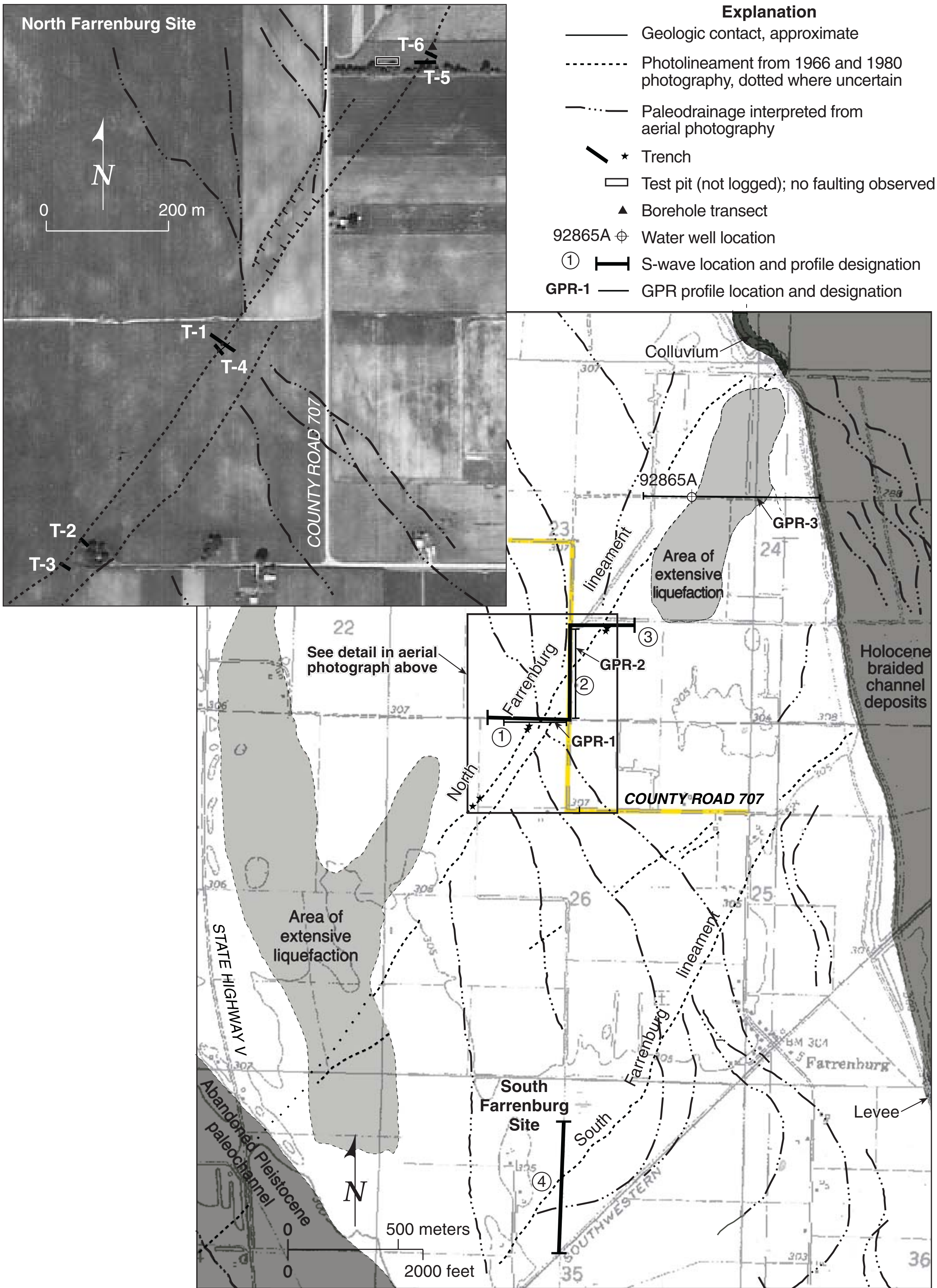

Figure 4. Mapped traces of the North and South Farrenburg lineaments. Surficial geologic mapping from Baldwin et al., (2001). Inset aerial photograph shows trench locations (aerial photography dated 9/29/66) at the North Farrenburg site.

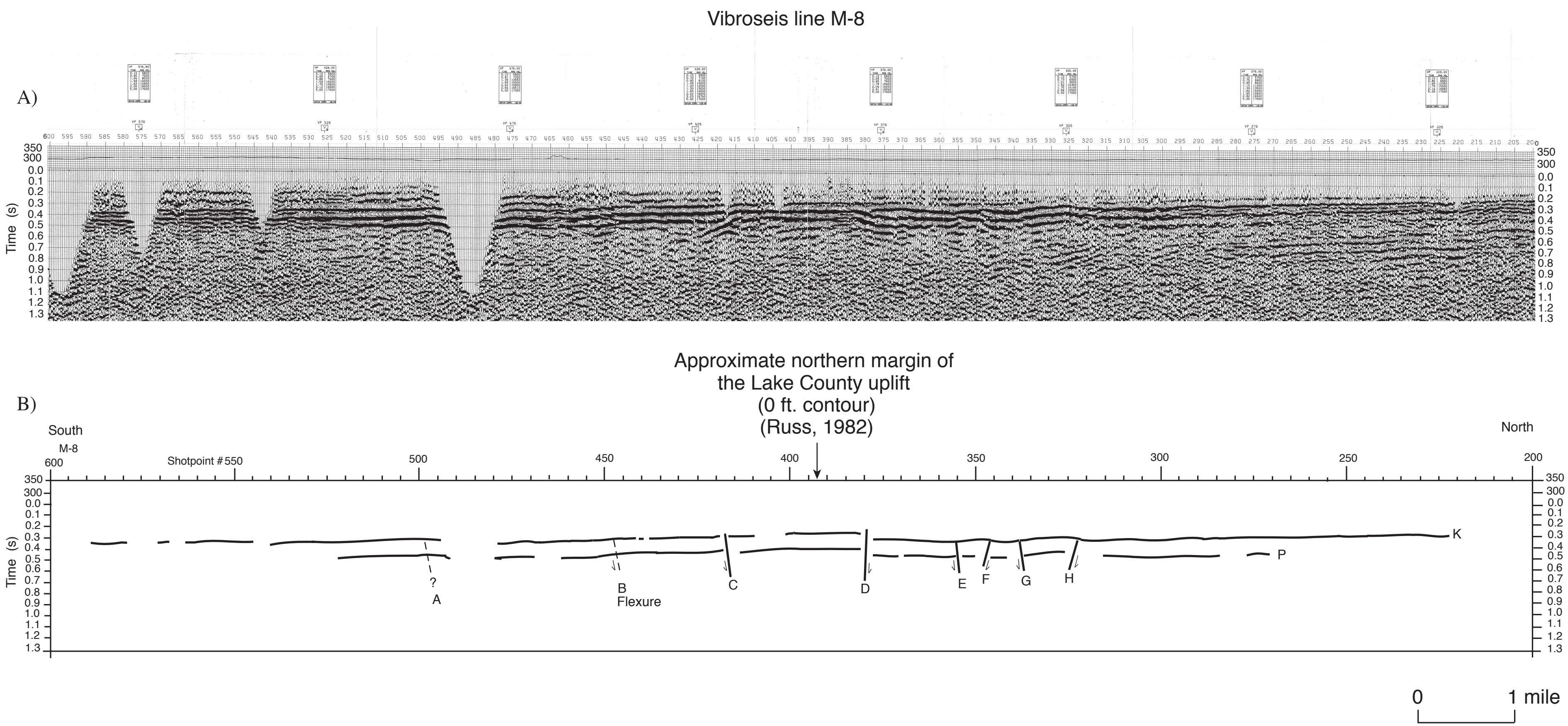

Figure 5. Dow Chemical vibroseis line M-8 trending north - south along Sikeston Ridge. Figure 5(A) shows uninterpreted seismic line. Figure 5(B) depicts interpreted seismic line. K = Cretaceous; P = Paleozoic; A - H refer to interpreted faults. See Figure 3 for section location. Triangular sections are where no data is available.

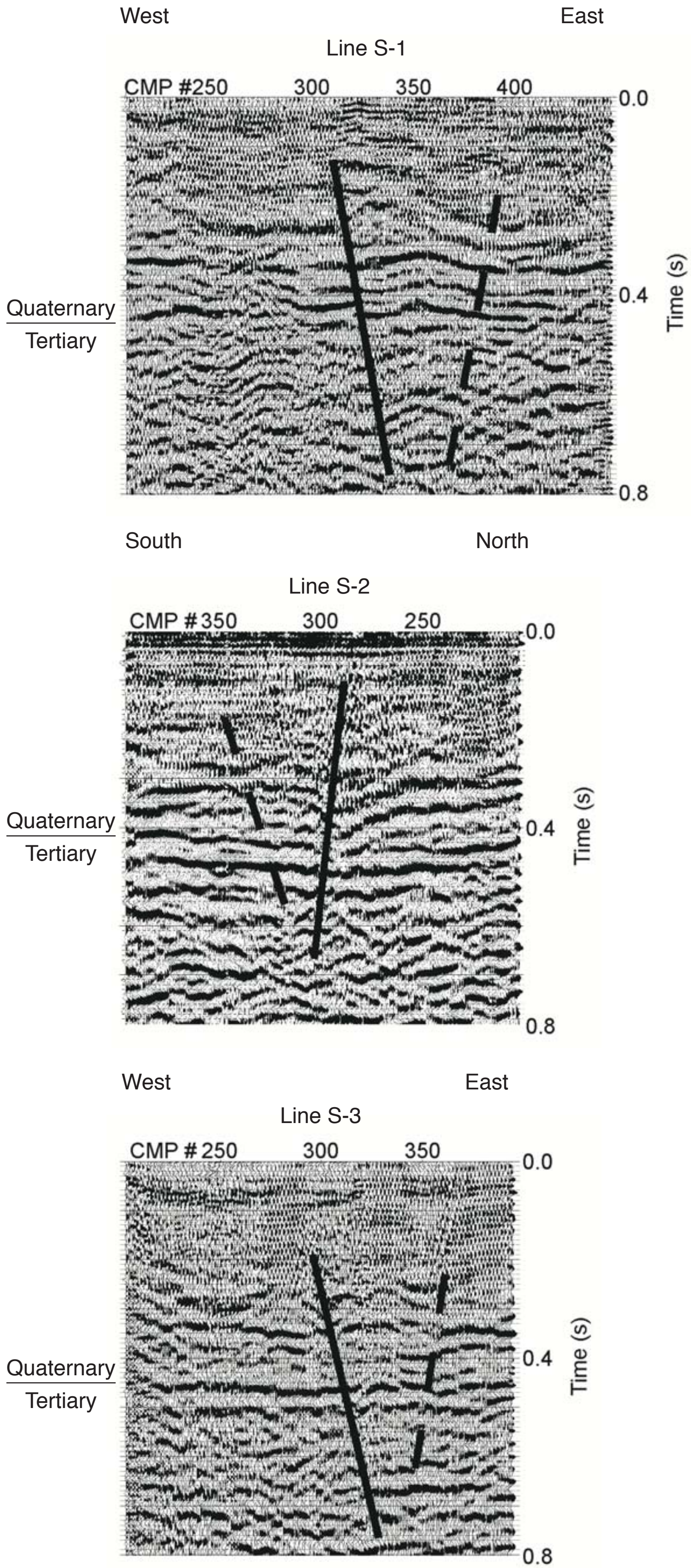

Figure 6. Interpreted S-wave seismic reflection profiles S-1 to S-3 acquired across the North Farrenburg lineament. See Figure 4 for profile locations.

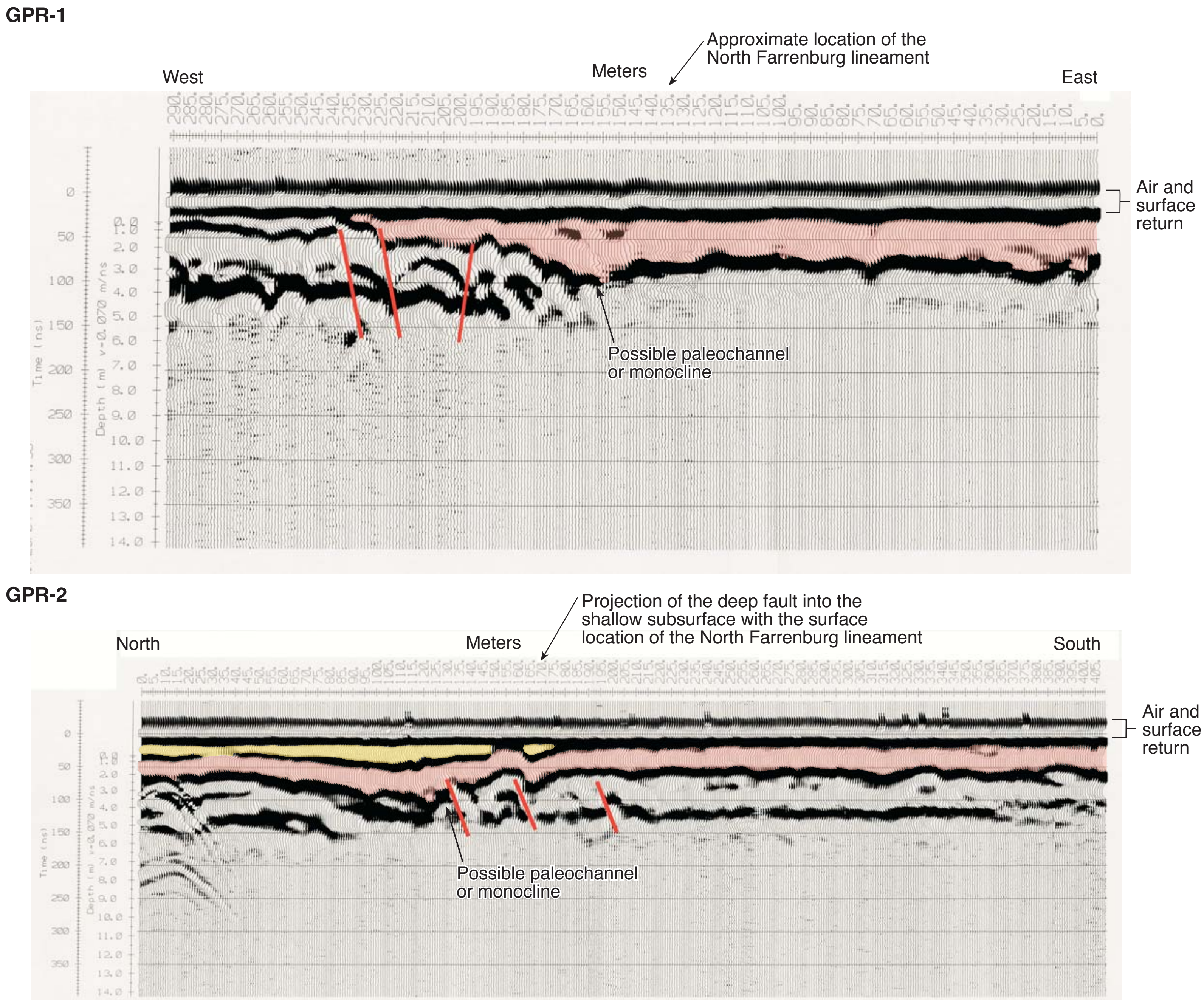

Figure 7. Preliminary interpretation of GPR profiles for the North Farrenburg site. See Figure 4 for locations (modified from Sexton and Lake, 2004).

GPR-3

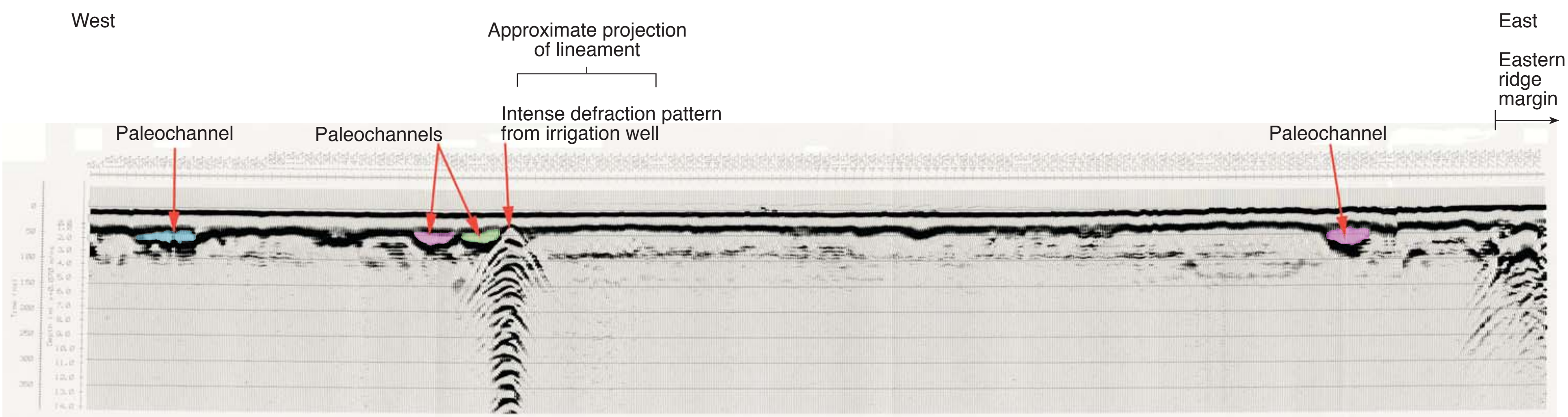

Figure 8. Preliminary interpretation of profile GPR-3 showing interpreted paleochannels east of North Farrenburg lineament (location of profile shown in Figure 4). Scale on upper horizontal is in meters. Preliminary data Farrenburg, Missouri, Georadar Line 5, Dr. John L. Sexton and Marshall A. Lake.

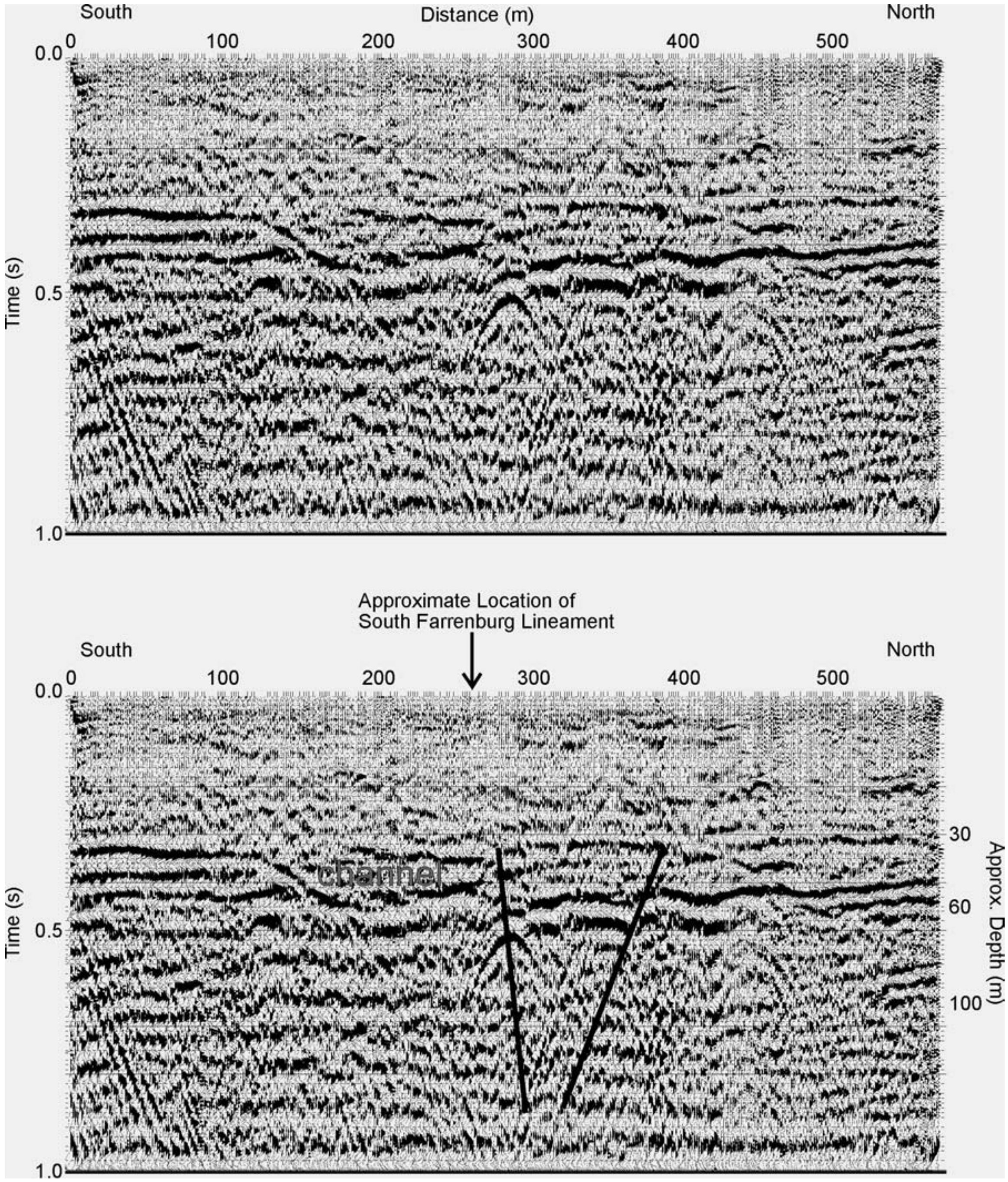

Figure 9. Seismic reflection line S-4 (12-fold stack) from the South Farrenburg site, uninterpreted (top), and interpreted (bottom). See Figure 4 for location.

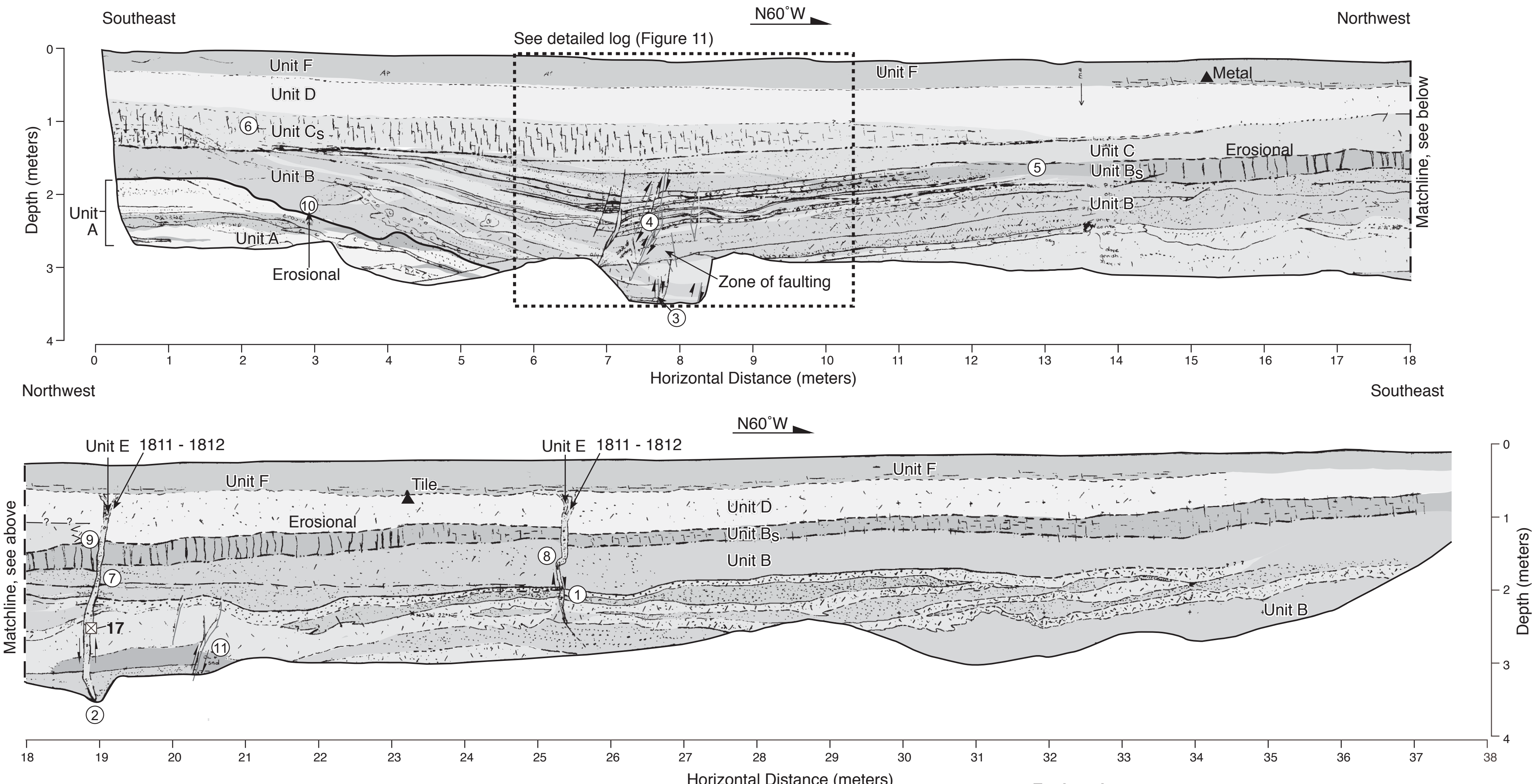

Notes:

1. Vent trends N19°E
2. Vent trends N55°E
3. Fault strikes N64°E
4. Fault strikes N42˚E
5. Relict interbeds of Unit B preserved in buried soil of Unit B_S.
6. Relict interbeds of Unit B preserved in buried soil of Unit C_S.
7. Apparent vertical displacement of 10 -15 cm of Unit B_S/Unit B contact
8. Apparent vertical displacement of 10 -15 cm of Unit B_S/Unit B contact
9. Apparent vertical displacement < 5 cm of Unit B_S/Unit C contact
10. Eastern margin of paleochannel deposits (erosional contact)
11. Fault shows about 8 cm apparent vertical displacement

Explanation

Unit F:	Dark gray to dark brown silty fine-grained sand (modern soil horizon/plow zone debris)
Unit E:	Light gray to tan clean fine to medium-grained sand with lignite (liquefaction deposits)
Unit D:	Massive grayish-brown to light brown silty sand to sandy silt (1811-1812 A/B horizon)
Unit Cs	Massive (occasional relict bedding) yellow-brown silty sand with pedogenic fractures and some mottling (soil developed in Unit C)
Unit C	Massive, friable tan to light yellowish-brown fine- to medium-grained sand
Unit Bs	Massive, strongly mottled gray to olive-brown silty fine-grained sand with well-developed pedologic structure (buried soil horizon developed in Unit B)
Unit B	Interbedded yellowish-brown to orange-brown silty sand and fine-grained sand ("tiger stripe" sands)
Unit A	Interbedded dark yellowish brown to light olive-brown fine- to coarse-grained sand with discontinuous lenses of clay.

Fault; dashed where uncertain; arrows point in direction of apparent displacement

◪ Radiocarbon sample location and designation; see Table 1

13,14 ☒ Sediment sample location and designation for textural analysis

▲ Historic artifact/metal, tile, glass

Figure 10. Log of trench T-1.

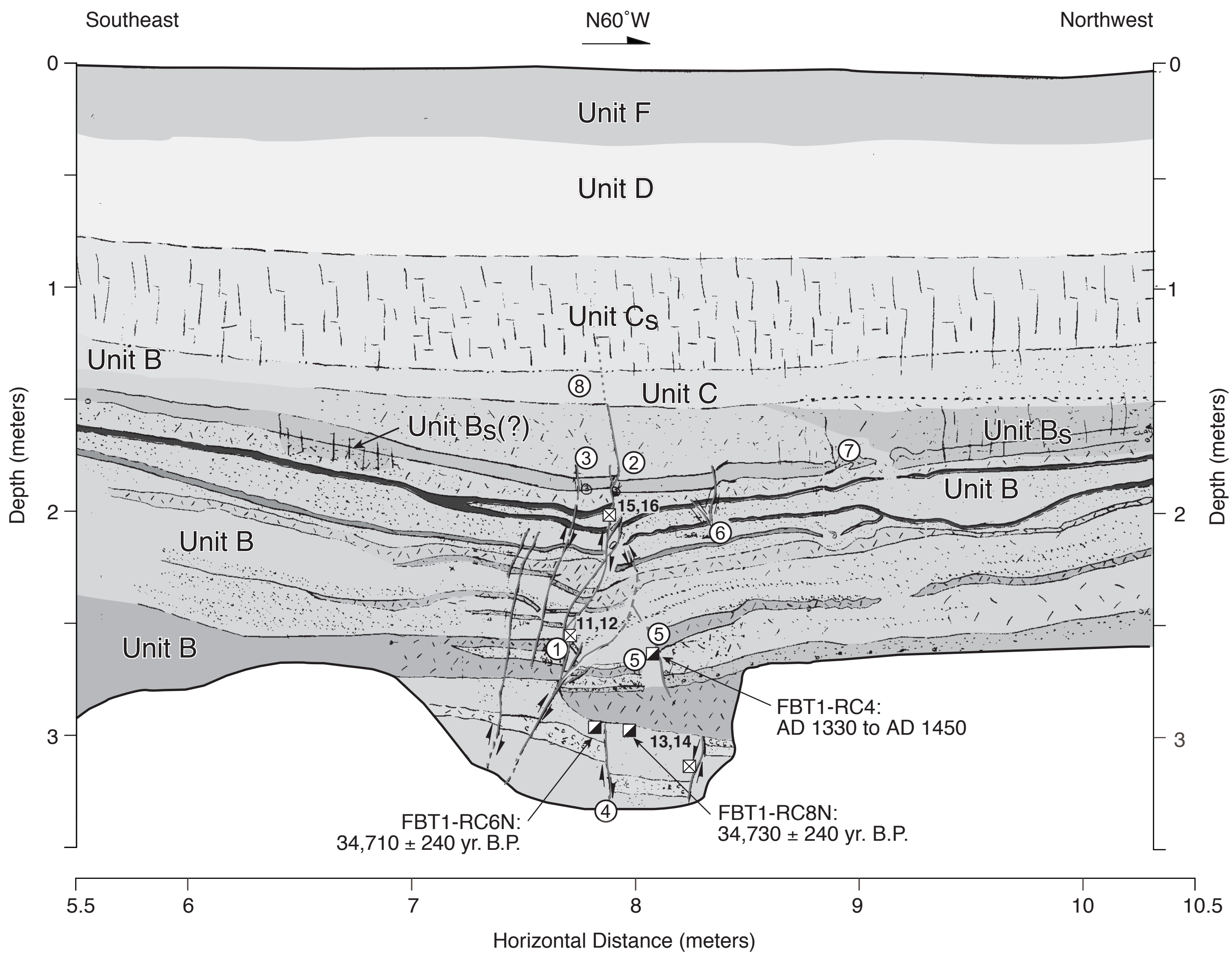

Notes:

1. Fault strike N42°E across trench
2. Fault strike N61°E across trench
3. Fault strike N53°E across trench
4. Fault strike N44°E across trench
5. Silty sand correlative across fault
6. Minor discontinuous shear zone
7. Tightly folded clay with interbeds of sand (soft-sediment deformation)
8. Upward fault projection obscured by soil processes

Figure 11. Detailed log of fault zone exposed in trench T-1. Note sediment sample locations 11 (vertical) and 12 (horizontal).

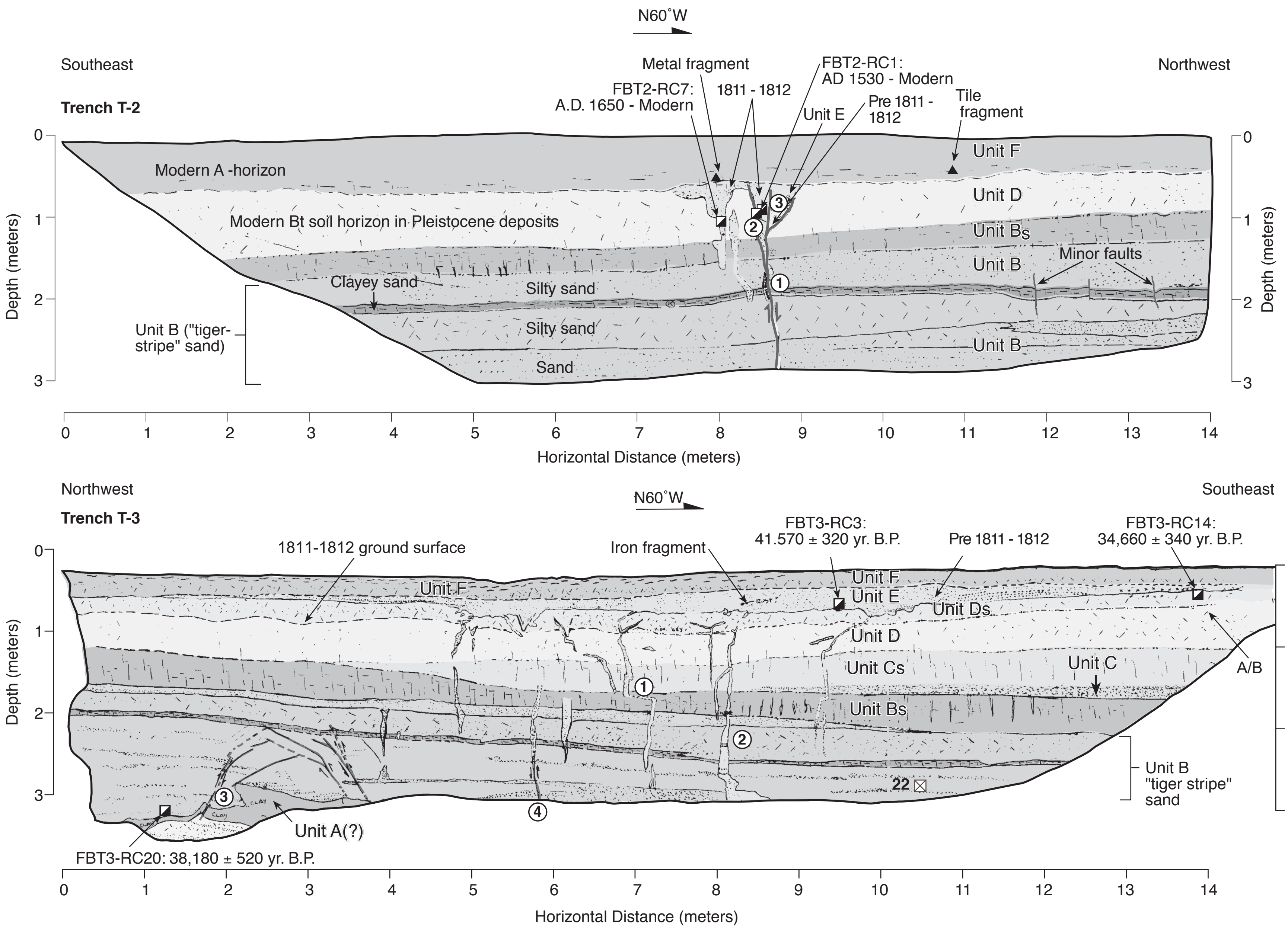

Notes for Trench T-2:

1. Apparent vertical displacement across clay unit < 5 cm
2. Vertically displaced Unit D within graben
3. Correlative Unit D block across graben fault

Notes for Trench T-3:

1. Vent trends N5°E across trench
2. Vent trends N38°E across trench
3. Clay appears warped with < 5cm apparent vertical displacement; opposite wall shows displacement is at least 10 cm or greater
4. Vent trends N23˚E (<1 cm vertical displacement)

See Explanation, Figure 10.

Figure 12. Logs of trenches T-2 and T-3.

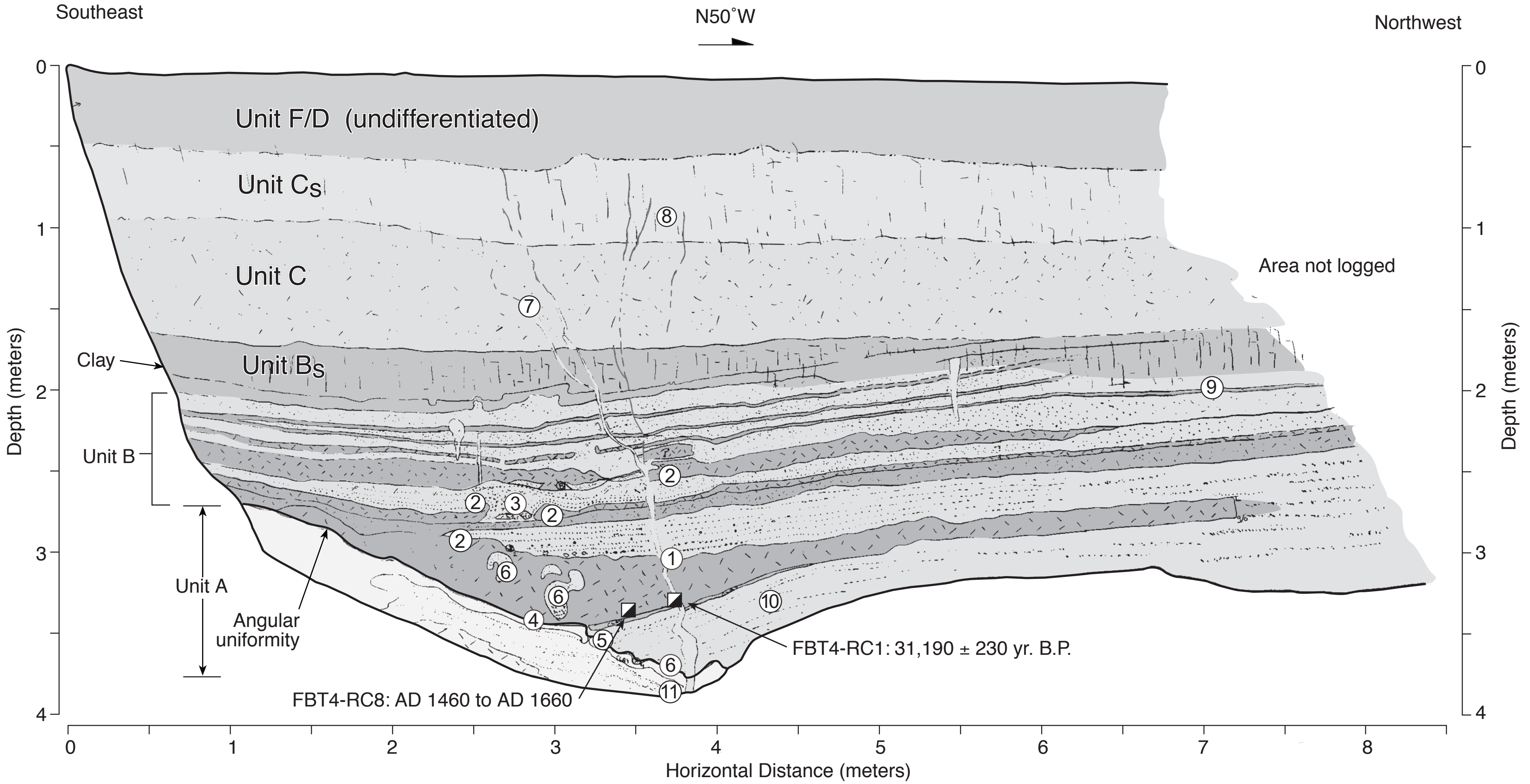

Notes:

1. Vent trends N30-33°E across trench; apparent vertical separation about 5 cm; up to about 15 cm in northeast wall across fault zone
2. Folded clay with occasional folded interbedded fine-grained sand (soft-sediment deformation)
3. Zone of disturbed fine-grained sand (liquefaction)
4. Channel fill trend across trench: N31°E
5. Possible older channel thalweg: trends about N42°E across trench
6. Silt and silty sand folded around liquefaction deposits (soft-sediment deformation)
7. Liquefaction fractures/fault obscured due to bioturbation and soil processes
8. Very strong soil partings (less prominent east and west of this zone)
9. Pedologic structure becomes more developed to west similar to trench T-1
10. Steep east-dipping laminated sand: possibly warped
11. Steep west dipping laminated sand: possibly warped

Figure 13. Log of trench T-4 showing venting, warping and soft-sediment deformation of the glacial outwash deposits.

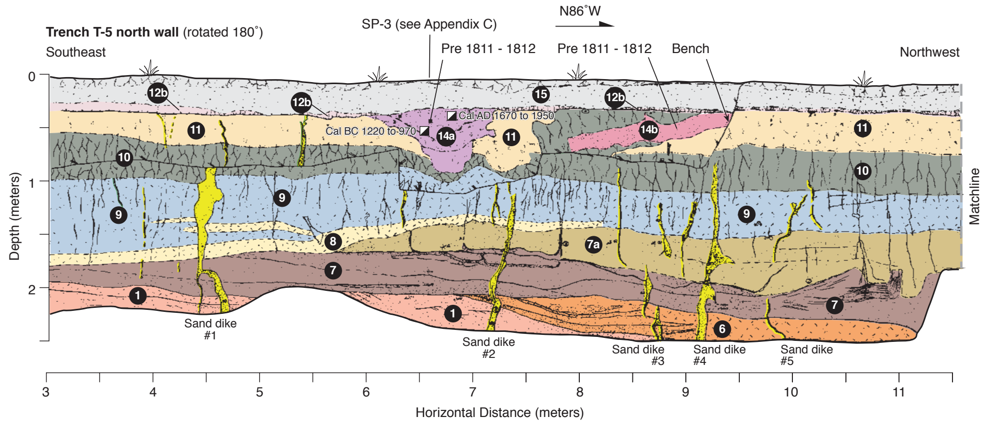

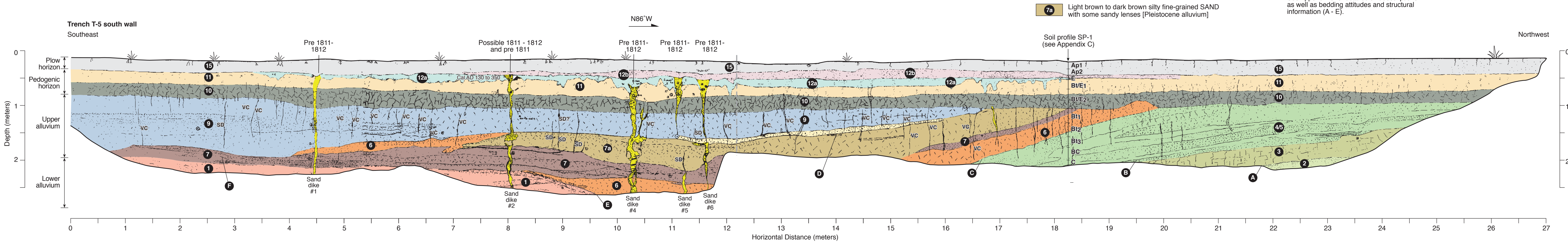

Explanation

- 15 — Light brown fine-grained SAND [Ap-soil horizon]
- 14b — Dark grray to grayish-brown, mottled, poorly sorted fine-grained SAND (liquefaction deposit)
- 14a — Dark gray to brown, very fine-grained SAND and SILT (buried swale within reworked liquefaction deposits)
- 12b — Dark brown organic rich fine-grained SAND [pedogenic A-soil horizon partly modified by plow zone]; like correlative with unit D_S of T-3
- 12a — Light grayish brown mottled silty SAND [pedogenic A/E - soil horizon]
- 11 — Light brown mottled orangish brown fine-grained sandy SILT to silty SAND [Bt/E1-soil horizon]
- 10 — Dark brown to orangish brown silty CLAY [Bt/E2 soil horizon]
- 9 — Orangish light brown sandy SILT to silty very fine-grained SAND [Pleistocene alluvium]
- 8 — Light orange-brown mottled SILT with very fine-grained sand [Pleistocene alluvium]
- 7a — Light brown to dark brown silty fine-grained SAND with some sandy lenses [Pleistocene alluvium]
- 7 — Oxidized brown to fine- to medium-grained SAND [Pleistocene alluvium]
- 6 — Gray to orange mottled sandy SILT with lenses of fine-grained sand and clay [Pleistocene alluvium]
- 5/4 — Oxidized light brown to reddish brown alternating beds of fine-grained SAND, sandy SILT, and silty CLAY [Pleistocene alluvium]
- 3 — Olive-brown to pinkish gray CLAY, reduced with abundant iron oxide nodules [Pleistocene alluvium]
- 2 — Olive-gray silty fine- to medium-grained SAND [Pleistocene alluvium]
- 1 — Light brown to reddish brown fine-grained SAND, planar to cross-bedded [Pleistocene alluvium]
- Radiocarbon sample location and age (generally 2-sigma); see Table 1
- VC — Vertical clay seam
- SD — Vertical sandy seam

See Appendix C for detailed unit descriptions as well as bedding attitudes and structural information (A - E).

NEW MADRID NORTH FAULT FARRNEBURG, MISSOURI	
Trench T-5	
William Lettis & Associates, Inc.	Figure 14

1504 New Madrid North fault

Explanation

- 15 — Light brown to light gray SILT with very fine-grained SAND [Ap soil horizon]
- 14 — Dark grayish brown poorly sorted silty very fine-to medium-grained SAND [sand blow deposit mixed with A/E soil horizon]
- 13 — Unit 13 Grayish brown sandy SILT [A/E soil horizon that collapsed into liquefaction-related crater or chemically stripped Unit 14]
- 12 — Dark grayish brown very fine-grained SAND with silt and trace of clay [soil with A- and E-soil horizon properties]
- 11 — Brownish gray very fine-grained sandy SILT [Bt1/E-soil horizon]
- 10 — Oxidized orangish brown clayey SILT [Bt2/E-soil horizon]
- 9 — Orangish brown silty very fine-grained SAND with clay [Pleistocene alluvium]
- 8 — Oxidized gray to orange-brown clayey SILT with very fine-grained sand to silty clay [Pleistocene alluvium]
- 7 — Orange-brown silty very fine-grained SAND with trace of clay [Pleistocene alluvium]
- 6 — Oxidized orange-gray silty CLAY to clay [Pleistocene alluvium]
- 5 — Orange-brown, very fine-grained SAND with silt [Pleistocene alluvium]
- 4 — Oxidized orange bedded fine-grained SAND
- 3 — Olive-gray CLAY, reduced with common iron oxide concretions [Pleistocene alluvium]
- 1 — Light brown to reddish brown fine-grained SAND, planar to cross-bedded [Pleistocene alluvium]
- ◪ — Radiocarbon sample location and age (generally 2-sigma); see Table 1
- ⊠ — Sediment sample location for microtextual analysis
- ⊗ — IRSL sample location and age; see Table 1
- VC — Vertical clay seam
- SD — Vertical sandy seam

See Appendix B for detailed unit descriptions as well as bedding attitudes and structural information (A - E).

Trench T-6 north wall (rotated 180˚)

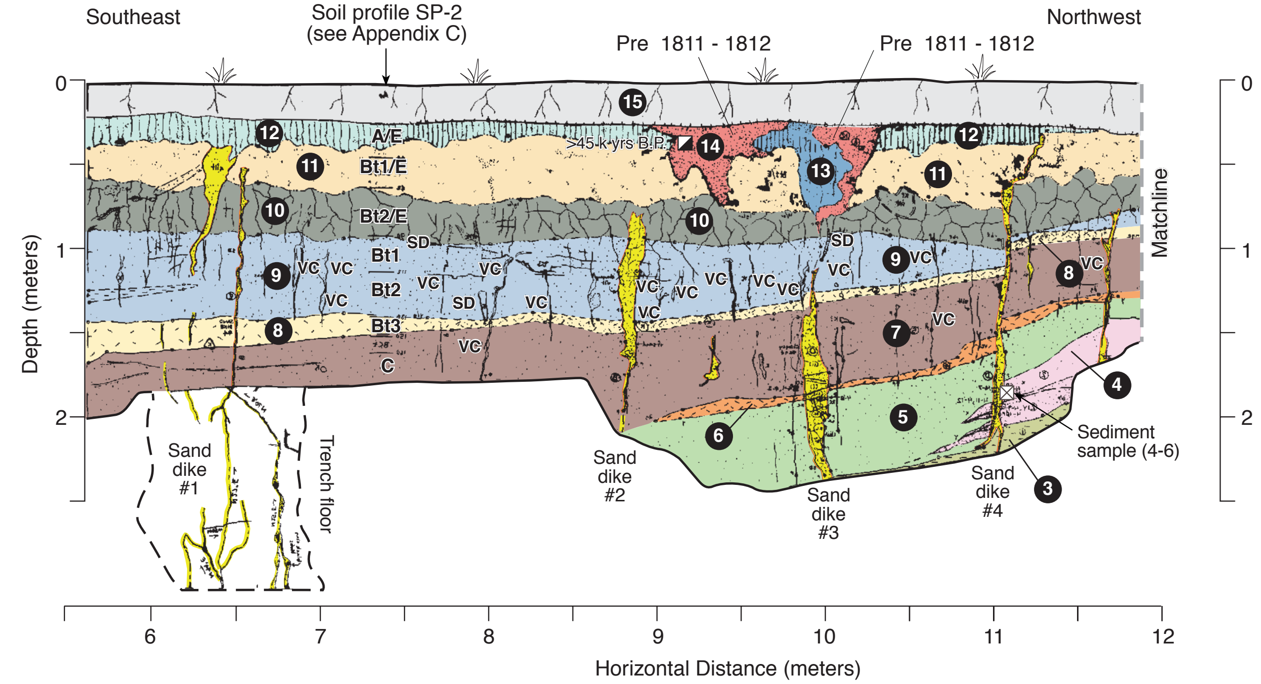

Trench T-6 south wall

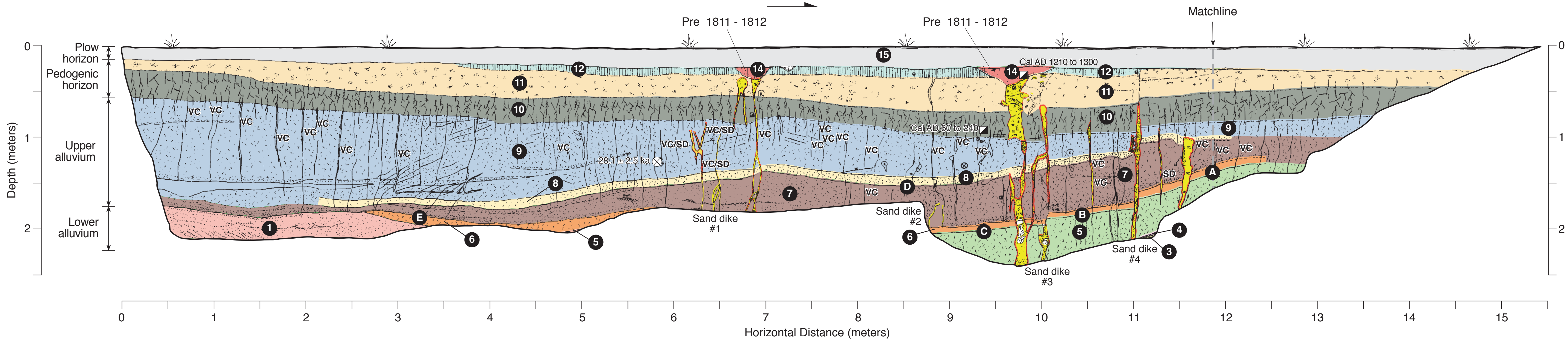

NEW MADRID NORTH FAULT
FARRNEBURG, MISSOURI

Trench T-6

WLA William Lettis & Associates, Inc. | Figure 15

1504 New Madrid North fault

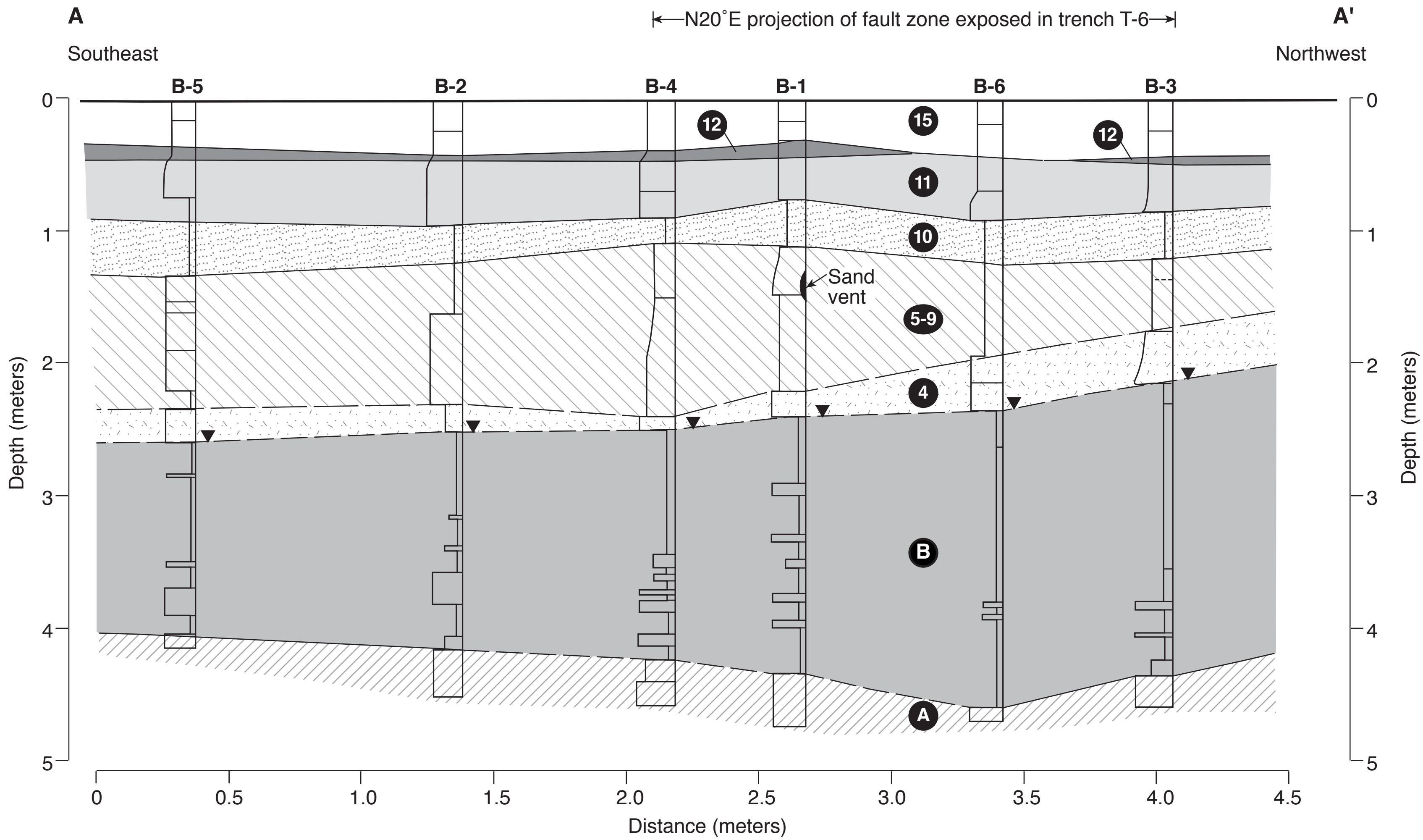

Explanation

- 15 — Yellow-brown to brown, massive silty fine-grained sand (Plow zone)
- 12 — Dark grayish brown, massive, very fine-grained sand to fine-grained sandy silt (pedogenic A-horizon)
- 11 — Light brown to grayish light brown, massive, silty very fine-grained sand (pedogenic A/E-horizon)
- 10 — Oxidized orange-brown clayey silt to silty clay (pedogenic Bt-horizon)
- 5-9 — Yellow-brown to orange-brown, interbedded fine-grained sandy silt to clayey silt (Pleistocene glacial outwash deposit)
- 4 — Strong reddish brown, thinly bedded, fine-grained sand with iron-oxide staining (Pleistocene glacial outwash deposit)
- B — Reduced olive-gray clay with thin interbeds of reddish brown silt and fine-grained sand; common iron-oxide stained root concretions (Pleistocene glacial outwash deposit undifferentiated Units 1 to 3 of trenches T-5 and T-6)
- A — Reddish brown to dark brown fine- to medium-grained sand with rip-up clasts of silt (Pleistocene glacial outwash deposit)
- ▼ Depth to groundwater (April 6, 2004)

NEW MADRID NORTH FAULT
FARRNEBURG, MISSOURI

Cross Section A-A'
(viewed to the south)

WLA William Lettis & Associates, Inc. | Figure 16

1504 New Madrid North fault

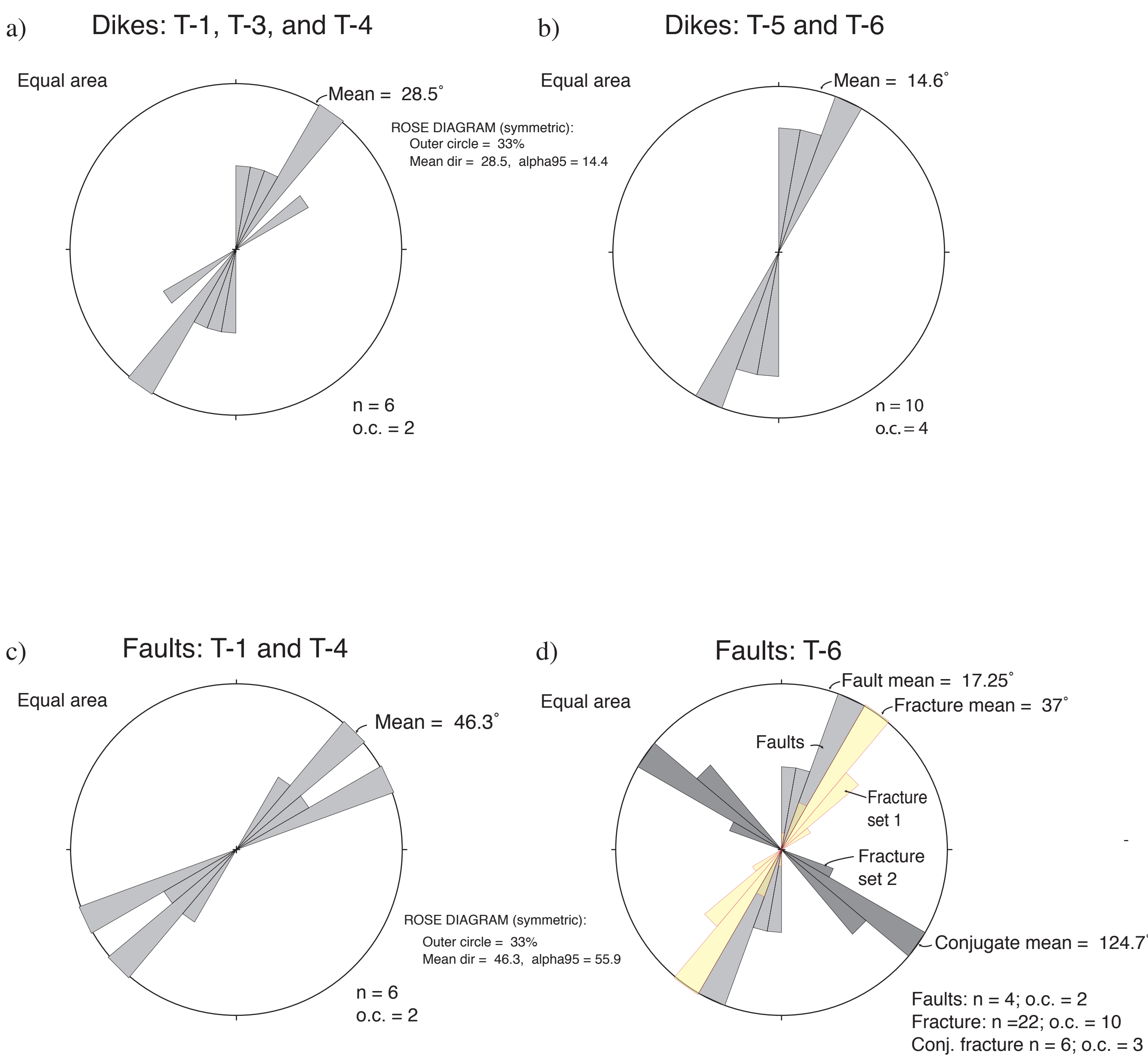

Figure 17. Rose diagrams of fracture, dikes, and fault data from North Farrenburg site.

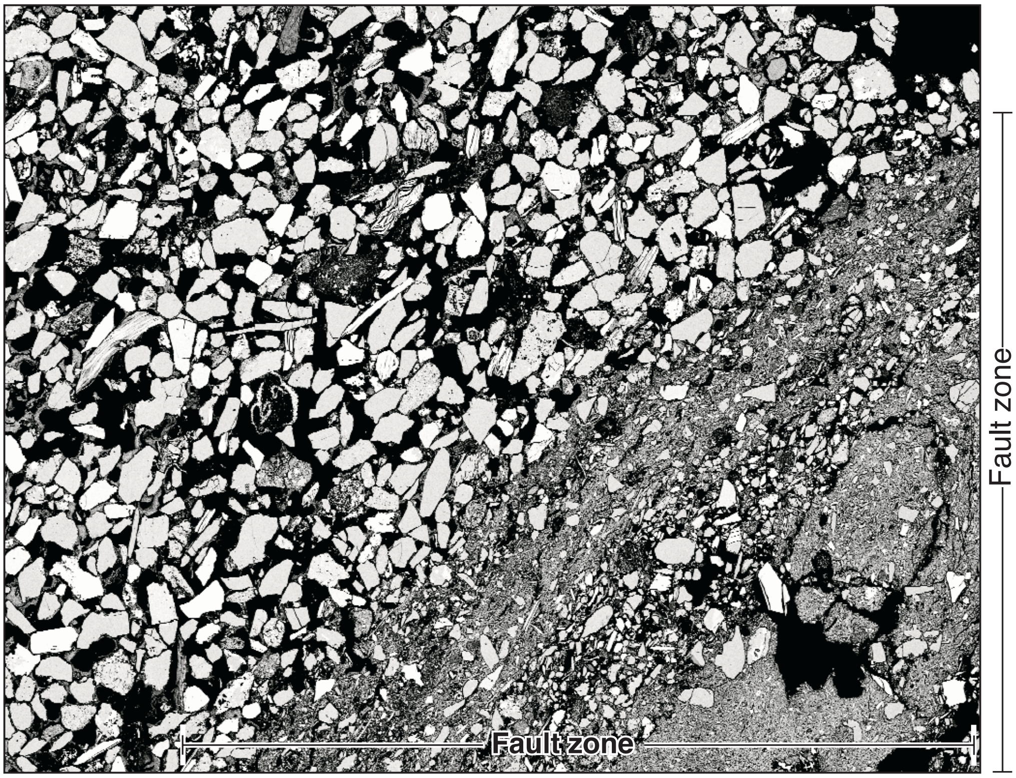

Figure 18. SEM image of sample number 12 (horizontal), collected along the main fault zone exposed in trench T-1. Sample is horizontal and is oriented about N60°W and normal to the trench wall. Note the reduced porosity, grain size, and anastamozing nature of the fault zone. Scale: 1.2 mm wide and 1 mm high.

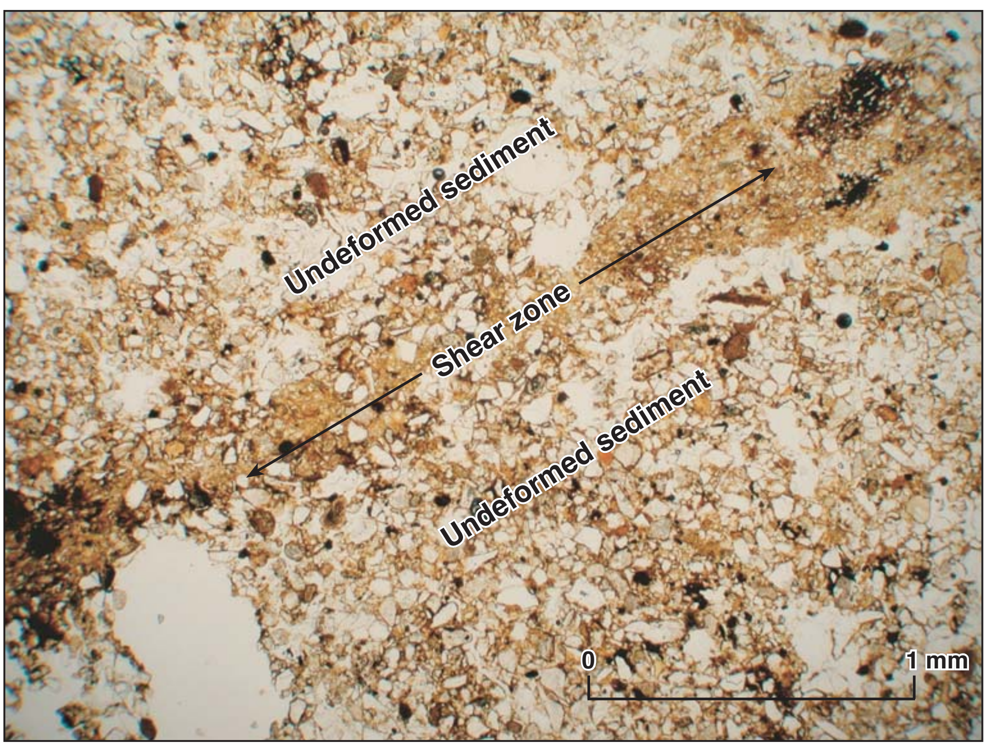

Figure 19. Photomicrograph of a small, ~N05˚W trending fault zone in silty fine sand unit, north wall T-6 (horizontal sample 4-6). Silty fine sand of the country rock is cut by a fracture zone 0.25 to 0.5 mm in width. The fracture zone has lower porosity than the adjacent sediment and consists of angular grain fragments that are smaller than surrounding material.

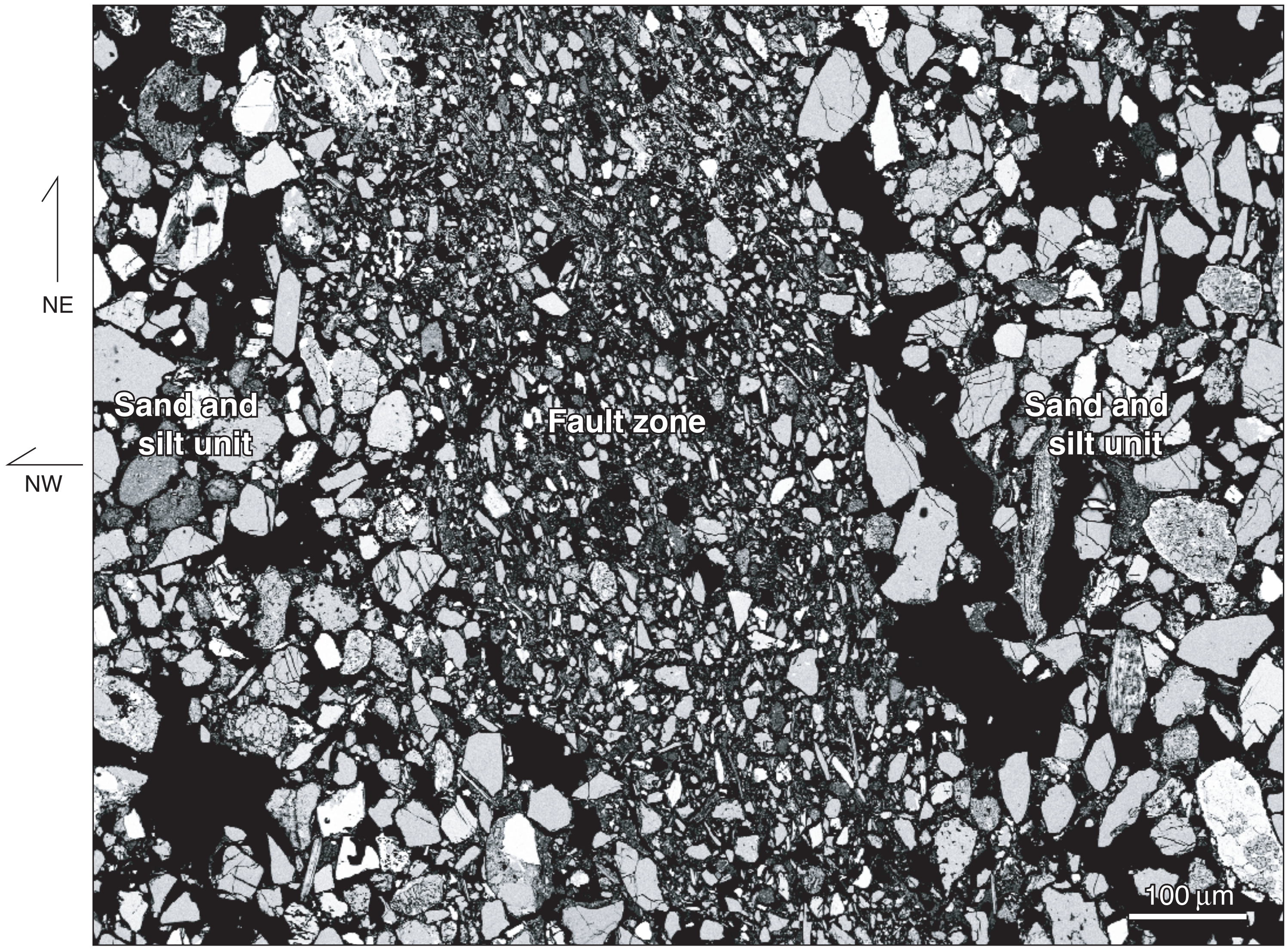

Figure 20. SEM image of a small, ~N05˚W trending fault zone in silty fine sand unit from the north wall T-6 (horizontal sample 4-6). The fault zone has a finer grain size and lower porosity than the adjacent sediment. Elongate grains in the fault zone show a preferred orientation roughly parallel to fault zone boundaries.

N60˚W

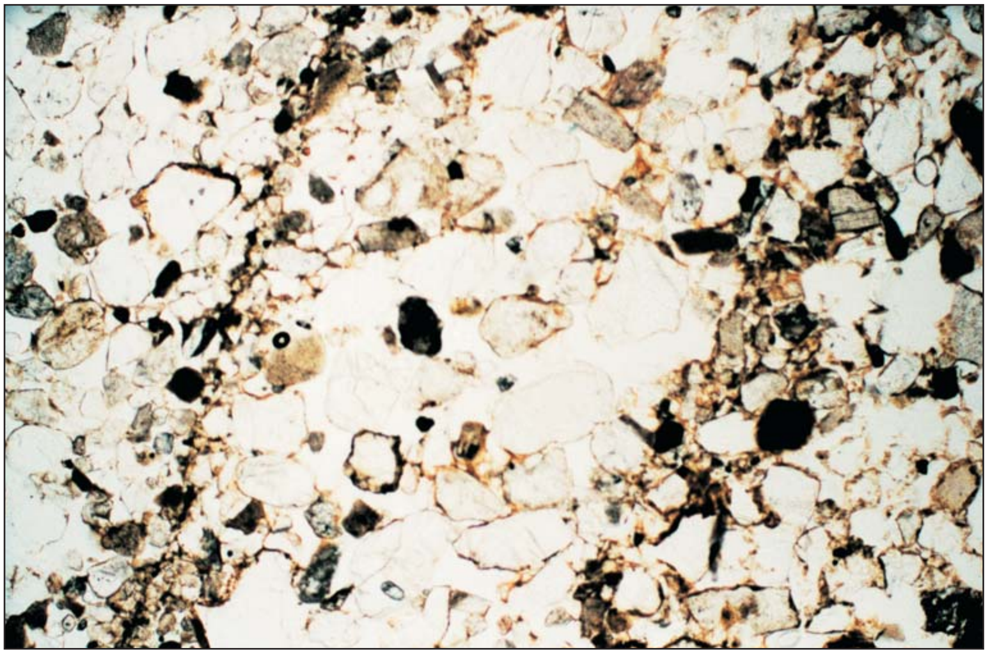

Figure 21. Photomicrograph of sample number 17 collected along the edge of a sand dike exposed in trench T-1. The country wall rock and dike consist of silty sand and and fine-grained sand, respectively. Note the absence of grain size reduction and shearing compared to Figure 18. Scale: 3.2 mm wide and 2 mm high.

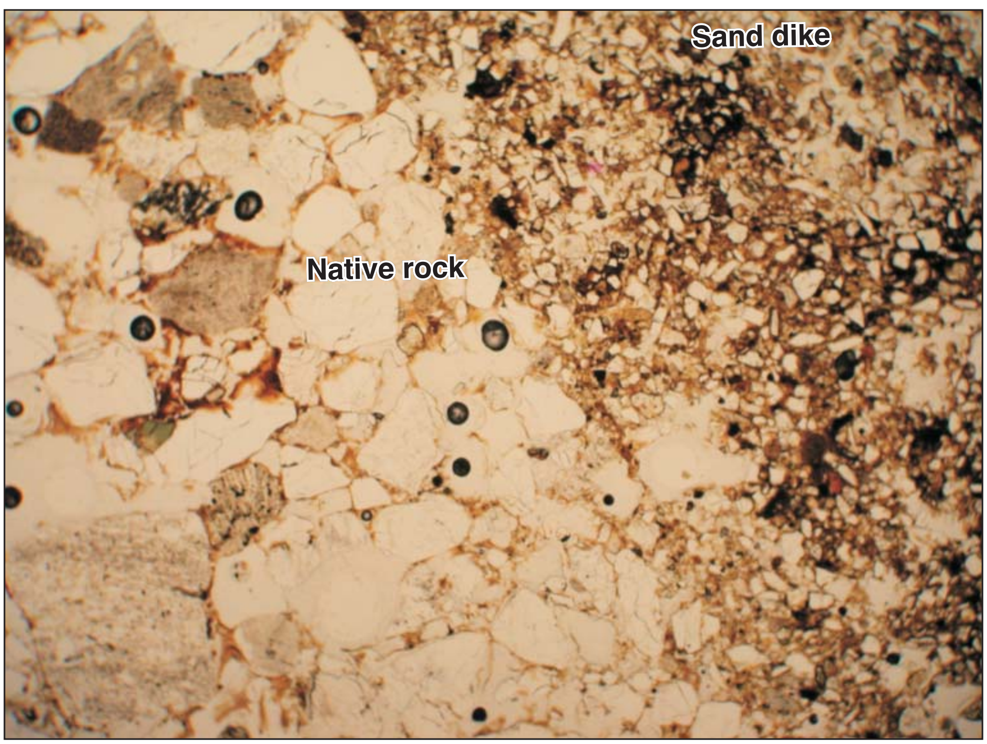

Figure 22. Photomicrograph of sample number 4-6 along sand dike margin exposed in trench T-6. Note lack of preferred grain orientation.

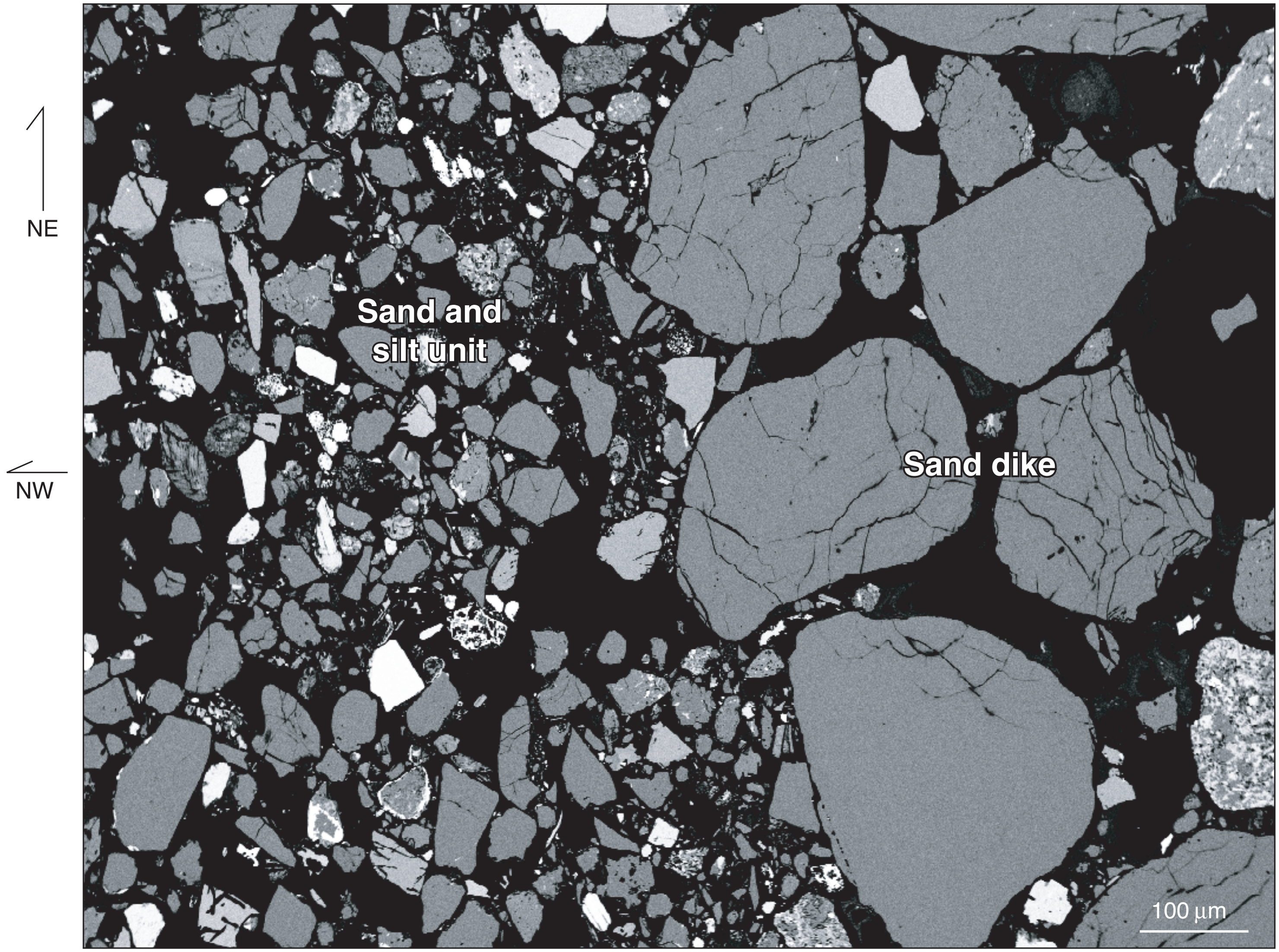

Figure 23. SEM image of the margin of the west margin of a sand dike intruded along a fault, north wall T-6 (horizontal sample 4-6). The sand dike is significantly more coarse grained than the adjacent sediment. Although the fault shows 15 cm of SE-side down displacement (Figure 16; T-6 trench log) no textural evidence of faulting is preserved at this contact. We infer that injection of the sand dike has removed any pre-existing fault texture.

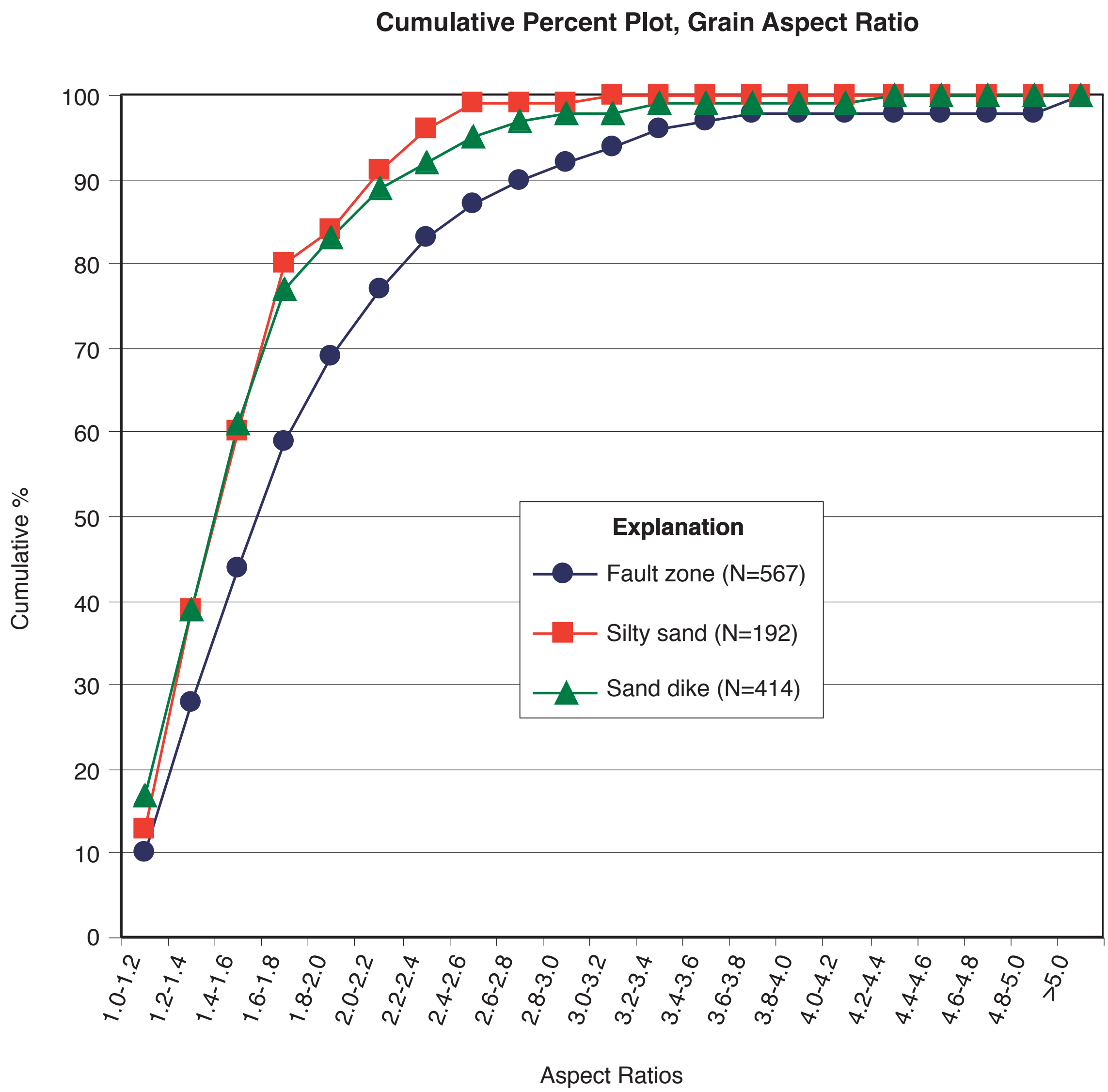

Figure 24. Cumulative plot of grain aspect ratios of sand in fault zone and in other sediments in trench T-1, from samples 12 and 17.

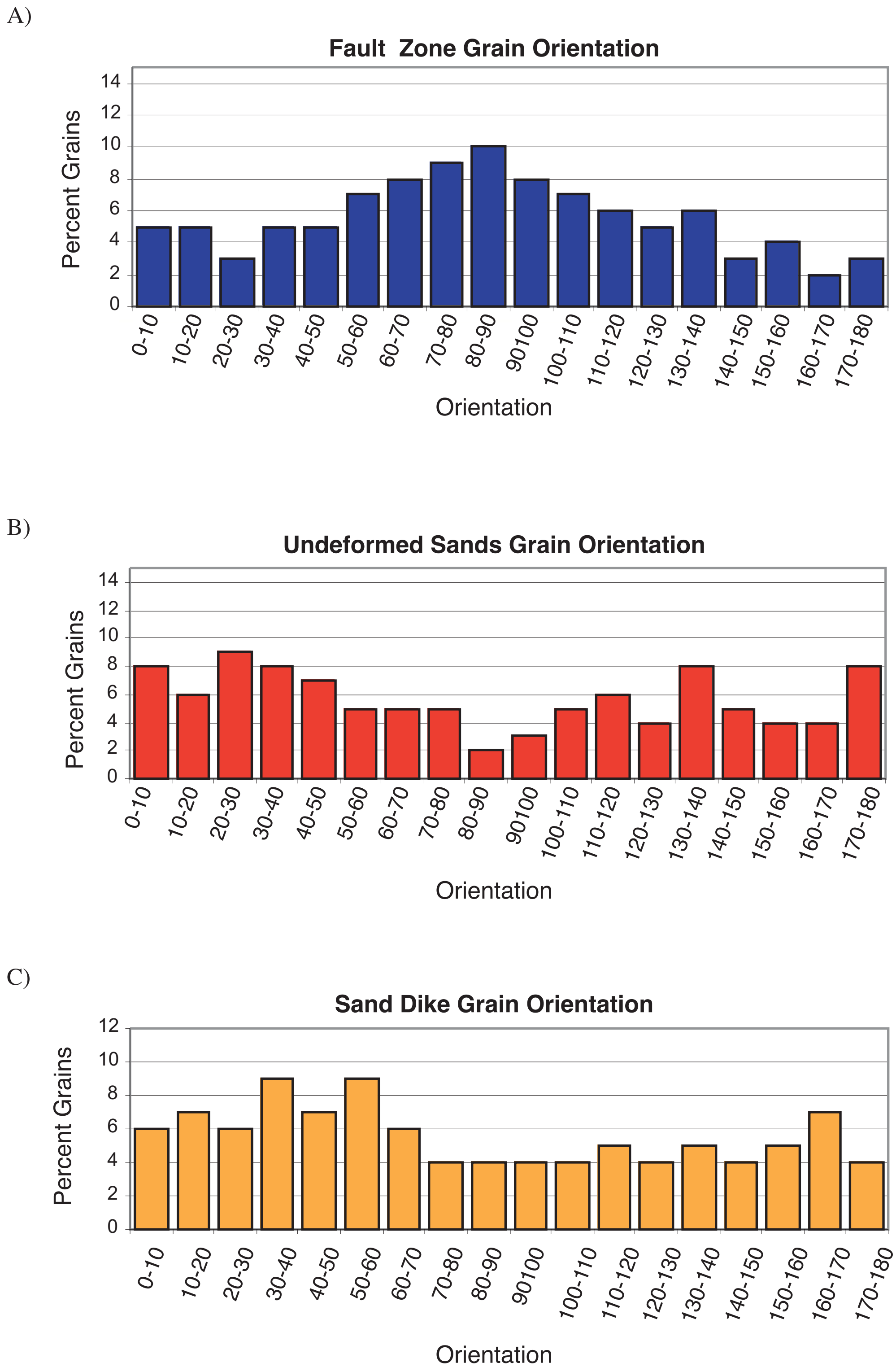

Figure 25. Histograms of orientation of sand grains in fault zone and in other sediments in trench T-1. Orientations are measured counterclockwise from horizontal. A) Grain orientations in the fault zone, sample 12, N=567. B) Grain orientations in undeformed silty sand, sample 17, N=192. C) Grain orientations in sand dike, sample 17 , N=414.